POLYMER-BASED MICRO CRYOGENIC COOLERS

By

YUNDA WANG

B.Eng. Electrical Engineering, Xi'an Jiaotong University, 2005

M.Eng. Electrical Engineering, Peking University, 2008

A thesis submitted to the

Faculty of the Graduate School of the

University of Colorado in partial fulfillment

of the requirement for the degree of

Doctor of Philosophy

Department of Mechanical Engineering

2012

This dissertation entitled:

Polymer-based Micro Cryogenic Coolers

written by Yunda Wang

has been approved for the Department of Mechanical Engineering

_____

Y.C. Lee

_____

Ray Radebaugh

Date_____

The final copy of this thesis has been examined by the signatories, and we find that both the content and the form meet acceptable presentation standards of scholarly work in the above mentioned discipline.

Abstract

Wang, Yunda (Ph.D., Mechanical Engineering)

Polymer-based Micro Cryogenic Coolers

Dissertation directed by Professor Y. C. Lee

This dissertation studies the design and fabrication of polymer-based planar, Joule-Thomson (J-T) micro cryogenic coolers (MCCs). The polyimide layers are used for fluid channels defined by copper sacrificial layers. The first planar MCC consists of a micro machined polyimide counter-flow heat exchanger and a silicon/glass anodic-bonded coldhead with a J-T expansion valve. Main features of the MCC demonstrated are: 1) the J-T valve with a size of 1.2 mm by 1.7 mm and a 3 μm gap ; 2) the high pressure fluid channel with a size of 12 mm by 2 mm and a 20 μm gap ; 3) the low pressure fluid channel with a size of 12m by 2mm and 10 μm gap ; 4) the DRIE-etched opening for the fluid coupling between the heat exchanger and a compressor with a size of 1.6mm by 300 μm and a through-wafer depth of 550 μm; 5) the staggered posts with a diameter of 60 μm inside the fluid channels for withstanding high pressure 6) the O-ring like trenches with a depth of 5 μm for the fluid coupling between the heat exchanger and the substrate. This planar MCC is functional with the coldhead temperatures reaching 233K; however, it suffers a leakage problem at the soldered-interface between the heat exchanger and the coldhead. This assembly problem is solved by an improved wafer-level processing for a monolithic polyimde MCC. The new cold stage including the heat exchanger and the J-T valve is fabricated using copper-polyimide processes, monolithically on a wafer . Improved features are: 1) the polymer J-R valve with a size of 1.2 mm by 1.4 mm and a 3.2 μm gap ; 2) the polyimide tethers to support the suspended heat exchanger; 3) the 3-dimensional fluid interconnects in different layers. This monolithic polyimide MCC does not encounter the mechanical leakage problem since the soldered-interface is removed. It also enhances the

manufacturability and scalability of the MCC through the wafer-level processing. The coldhead temperatures improve from 233 K to 190 K with a flow rate reduced from more than 260 sccm to about 60 sccm. The cryogenic demonstration is accomplished by using a custom-designed 5 components refrigerant (8% methane, 46% ethane, 14% propane, 4% butane and 26% pentane) optimized by scientists in NIST.

During the demonstration studies, an accurate model to design a polymer J-T valve is identified as a critical need. Therefore, this thesis experimentally measures flow characteristics of different polymer J-T valves in order to establish the design model. Specifically, an apparatus is built to measure pressure drop vs. flow rate corresponding to pure nitrogen and a gas mixture consisting of methane 34%, 22% ethane, 20%, ethylene 12% isobutane and 12% isopentane. A valve resistance prediction model is established with a homogeneous assumption for a multiphase flow assisted by the calculation of fluid properties using NIST-REFPRO. The model is proven accurate with a mean deviation < 10% for the cases studies at temperatures of 295 K, 265 K and252 K.

Keywords: cryogenic cooler, MEMS, polyimide, planar structure, heat exchangers, tethers, thermal isolation, Joule - Thomson valve

Dedication

To my parents and family who gave me the greatest support towards the completion of this thesis.

Acknowledgements

I would like to express my sincere gratitude to my dissertation advisor, Professor Y. C. Lee, for his enthusiastic support and invaluable advice provided throughout this study. I would also like to thank Dr. Ray Radebaugh whose insights and knowledge in cryogenics have been instrumental to this process.

I am also thankful to Professor Victor M. Bright, Professor Scott Bunch, and Dr. James Booth for serving in my dissertation committee. I would also like to thank my colleagues, collaborators, and friends in Boulder for their critical inputs, discussions, and support. In particular, I would like to express my appreciation to Ryan Lewis, Dr. Martin Lin, Collin Coolidge, Paul Schroeder, Ben Britton, Hayley Schneider, Peter Davis, Dr. Yadong Zhang, Dr. Jen-Hau Cheng, Hsin-Ray Wu, Dr. Ming Kong, Xinghui Liu, Jian Wang, Qian Li, Dr. Christopher Oshman, Dr. Joseph Brown and Harris Hall from the Department of Mechanical Engineering, University of Colorado at Boulder, and to Dr. Li-anne. Liew, Peter Bradley, Dr. Marcia Huber, Dr. Yu Wang, Dr. Jim Beall, Dr. Gene Hilton, Dr. John Nibarger and Dr. Adriana Litafrom National Institute of Standards and Technology (NIST).

Finally, I would like to thank the Defense Advanced Research Projects Agency (DARPA) for providing funding for this research. This research is supported by DARPA Micro Cryogenic Coolers program (NBCHC060052 and W31P4Q-10-1-0004).

Content

Figures

Tables

CHAPTER 1: INTRODUCTION AND BACKGROUND

1.1 Thesis motivation

Cryogenic coolers are intended to cool low power-consumption sensors thereby lowering thermal noise, enhancing bandwidth, and enabling superconductivity in the sensor [1]. For example, the signal-to-noise ratio of a preamplifier can be improved when the thermal noises are reduced substantially as the temperature reaches a cryogenic level. The parasitic resistance which is induced by inductors in electrical filters as LRC filters often limits the Q (quality) factor. The Q factor can be improved dramatically assisted with superconductor materials operating at cryogenic temperatures. Another example is for the mixers used in terahertz frequencies imaging system based on high temperature superconductor hot-electron bolometers (HTS HEBs) operated at cryogenic temperatures, e.g. 70 K [2]. According to DARA's MTO MCC project description [3], applications that benefit from operation at cryogenic temperatures include cooled IR detectors for heat-seeking missiles and night vision; low-noise amplifiers for ultra-sensitive, long-range communications such as needed for deep space applications; front-end passives in communication systems; myriad sensors that have substantially lower noise floors and improved stability when operated at cryogenic temperatures (including and especially sensors for inertial navigation); and nextgeneration nanoscale devices such as atom optical inertial sensors and timing references, single electron transistors, biosampling devices, and other nano-applications that operate best at cryogenic temperatures.

However, most current cryogenic cooler systems are of large volumes and do not match the size of devices or systems targeted to be cooled. Coolers with rather large size will make the whole system to be large, power consumptive and expensive which impedes the use of cryogenic cooling. It is desirable to design and fabricate miniature cryogenic cooler systems with small size

and low power. However, to offset economies of scale and to enhance the performance, some key elements involving new fabrication technologies remain to be developed. Improved miniature heat exchangers and regenerators are needed [4].

This thesis will report the first polyimide-based planar cold stage for micro Joule-Thomson cooler. Fabricated through wafer-level processing, this novel component will make the MCC very compact, manufacturable, reliable and cost-effective. The details of the designs, fabrication and characterization of the MCC's planar cold stage are to be presented and discussed in the thesis.

1.2 Micro Joule-Thomson (J-T) cooler

Figure 1.1 shows the schematics of the operation principle of the J-T micro cryocooler. Refrigerant flows continuously through the compressor, heat exchanger (high-pressure channels), JT expansion valve, evaporator, heat exchanger (low-pressure channels), and then through the compressor again to form a closed loop cycle. The gas mixture (refrigerant) is pressurized by a compressor (see Figure 1.1, a→b), and then it flows through a cooler to be precooled (see Figure 1.1, b→b'). After precooling, the gas mixture flows through a counter flow heat exchanger, where it exchanges heat with the gas flowing in the opposite direction inside the low-pressure line (see Figure 1.1, b'→c). When the gas mixture enters a flow restriction (see Figure 1.1, J-T orifice), it undergoes an isenthalpic expansion and the pressure drops from high to low. During the expansion process, the gas mixture cools and partially vaporizes (see Figure 1.1, c→d). The liquid evaporates or boils while absorbing heat from the device and from the environment (see Figure 1.1, d→e). From the cold head, the low-pressure two-phase fluid flows back into the heat exchanger (see Figure 1.1, e→a) to cool the incoming high-pressure warm fluid for enhancement

of efficiency. The gas eventually goes back to the compressor system to complete a closed-loop Joule-Thomson cooling cycle.

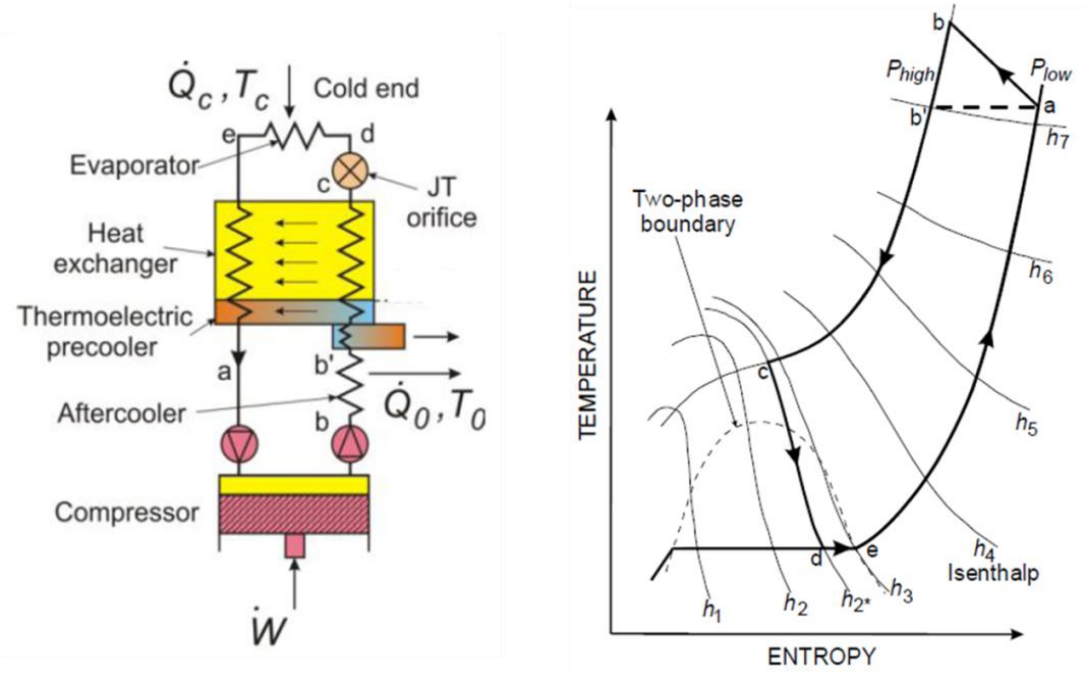

Figure 1.1: On the left side, a schematic diagram of the J-T cycle. On the right side, the T-S diagram of nitrogen with isobars and isenthalps. The bold line with numbers represents the cycle.

In the past decades, the miniaturization of J-T coolers attracted considerable interest due to its great potential for small size, low noise, fast response, and high efficiency [5]. Figure 1.2 compares J-T MCCs, thermoelectric (T/E) coolers and Stirling coolers for a temperature range from 300 K to 200 K. As indicated, for the same heat lift, MCC input power is about 10 % of the T/E cooler's. MCC's size is about 10% of the Stirling cooler's. The T/E cooler is well known for its poor efficiency at temperatures below 240 K. The Stirling cooler's size is limited by the operation frequency (<120 Hz) of the compressor, which is limited by the oscillating flow. With the simple configuration, MCC's compressor can be operated at high frequencies, e.g. 1 kHz or

100 KHz. Dr. Ray Radebaugh at NIST has also derived other comparisons corresponding to different temperature ranges with conclusions similar to those illustrated in Figure 1.2 [6].

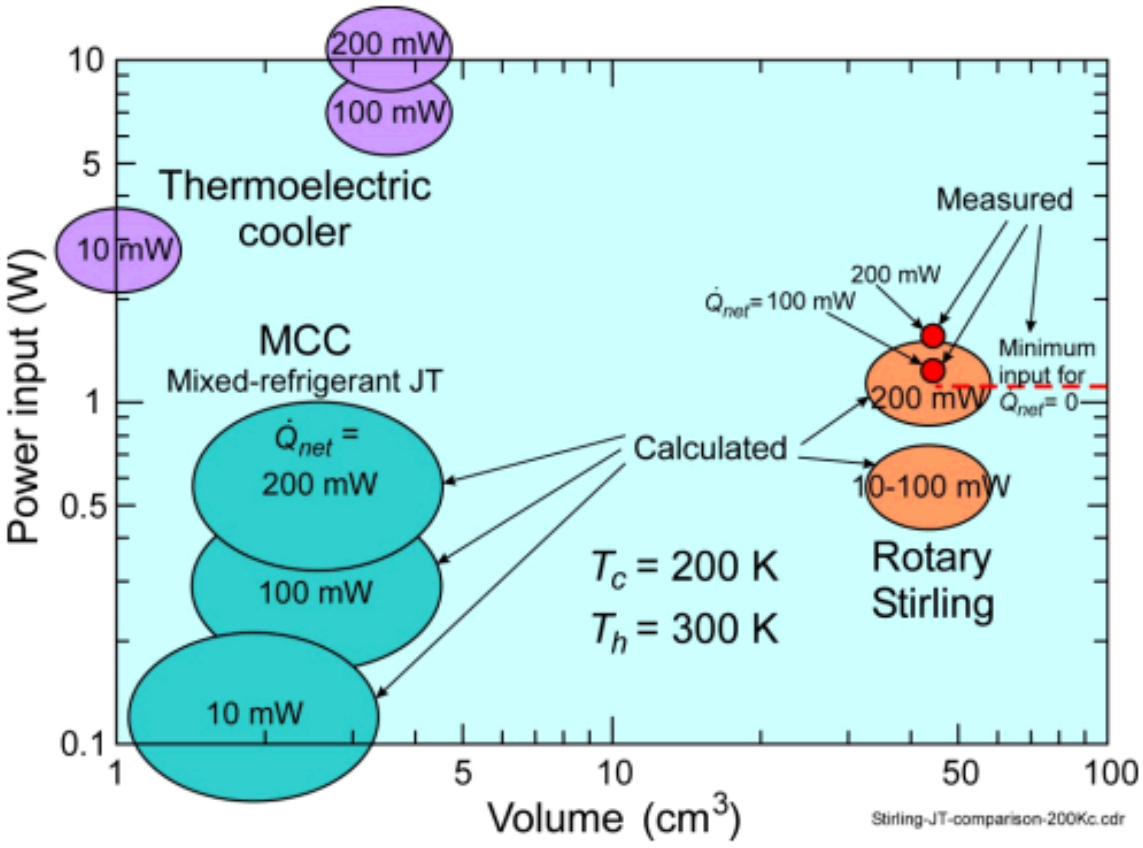

Figure 1.2: J-T cooler compared with thermoelectric and Stirling coolers for a 300K to 200K temperature range.

1.3 Previous work on MCC

According to our knowledge, Jim Mercereau was the first pointing out the need for microminiature refrigeration [7] and together with Little, W. A. submitted a proposal to the Navy in 1972 to develop a microminiature refrigeration system and integrated superconducting magnetometer [4].

For fabrication of the micro cooler's cold stage, most of recent works have highly relied on assembly processes. For example, in 2006, Lerou et al. reported a micro cryocooler made of

glass wafers as seen in Figure 1.3a [7.1in1]. They used the HF wet etching technology to fabricate the channel for gas delivering, heat exchanger, and gas valve structure [8][9].Three glass chips were fusion bonded together (see Figure 1.3b).

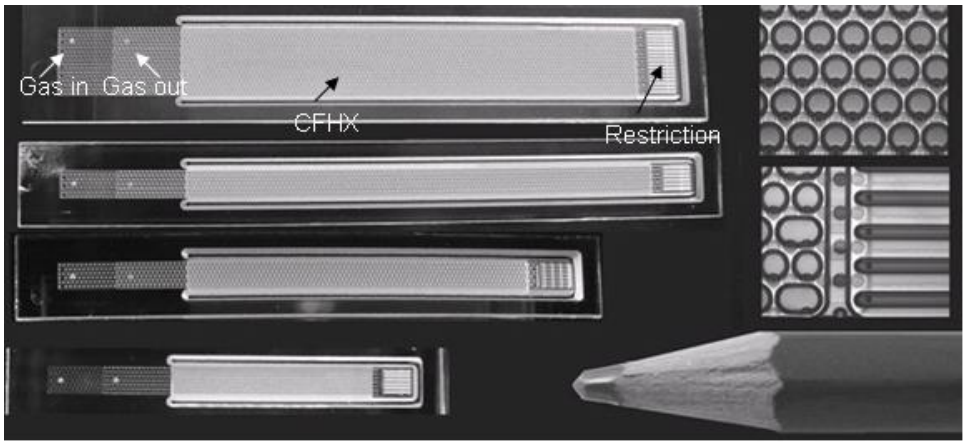

(a) *Left: four different micro cryogenic cold stages. Top right: magnification of the micro channel with supporting pillars. Middle right: the end of the high-pressure flow.*

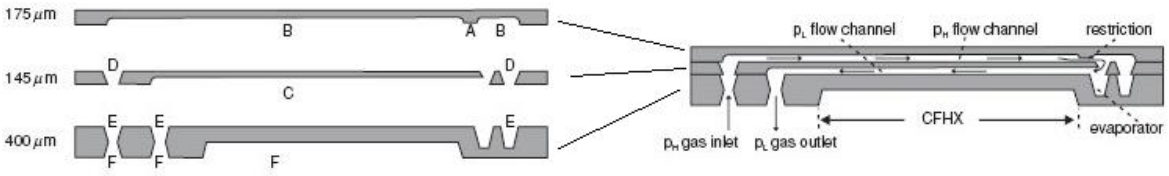

(b) Overview of the process scheme of the cold-stage fabrication.

Figure 1.3: Picture and schematics of 3 glass chips based microcrygenic cold stage reported by Lerou et al from University of Twente.(Figures from[20])

The smallest dimension of these coolers was around 30 mm × 2.2 mm × 0.5 mm. With 8.0 MPa nitrogen input and expanding to 0.6 MPa, the cold head reached a temperature around 100 K and the net refrigeration power was 12 mW [9]. However, these plates-based coolers which were usually fabricated with plates with up to several hundred micron thickness had significant heat conduction from the warm end to the cold end. Such conduction loss could dramatically decrease the net refrigeration power.

To reduce the loss, the Center for Integrated Micro and Nanoscale Transducers (iMINT center) at the University of Colorado cooperating with National Institute of Standards and Technology (NIST) developed a fiber/capillary based microcryogenic cooler in 2009 as shown in Figure 1.4. They used six internal hollow-core fibers inside a glass capillary to form the heat exchanger. As shown in Figure 1.4, the fiber-based heat exchanger was 25 mm long and 0.61 mm in outer diameter with six hollow-core fibers of 125 μm O.D./76 μm I.D. bundled internally. The cold head was 2 mm × 2 mm × 1.2 mm silicon-to-glass chip stack which provided fluid coupling structure and the J-T valve. Fibers were inserted manually into the coupling structure in the silicon chip. The fibers, the capillary tube and the silicon chip were soldered and sealed (Figure 1.5). Due to the very thin wall of the glass fiber and the capillary, this cooler achieved excellent thermal isolation with extremely low conduction and radiation. The corresponding MCC reached 140 K with 15 sccm mixed refrigerants under 14:0.08 MPa pressure ratio [10].

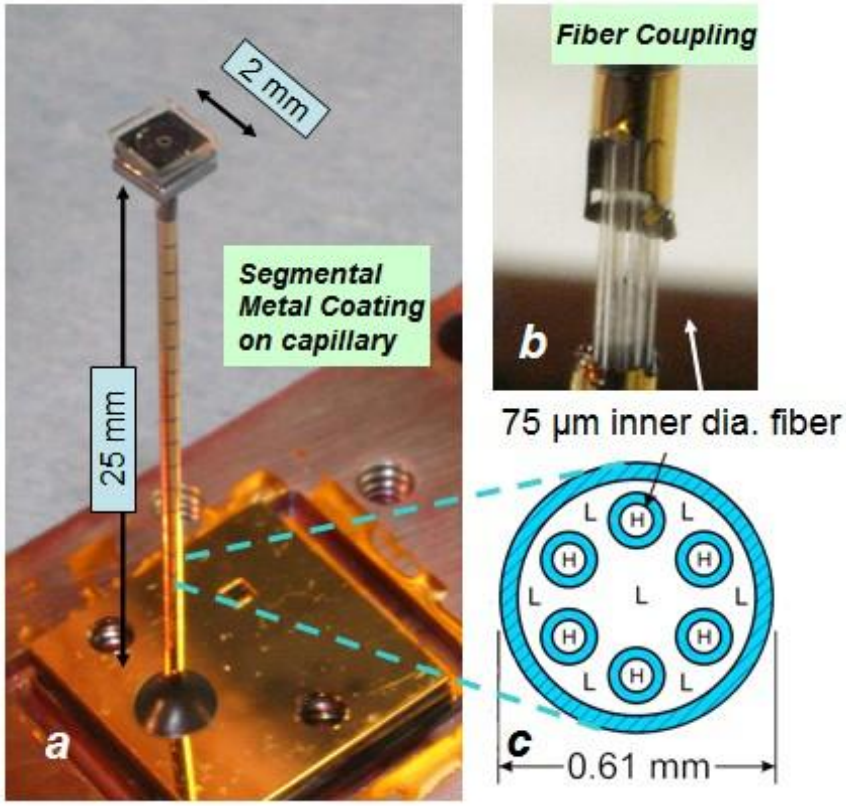

Figure 1.4:a) CU&NIST's fiber-based vertical MCC cold stage, by Martin Lin et al. in 2009. b) Six fibers in a capillary tube. c) Cross sectional view.

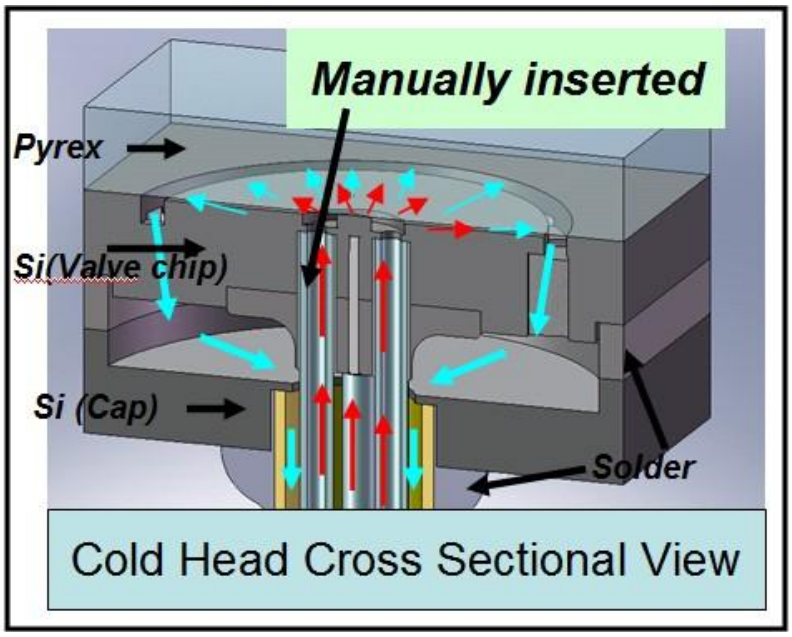

Figure 1.5: Cross-sectional view of a CU Boulder's cold head with fibers manually inserted into the cold head assembly.

However, the fabrication of the cold-stage was labor intensive and low yield. For example, inserting fibers into the small hole on valve chip (see Figure1.4) was challenging. There were many processing steps required for soldering and epoxy bonding to seal the fibers with the valve chip, the capillary tube with the cap chip and the cold-head with the coupler chip (see Figures1.4 and 1.5). In addition, the assembly was brittle and could be damaged easily in the after-assembly processing and characterization steps What's more, the vertical structure was a challenge to future packaging which was needed for providing a vacuum environment, protecting and making a fully integrated cooling system.

1.4 Mixed Refrigerant and Opportunity for Polymer Based MCC

In macro-scaled Joule-Thomson refrigeration systems, mixed refrigerants have been widely applied to enhance the efficiency and refrigeration power. Radebaugh [11], Missimer [12], and Boiarski [13] reviewed recent developments and history of mixed refrigerants. Fuderer and Andrija [14] first used mixed gases in a single stream without phase separators in 1969. They found that the mixtures experienced mostly two-phase flow in the heat exchanger. As a result, boiling and condensing heat transfer of two-phase flow greatly enhanced cooling efficiency [6].

The ideal cooling power of a refrigerant in a J-T cryogenic cooler is given by the product of flow-rate with the minimum isothermal enthalpy difference between the high-pressure refrigerant and low-pressure refrigerant [15].

$$\dot{Q} = \dot{n}\,(\Delta h|_T)_{min} \tag{1.1}$$

NIST scientists have successfully developed a series of refrigerants for different temperature ranges [16]. For example， a mixture with 5 composition (8% methane, 46% ethane, 14% propane, 4% butane and 26% pentane) was optimized by the program NIST-4 [17] to provide an optimum $(\Delta h|T)_{min}$ in the range from 300 K to 200 K with a high pressure of 4.0 bar and a low pressure of 1.0 bar. The enthalpy differences curve is shown in Figure1.6.

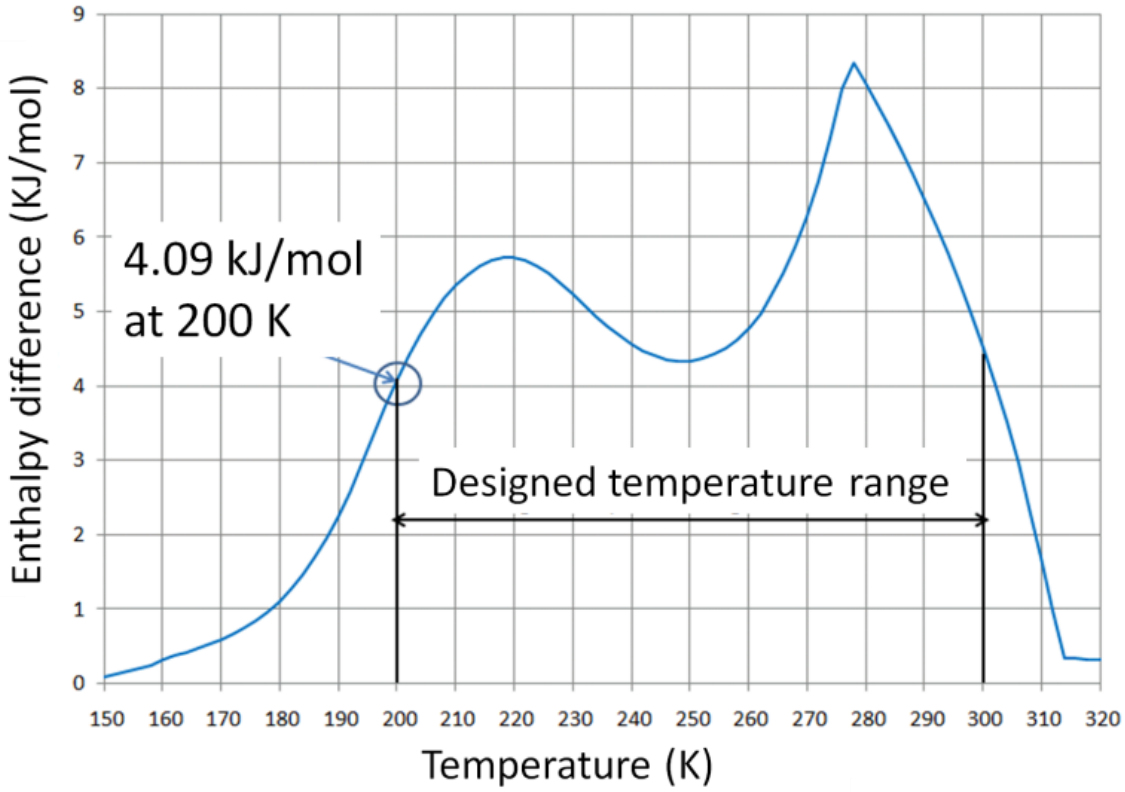

Figure 1.6: Isothermal enthalpy differences for a 5 component mixture with a high pressure of 4 bar and a low pressure of 1 bar. The minimum isothermal enthalpy difference is 4.09 kJ/mol for the temperature range between 300 K to200 K.

Compared with the pure fluids or mixtures used in previous studies, this novel mixture can deliver a reasonable refrigeration capability with a low pressure ratio. Without high pressures inside the heat exchanger, it allows us to use polymer instead of glass. By using polymer, we will benefit from wafer-level fabrication and sacrificial layer releasing processes developed for MEMS. We have an opportunity to fabricate monolithic cold stage including the heat exchanger and J-T valve. Specifically, polyimide is chosen since it has been used in cryogenic applications. Polyimide remains ductile even in cryogenic temperatures and can avoid failures resulting from mechanical loadings such as vibration, shock and impact. Its thermal conductivity (polyimide: k=0.17W/(m-K) was also lower than that of glass: k=2 W/(m-K)). For the sacrificial material,

copper is chosen. The copper-polyimide thin structures are standard configurations used widely in the manufacturing infrastructure for electronic packaging.

1.5 Thesis Outlines

This thesis will present the design, fabrication and characterization of polymer-based cold stage for micro cryogenic coolers (MCC). It should be noted that an MCC consists of a cold stage including a heat exchanger and a J-T valve and a compressor. However, MCC has also been used to describe the cold stage alone in the previous studies. In this thesis, we will use MCC to describe the cold stage. The planar compressor will be developed in the future, but it is outside the scope of this thesis work.

The thesis consists of the following chapters:

(1) Introduction including the project motivation, the review of previous works and opportunities offered by the polymer-based MCC as described in Chapter 1.

(2) System design considerations and optimization of the MCCs based on planar polyimide-based MCCs in Chapter 2

(3) Thermal and mechanical analysis of the MCCs based on planar polyimide-based MCCs in Chapter 3

(4) Fabrication and assembly of the polyimide-based MCCs in Chapter 4.

(5) In proved design and fabrication by making monolithic polyimide planar MCCs in Chapter 5.

(6) Cooling tests and measurements of the both the polymide-based and monolithic polyimide MCCs in Chapter 6.

(7) Study of the polymer J-T valve in Chapter 7.

(8) Summarization the conclusions of the thesis works, followed by recommendations for future works.

CHAPTER 2: SYSTEM DESIGN OF THE POLYMER-BASED MCC

2.1 Introduction to the structure of the polymer-based MCC and design features

Since polyimide material and MEMS technologies were considered to make the cold stage, a heat exchanger (HX) with a parallel-plate configuration rather than some other geometries, such as tube-in-tube, is chosen for the planar MCC. The structure of the MCC cold stage contained a polyimide heat exchanger which was fabricated on a silicon substrate by using polyimide/copper surface micro fabrication process, and a cold-head which contained a micro gap as a gas valve. The two parts were assembled by soldering. Figure 2.1(b) and Figure 2.1(c) illustrates the structure and major dimensions of the planar polyimide-based MCC both from a top view and a cross-sectional view.

Some other description of the features are shown in Figure 2.2, including: 1) 1.2 mm by 1.7 mm with a 3 μm gap for the J-T valve; 2) 12 mm by 2 mm with a 20 μm gap for high pressure fluid channel; 3) 12m by 2mm with 10 μm gap for low pressure fluid channel; 4) 1.6 mm by 300 μm 550 μm length of holes for fluid coupling between the heat exchanger and a compressor; 5) Polyimide tethers to support the suspended HX for better mechanical properties to avoid vibration or excessive displacement under shock); 6) Small posts with column diameter of about 60 μm staggered inside the two channels for both withstanding overpressure in the channels and increasing thermal exchanging surface area (see Figure 2.2). 7) O-ring like trenches in the HX-to-substrate coupling end to enhance the sealing between the interface of the substrate and polyimide HX. To understand this, as show in Figure 1(b), polyimide was embedded in the 5 μm deep trenches around the interconnecting channel to form a micro O-ring. Because the deep trench was etched by deep reactive ion etching (DRIE), scallop side walls formed a better

bonding interface between the polyimide and silicon. High pressure fluid can be stopped by the micro O-ring like trenches to provide a better seal.

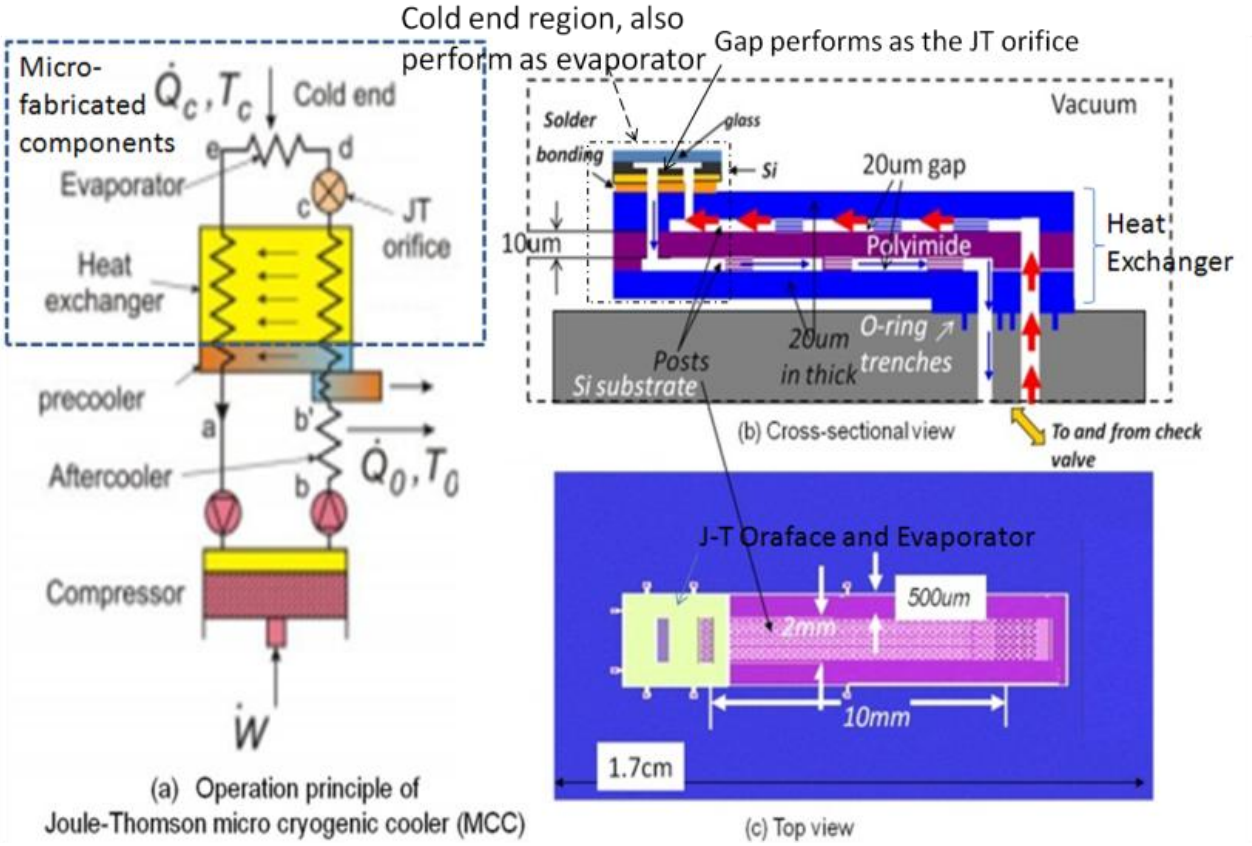

Figure 2.1: Schematics of the operation principle of the J-T micro cryogenic cooler system with top and cross-sectional views of the planar polymer-based MCC. Heat exchanger and cold end (or "cold head") are micro-fabricated and their schematics are shown in (b) and (c).

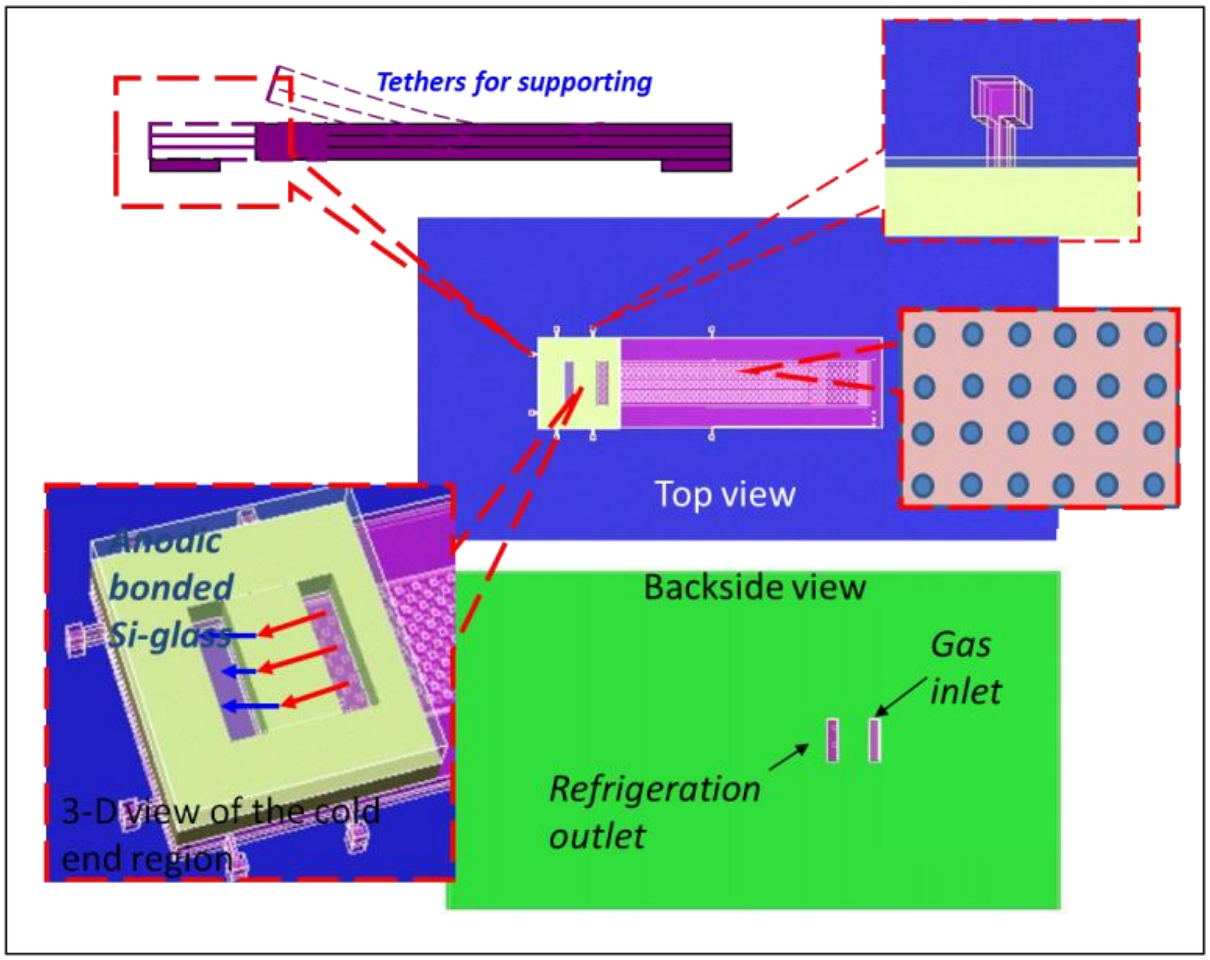

Figure 2.2: Schematics of the operation principle of the J-T micro cryocooler system with top and cross-sectional views of the planar polymer-based MCC.

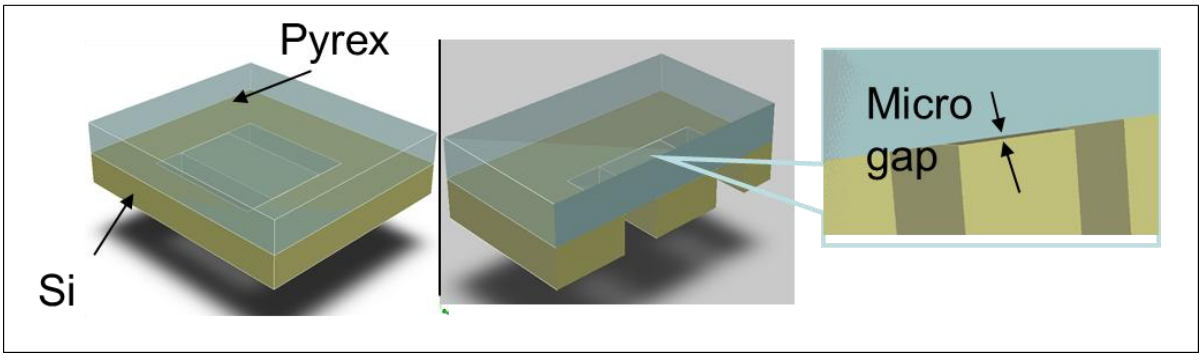

Figure 2.3: Schematics of the Cold head. Micro gap is formed with anodic bonded Pyrex and silicon chips.

The cold-head (or J-T valve chip) is made up of a silicon/glass bonded stack which contains a submicron (around 700nm to 3000nm) gap to provide the gas restriction. The footprint is about 2.5 mm × 2.7 mm. This valve was attached on the cold end of the heat exchanger by soldering (see Figure2.2 and Figure 2.3). More details about the fabrication and assembly of the cold head can be found in Chapter 4.

2.2 System Analysis of the MCC

2.2.1Gross Refrigeration and Mixed Refrigerant

As shown in equation (2.1) in Section 2.2.2, the gross refrigeration power is the product of the flow rate ṅ times the minimum isothermal enthalpy difference of the refrigerant $(\Delta h|_T)_{min}$. The minimum isothermal enthalpy difference of the refrigerant is approximately proportional to the pressure ratio applied up to some maximum pressure ratio [10]. With limited power consumption and stroke volume, a micro compressor is difficult to deliver both high pressure ratio and flow rate. A typical high-pressure that is possible to generate with a miniature compressor is in the range of 0.4-0.8 MPa. In order to provide a system which can operate with a shorter heat exchanger and low driving pressure, refrigerant mixtures need to be used. In fluids, the largest enthalpy difference usually occurs at or very close to the temperature of the phase change from liquids to gas. In mixed refrigerants, refrigerant mixtures are designed to have some fraction of the mixture in liquid-phase throughout most of the heat exchanger. This two-phase flow results in higher heat transfer parameters. Furthermore, refrigerant mixtures can have substantially higher enthalpy differences between the high and low pressure streams at any temperature, as the high-pressure stream can have a higher liquid fraction than the low-pressure stream at the same temperature, and the evaporation of some of that liquid will yield large enthalpy changes [37]. Dr. Huber and Dr. Radebaugh of NIST are the world leaders in

engineering refrigerants and maximize the minimum isothermal enthalpy difference $(\Delta h|_T)_{min}$ along the heat exchanger working temperature range. As shown in Figure 1.6 in Chapter 1, Dr. Huber has engineered the optimized five-component mixture with 4.09kJ/mol under 0.4MPa : 0.1MPa pressure ratio within temperature range of 300-200 K. Based on this mixture, the MCC heat exchanger has been optimized to minimize the refrigeration loss under a condition of 10 SCCM so that the gross refrigeration is about 40.9 mW. Details of the optimization of the heat exchanger using this mixture can be found in Section 2.3.

Some other optimized mixed refrigerants for different temperature range were also designed to meet different temperature and refrigeration requirement. For example, the enthalpy differences of refrigerants using 4 or 5 components under 0.4:0.1MPa pressure ratio within temperature range of 300-140K are shown in Figure 2.4.

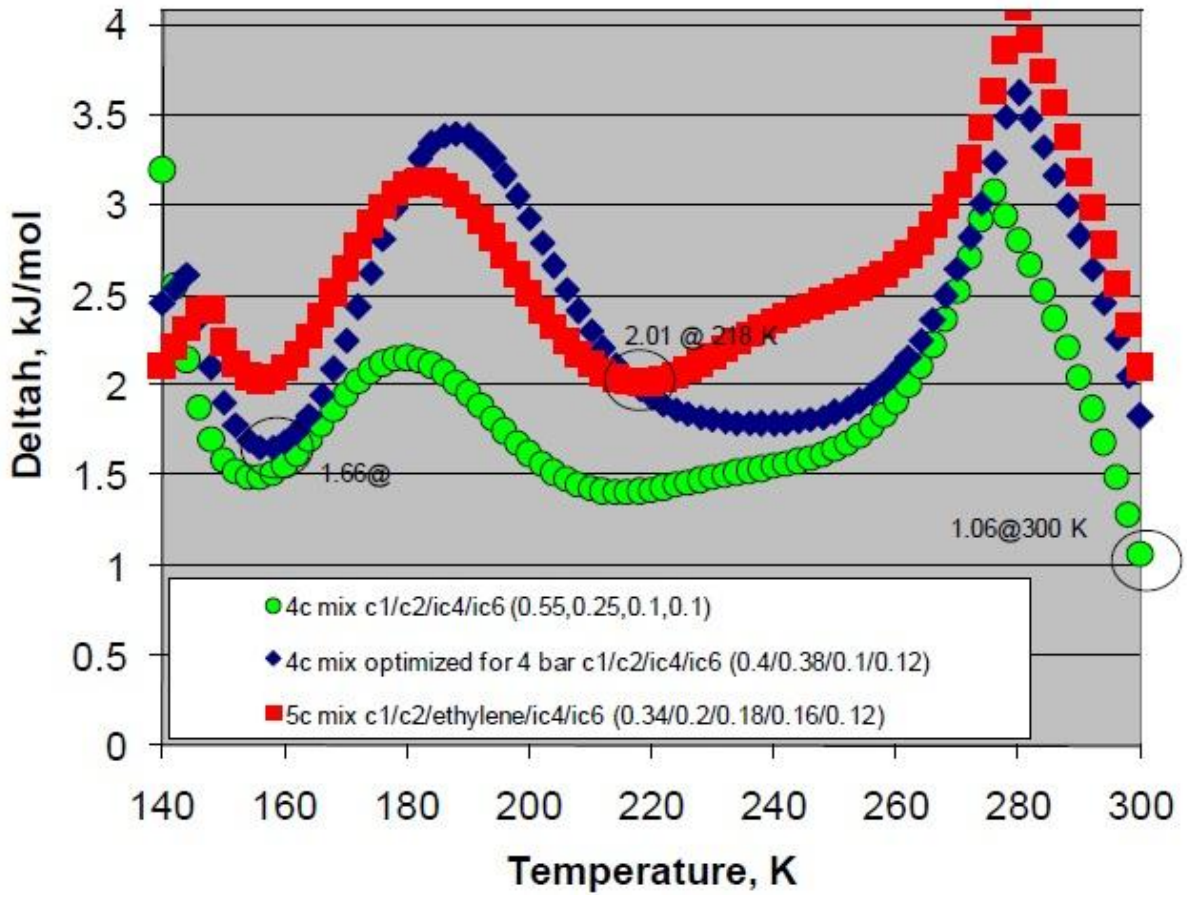

Figure 2.4: Gas mixtures designed for a 300-to-140 K temperature range and 4:1 pressure ratio. Gas mixture of methane/ethane/ethylene/isobutane/isohexane with mole fractions 0.34/0.20/0.18/0.16/0.12 achieved a 2.01 kJ/mol refrigeration capability. (Figure from [6])

2.2.2 Refrigeration losses in the MCC system

For a system requirement, the MCC is designed to have maximal gross refrigeration and minimal refrigeration losses due to the heat exchanger ineffectiveness, pressure drop, and heating from the environment. The ideal cooling refrigeration of a refrigerant in a J-T cryogenic cooler is given by the product of flow-rate with the minimum isothermal enthalpy difference between the high-pressure refrigerant and low-pressure refrigerant [9].

$$\dot{Q}_r = \dot{n}\,(\Delta h|_T)_{min} \tag{2.1}$$

where $\dot{Q}_r$ is the gross refrigeration delivered by the mixed refrigerant pumped by the compressor; $\dot{n}$ is the flow rate in mol/s; $(\Delta h|_T)_{min}$ is the minimum molar isothermal enthalpy difference of the refrigerants between the high pressure and low pressure enthalpies within the temperature range of interest. However, for the realistic situation, there will be refrigeration losses associated with imperfect heat transfer, pressure drop, and environment heating as given in [15],

$$\dot{Q}_{net} = \dot{Q}_r - \dot{Q}_{\Delta P} - \dot{Q}_{HX} - \dot{Q}_{cond} - \dot{Q}_{rad} \tag{2.2}$$

where $\dot{Q}_{net}$ is the net refrigeration (heat lift) of the MCC; $\dot{Q}_{HX}$ is refrigeration loss due to heat exchanger ineffectiveness; $\dot{Q}_{\Delta P}$ is the refrigeration loss resulting from the pressure drop along the heat exchanger; $\dot{Q}_{cond}$ is the conduction heat load through the heat exchanger or DC leads used to power the device; and $\dot{Q}_{rad}$ is the radiation heat load from the environment. Calculations of the each of the components have been elaborated by Radebaugh in [15]. Since the cold stage will

be operated in a vacuum chamber with air pressure less than 10^{-4} torr, conduction heat load through the air is negligible. Figure 2.5 shows all the refrigeration losses of the MCC system.

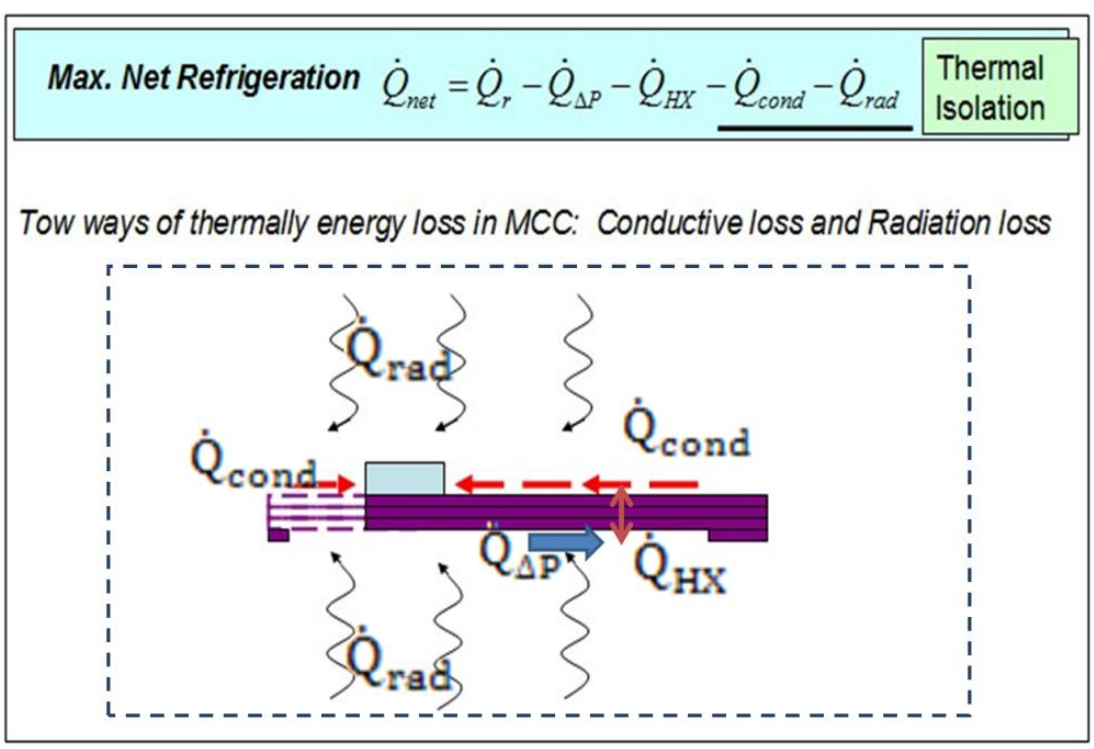

Figure 2.5: Schematics of heat flow in and out in the micro cryogenic cooler.

2.3 Optimization of the Heat Exchanger

The objective in optimizing the heat exchanger geometry is minimizing the volume of the heat exchanger. Heat exchangers are usually the largest components of the J-T cryogenic coolers so the objective is particularly important for the development of micro cryogenic coolers. To optimize the heat exchanger, we chose to consider the fractional losses associated with imperfect heat transfer, pressure drop, and heat loss as functions of heat exchanger geometry. These losses are normalized by the gross refrigeration power $\dot{Q}_r$. The design will be considered reasonable

once the ratio of the refrigeration loss to the total refrigeration power is less than 60% which mean at least 40% of the gross refrigeration power will be successfully used [15].

For an ideal parallel plates counter-flow heat exchanger, the thickness of each wall needs to be minimized both to increase the thermal isolation between the warm end and cold end and to increase the heat transfer between the two lines; however, due to a consideration of the process and mechanical properties, the thickness was chosen to be 20 μm, 10 μm and 20 μm for each layer respectively as shown in Table 2.1. We then started by using a flow-rate of 10 standard cubic centimeters per minute (sccm) of a five components mixed refrigerant under operating pressures of 4 bar and 1 bar for high and low pressure sides. For a fixed width of 2 mm, channel gap of 20 μm, and flow-rate of 10 sccm, the optimization of length was obtained as shown in Figure 2.6. The fixed parameters are determined by manufacturability, cooling power requirements, and size requirements.

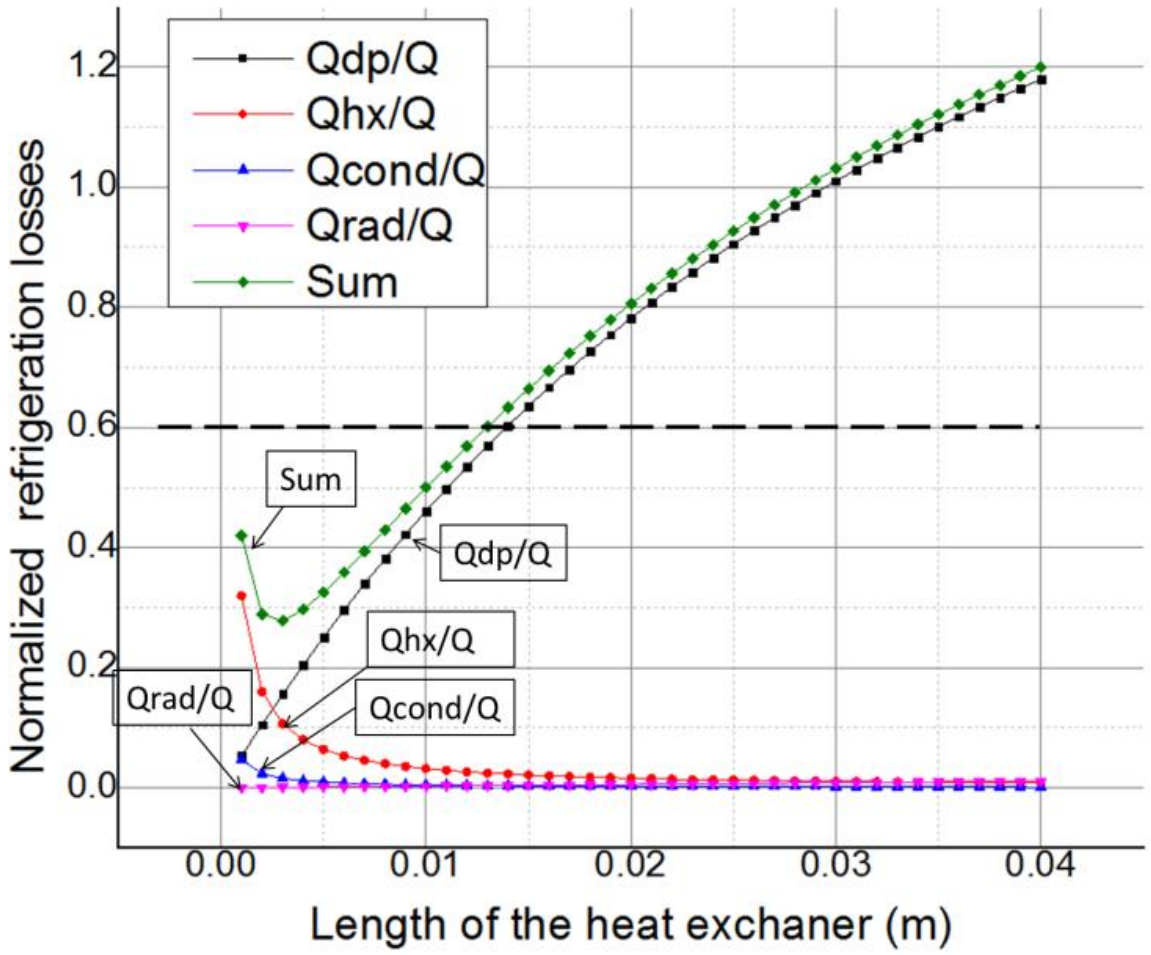

Figure 2.6: The ratio of the refrigeration losses to the total gross refrigeration power. Each refrigeration loss is calculated according to the method presented in [9].

Since the ratio of the refrigeration loss to the total refrigeration power in an optimized design is constant for a constant ratio of the flow rate to heat exchanger width, the gross and net refrigeration powers are proportional to the flow rate as long as the width is changed equally. It means that the gross refrigeration can be increased simply by increasing flow rate which can be gained with scaling up the width. The dimensions we chose to demonstrate the MCC is shown in Table 2.1.

Table 2.1 Key dimensions of the MCC

Symbol	Description	Value
t_{top}	thickness of the top layer	10 μm
t_{bottom}	thickness of the bottom layer	20 μm
t_{center}	thickness of the center layer,	10 μm
D_{post}	diameter of the posts	60 μm
L_c	length of the channels	12 mm
W_c	width of the channels	2 mm
h_c	height of the channels	20 μm
W_{HX}	width of the heat exchanger	3 mm
S_{post}	space between the posts	150 μm

CHAPTER 3: THERMAL AND MECHANICAL ANALYSIS OF THE POLYIMIDE-BASED MCC

3.1 Thermal isolation of the MCC

3.1.1 Requirement of analysis of thermal isolation.

Environmental and parasite heat load is one of the major refrigeration losses of the MCC. Due to the high surface-to-volume ratio and short path for heat conduction from the worm end to the cold end, the heat leak from the environment (radiation and conduction losses) is particularly significant in the micro cryogenic cooler with limited gross refrigeration power as illustrated as in Figure 3.1[10]. High thermal isolation design is essential to manage the heat losses and increase the net refrigeration power for a given gross refrigeration power.

In the previous MCC studies, one solution was to increase the gross refrigeration power to compensate the loss to environment [10]. In Little's work [4][18][19][21], they reached high gross refrigeration powers by using relative high pressure ratio nitrogen (16.5:1 MPa) and flow-rate (107 μmol/s). In Lerou's work [9][20], a low emissivity metal thin film was coated on the heat exchanger to reduce its radiation loss, however, they still needed to use a much higher pressure (8 MPa) and flow-rate in order to compensate the loss. As described in Lin's work [10], even using a high refrigeration mixture as the refrigerant, to achieve the temperature at which they aimed, and to provide required refrigeration power, the MCC has to be well thermally isolated to minimize heat loads from the environment. In a 77 K cold head under a 300 K shielding temperature, the glass capillary based test vehicle, the hollow-core fiber-based MCC with a segmental low emissivity metal coating, and the hollow-core fiber-based MCC without the segmental coating enclosed by an enhanced low emissivity shielding are tested and achieved

a heat leak of 5.1 mW, 9.6 mW, and 3.8 mW, respectively [10]. It seems that the thermal isolation is extremely important for such a small size micro cryogenic cooler with limited gross refrigeration.

In this thesis work, the conduction and radiation losses due to the polyimide heat exchanger were considered in the design optimization in Chapter 2. However, it is good to understand contribution of each part of the MCC to the refrigeration losses for potential adjustments, e.g. by knowing the radiation loss of each part, one can decide whether it is necessary to apply reflective shielding for some part or not. In addition, tethers are used to make a mechanical support of the MCC. Their contribution to refrigeration loss was not considered in the optimization in Chapter 2, and the reason is that tethers' dimension will not affect the design of the functional part of the heat exchanger itself while on the other hand, it's a trade-off design between the thermal losses and mechanical design, it should be more convenient to isolate the design of the tether from the optimization of the heat exchanger. A conduction loss analysis is needed for us to come with a reasonable design including the tethers.

3.1.2 Calculation of the thermal refrigeration losses of the polyimide-based MCC

Conductive refrigeration loss

In the polyimide based MCC, heat is transferred from the environment to the cold end by conduction and radiation (see Figure 3.1).

The conduction can happen both along the heat exchanger (HX) and air from surrounding to the cold end. However, in our system, the cold stage of MCC is in vacuum with 1E-4 Torr (0.01333 Pa) or smaller number, the conduction heat transfer through air can be negligible.

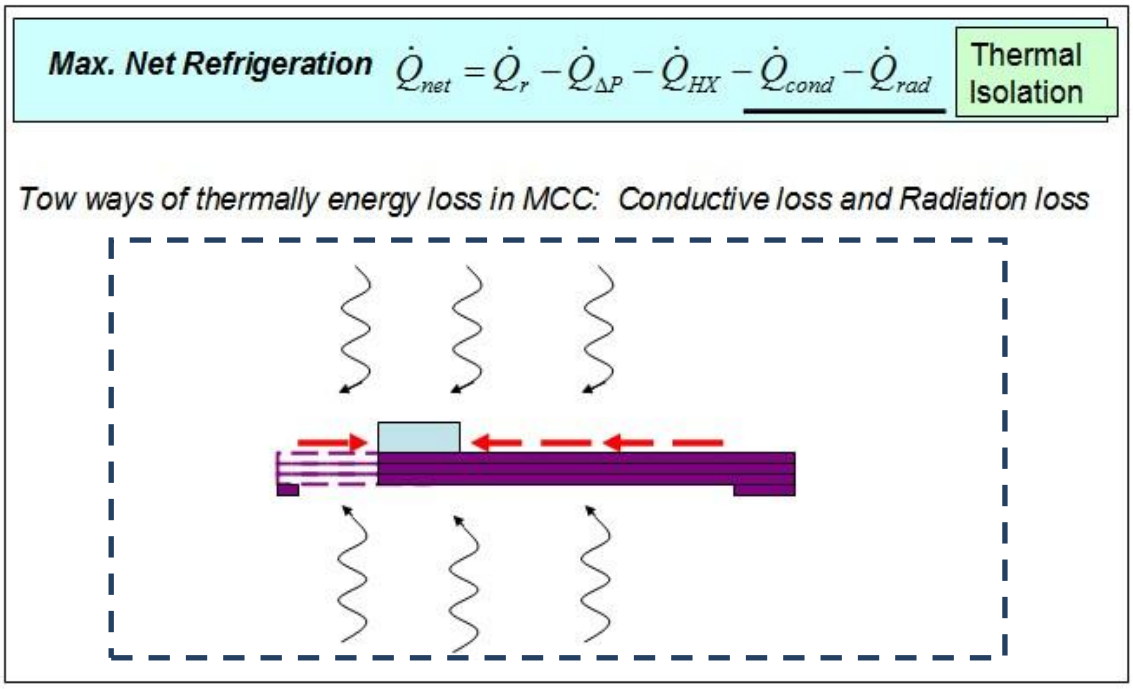

Figure 3.1 Schematic of the heat transfer mechanisms in the MCC system.

Specifically, for two parallel plates in a vacuum environment as the effective air thermal conductivity can be calculated using the following equation [22]:

$$k_{eff} = k_{air} \frac{1}{1 + \frac{(7.6E-5)T}{Pd}} \tag{3.1}$$

where T is the absolute temperature (K); P is pressure (Pa); and d is the air gap (m). The air thermal conductivity (W/m·K) is calculated using the following equation:

$$k_{air} = (1.5207\,E-4)T^3 - (4.8574\,E-8)T^2 + (1.0184\,E-4)T - (3.933\,E-4) \tag{3.2}$$

In the test of our MCC, pressure is kept lower than 1E-4 Torr (0.01333 Pa). As a result, air conduction is negligible. The conduction loss therefore is mainly due to the heat transfer along the solid parts of the HX. This loss can be expressed by Fourier's law of heat conduction as equation (3.3) [23].

$$\dot{Q}_{cond} = -kA\frac{\partial T}{\partial x} \tag{3.3}$$

where $\dot{Q}_{cond}$ is the heat transfer rate, A is the cross sectional area, T is the temperature, x is the length along the temperature gradient and k is the thermal conductivity of the material.

For a rectangular heat exchanger of which the cross-sectional area does not change along the x direction, the temperature along the x direction can be seen as a liner distribution if the radiation energy transfer can be ignored compared to the conduction one. By making such an assumption, the conduction heat transferred from the worm end of the heat to the cold end of the HX is simplified as:

$$\dot{Q}_{cond} = kA(T_{worm}-T_{cold})/\Delta x \tag{3.4}$$

where T_{worm} and T_{cold} are the temperature of the worm end and cold end respectively. The dimensions and material properties of our device are given in Table 3.1 and 3.2, a conduction refrigeration loss due to the HX is shown in Figure 3.2 for an interested cold end temperature range (from 140 K to 250 K).

Table 3.1 Dimensions of the MCC for thermal calculation

Parameters of the MCC for thermal calculation	Dimensions
HX total solid thickness (t)	50 µm
L_1 (indicated as in Figure3.2)	3 mm
L_2 (indicated as in Figure3.2)	8 mm
HX Width (W)	3 mm
Gap (g)	15 µm
Acs (Side area of cold head)	9.36e-6 m^2
Lt (Length of the tethers)	300 µm
Wt(Width of the tethers)	60 µm

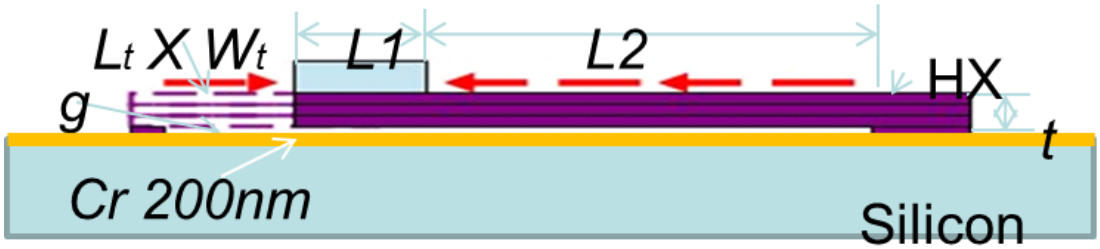

Figure 3.2: Illustration of the parameter of the MCC for thermal calculation.

Table 3.2 material properties of the MCC for thermal calculation

Parameter of material	**Thermal Conductivity** ($W \cdot m^{-1} \cdot K^{-1}$)	**Thermal Emissivity**
Polyimide	0.18 (0.175@200K to 0.186@300K) [24]	0.95
Cr	-	0.05
Au	318	0.025

Thermal conduction loss with varies of the cold head temperature from 140 K to 200 K were calculated as shown in Figure 3.3. As a result, there is a 0.33 mW conduction refrigeration loss due to the HX and 0.18 mW due to one tether of a dimension of 300 µm × 60 µm.

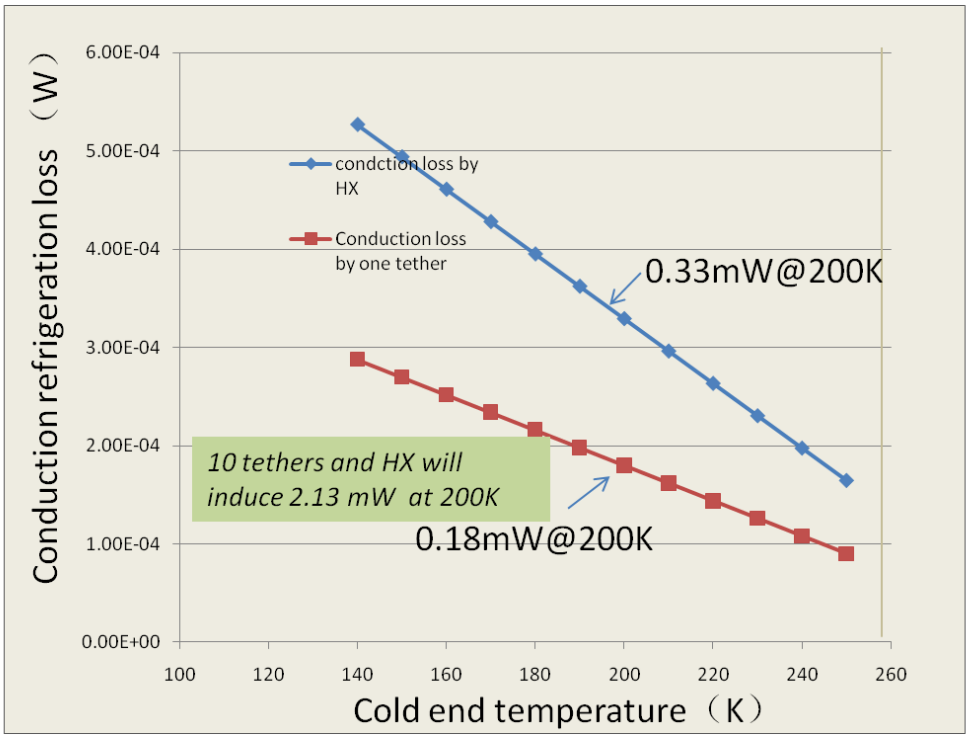

Figure 3.3: Refrigeration losses due to conduction

Radiation refrigeration loss

Heat energy transferred through electromagnetic waves is called thermal radiation. The heat transfer from an ideal thermal radiator, or a black body, can be modeled by the Stefan-Boltzmann law of thermal radiation [23].

$$\dot{Q}_{rad} = \varepsilon\sigma A(T_{obj}{}^4) \tag{3.5}$$

where σ is the Stefan-Boltzmann constant with the value of 5.669E-8 W/m^2·K. A is the surface area of radiator, and T_{obj} is the surface temperature of radiator. Most of the time the object material is not an ideal radiator or blackbody, and a factor called emissivity ε is introduced to correct this. Values of emissivity of the materials we are using are shown in Table 3.2. Considering that a thermal radiator with enclosed by a surface which will also emit EM, a more popular used equation for calculation is:

$$\dot{Q}_{rad} = \varepsilon_{eq}\sigma A_1(T_2^4 - T_1^4) \qquad \text{for} \qquad T_2 \geq T_1 \tag{3.6}$$

where T_1 is the temperature of the radiator and T_2 is the temperature of the environment material, ε_{eq} is the equivalent emissivity which is determined by emissivity of the radiator (ε_1) and environment material (ε_2) and there geometries.

For $A_2 >> A_1$, $\varepsilon_{eq} \doteq \varepsilon_1$

For a infinite parallel plates structure $\varepsilon_{eq} = 1/ (1/\varepsilon_1+1/\varepsilon_2-1)$

In the HX fabricated for this thesis study, the bottom of the HX was very close to a Cr coated silicon substrate therefore being considered with a good shield condition. The upper side of the HX was not coated with low emissivity material. However, further shielding of the upper side of

the HX can be achieved by sputtering metal layer, for example gold layer with 100 nm thickness, to dramatically decrease the emissivity of the surface (see Figure 3.4).

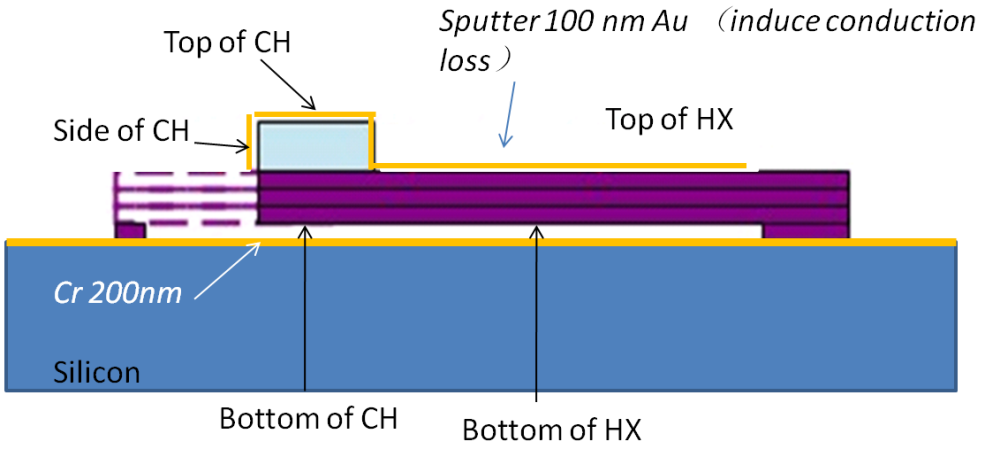

Figure 3.4: Shielding method of the planar MCC.

Radiation refrigeration loss of each part of the cold-stage was then calculated according to a cold head temperature range from 140K to 250K (see Figure 3.5). The result indicates that, with a thin layer of metal (Au 100 nm in thickness) coating to cover the top surface of the HX, the total radiation loss can be reduced dramatically with only adding much smaller extra conduction loss. For example, the MCC's radiation loss can be reduced from 12 mW to 0.73 mW with only inducing 1.16 mW of conduction loss for a 200K cold end temperature condition. For such a reason, we can benefit a lot from the shielding process by reducing the radiation loss exponentially.

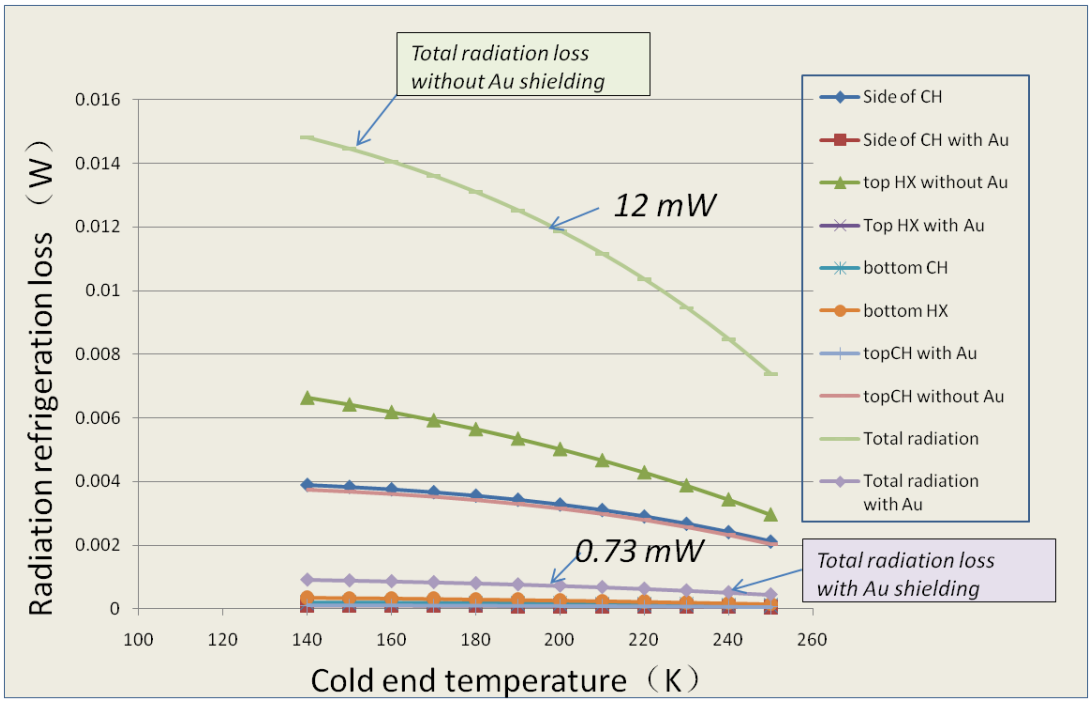

Figure 3.5: Radiation refrigeration energy loss of the MCC.

3.2 Mechanical analysis of MCC

3.2.1 Deformation of polyimide HX under pressures

For a functional mechanical design of the MCC, firstly, numbers and size of the posts inside the channels need to be optimized to minimize the pressure loss along the channels while still keeping the channels stiff enough under pressures. To make the posts more efficient on supporting the center layer which was the thinnest layer (10 μm) of the heat exchanger, the posts were staggered (see Figure 3.6).

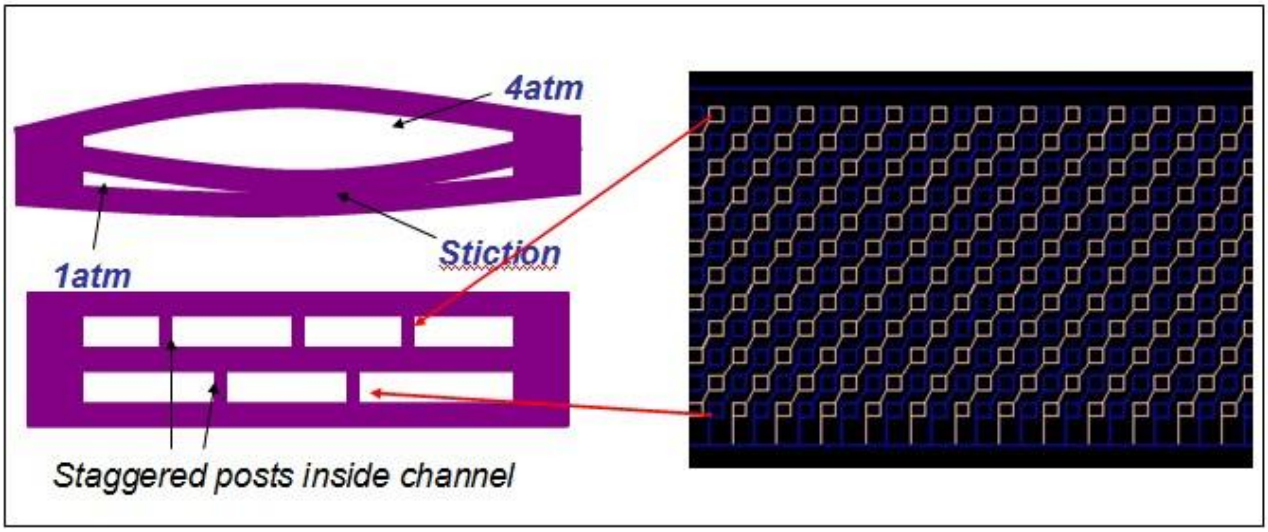

Figure 3.6: Left: schematic of staggered posts; right: posts lay out in the channels.

A series FEA study results by using Coventorware showed that by using 80 µm × 80 µm staggered posts array with 150 µm distance of rows and columns can gave us a stiff enough supporting under a 4:1 bar pressure ratio under a vacuum environment with maximum channel gap variation of only 2 µm. Figure 3.7 shows the deformation of each layers deformation under an internal pressures condition of 4:1 bar for high and lower pressure channels. By comparing the deformation of each layer, we were able to tell the channel size deformation.

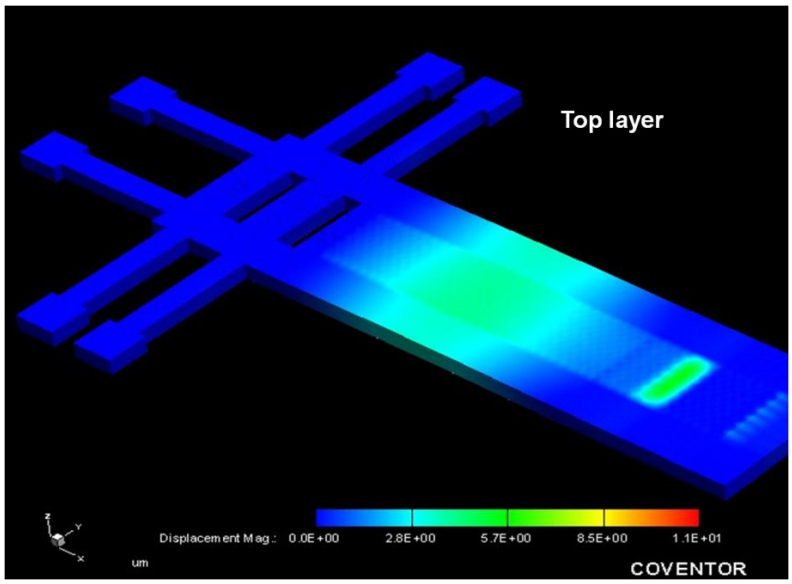

(a) Deformation of the top layer with 20 µm thickness.

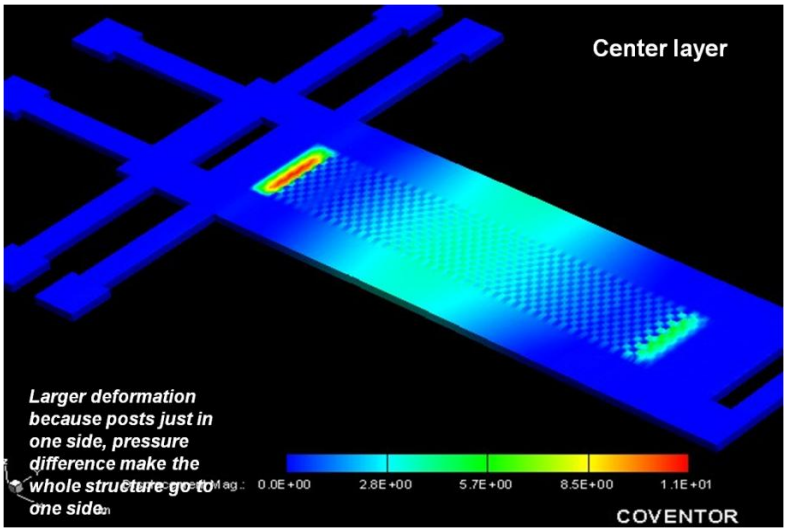

(b) Deformation of the center layer with 10 µm thickness.

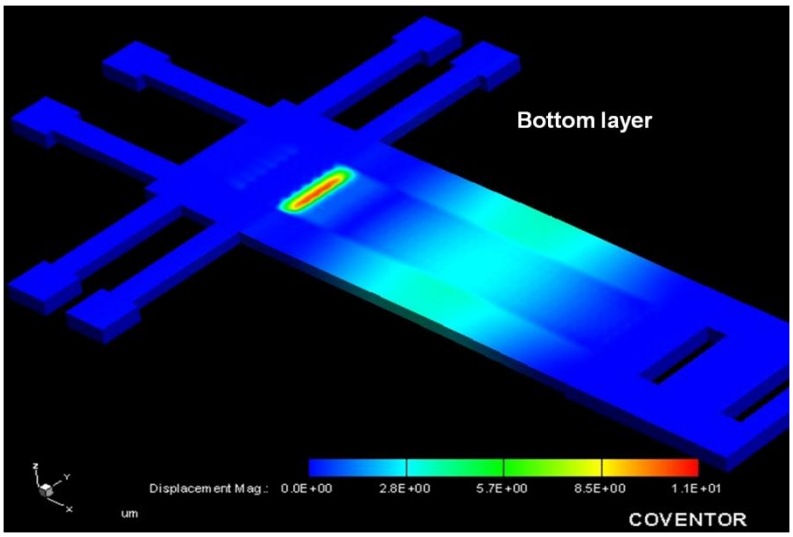

(c) Deformation of the bottom layer with 20 µm thickness.

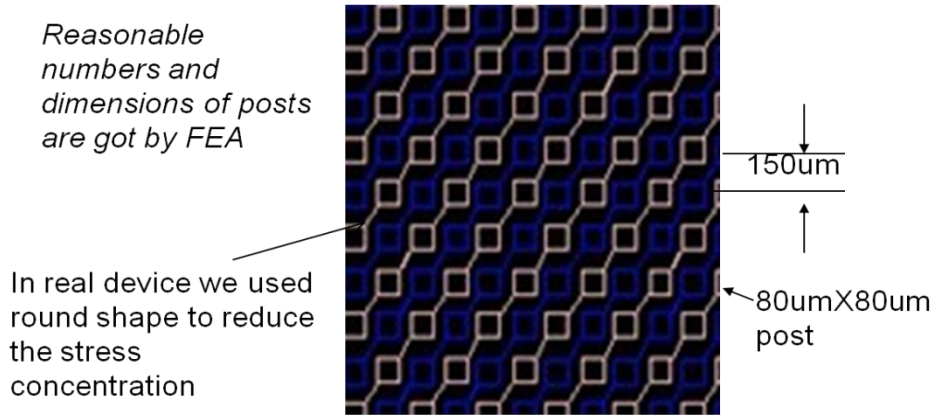

(d) Schematic of the posts strategies for both channels

Figure 3.7: Deformation of each layer under pressure difference of 4 bar and 1 bar.

3.2.2 Mechanical analysis of the tethers

Stiffness design of the tethers

For the polymer-based MCC, because of the complaint property of polyimide material used, tethers design became very important to prevent the suspended device structure from large vibration excessive displacement under shock or gravity of the device to be cooled. In our case,

as a simplification, when the deformation of the cold end is small, tethers can be considered as cantilever beams with ends load (see Figure 3.8). In such a case, the deformation of the free end of a tether can be calculated by [25]

$$y = \frac{-FL^3}{3EI} \tag{3.7}$$

where F is the force applied on the end, L is the length of the tether, E is the young's modulus of the material and I is the moment of inertia of the beam, which is given in [25] by

$$I = \frac{bh^3}{12} \tag{3.8}$$

in which b is the width and h is the height of the tether. We can combine equation (3.7) and (3.8) to obtain

$$F = -y\frac{Ebh^3}{6L^3} \tag{3.9}$$

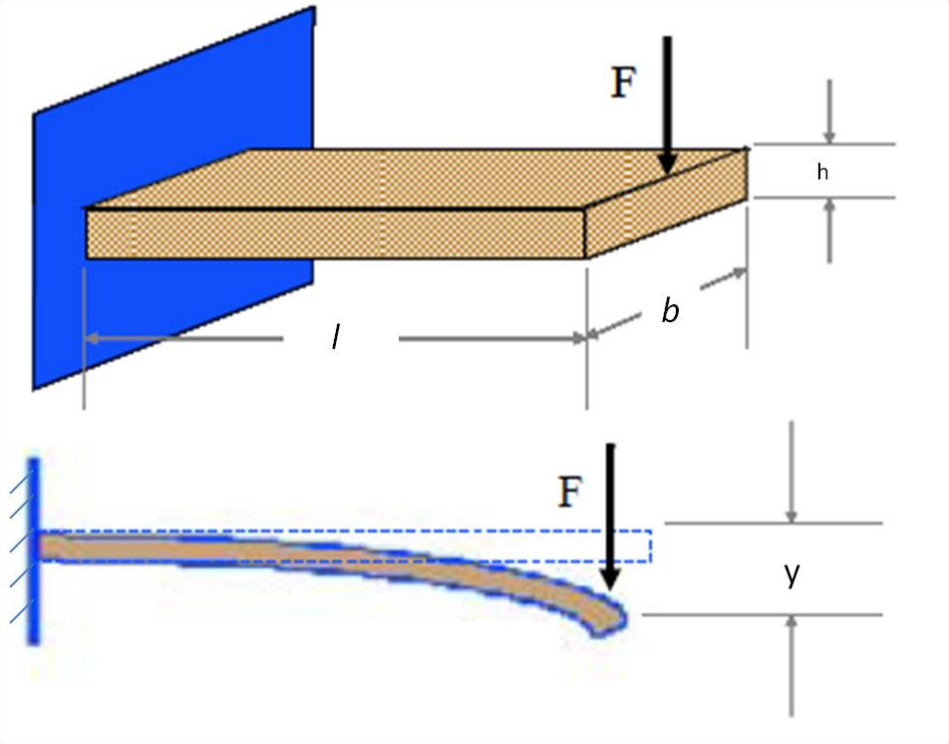

Figure 3.8: Schematic of the cantilever with end load.

In such a relationship, when the h is fixed by considering the design and optimization of the heat exchanger, the effective spring constant is proportional to the width of the tether b and inversely proportional to the L3. From equation 3.4, we can see that if the ratio of b to l is kept as a constant, the heat leak along the tether will be the same. For such a reason, to obtain a larger stiffness design with same refrigeration loss, smaller tethers are preferred. Numerical study can be used to get the more accurate deformations under different loads. For example, in Figure 3.9, it shows the deformations of the heat exchangers with different tether dimensions, under a loading of 80 mg which was estimated to be a typical weight from the cold head and a chip to be cooled. The material properties used in the simulation of PI-2574 is shown in Table 3.3. The results also suggest using smaller tethers to achieve better stiffness with same conduction loss.

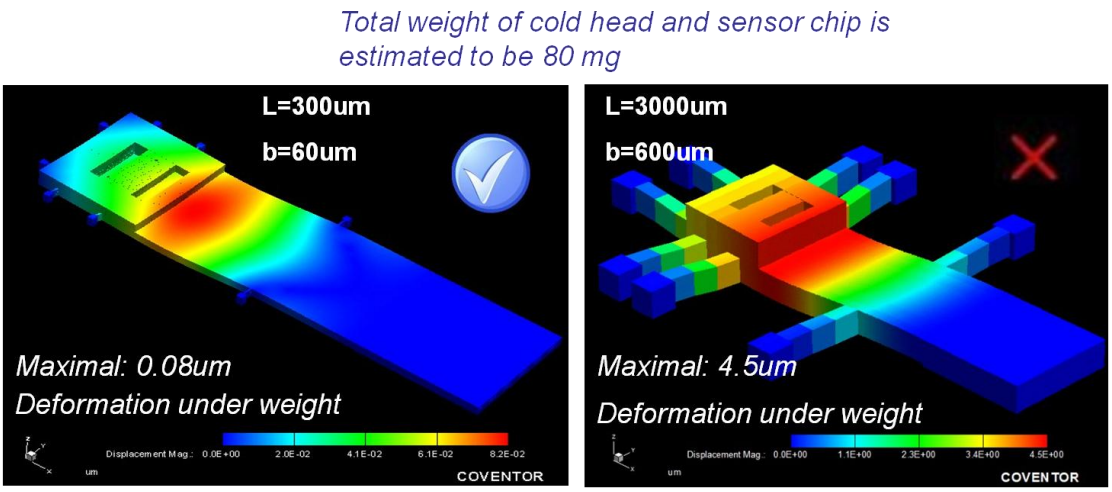

Figure 3.9 Deformation of the heat exchangers with different tether dimensions, under a loading of 80 mg.

Failure analysis of the tethers

When the tether becomes too small, failure of the tethers could happen due to potential stress in them. As can be seen in Chapter 4, some of the tethers of the heat exchanger made of PI-2574 are broken after releasing. The reason is because of the CTE mismatch between the Si substrate and the polyimide used. After the releasing, without filling of the copper, the suspended structure tuned to be stretched and then a tensile tress concentration was applied on the thinnest part of the suspended structure.

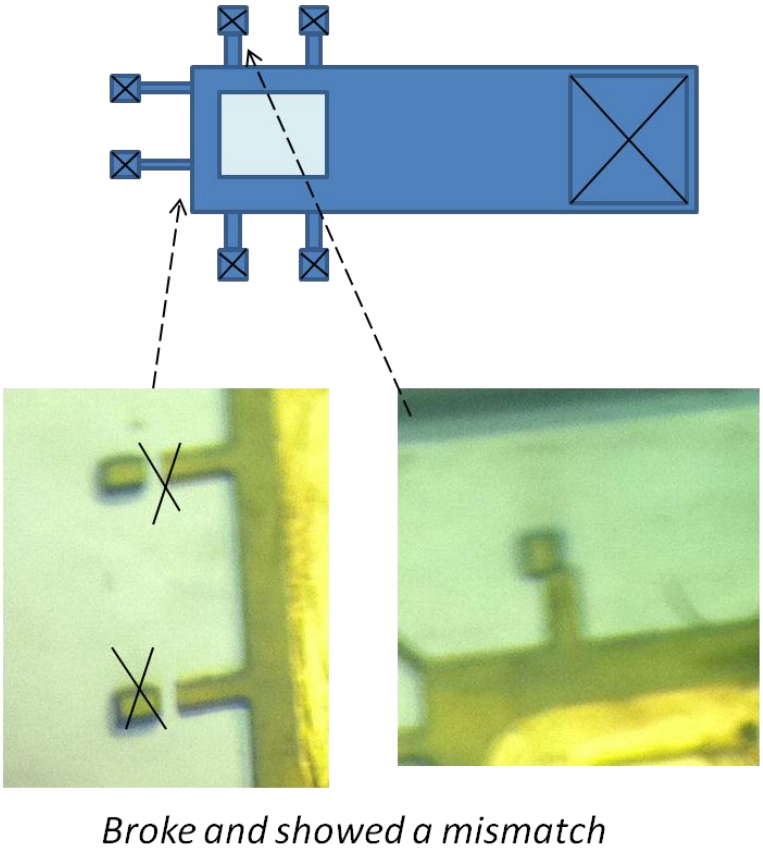

Figure 3.10 Photos of the broken tethers after metal etching

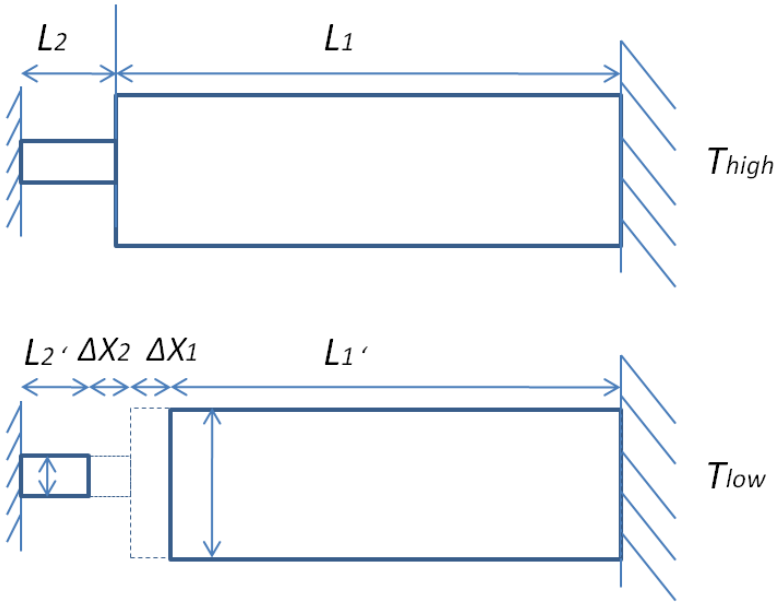

Figure 3.11 Schematic of a simplified case with only one tether supported.

Figure 3.11 shows a very simple situation. In such a situation, the HX is only supported by one tether, after the structure cooled down from the curing temperature of the polyimide T_{high} to the room temperature T_{low}, the Polyimide will shrink much more than the Si substrate do therefore generating a mismatch to the silicon substrate. The total linear mismatch is given by:

$$\Delta x_1 + \Delta x_2 = (L_1 + L_2)(\alpha_{PI} - \alpha_{Si})\Delta T \tag{3.10}$$

where L_1, L_2 are the original length of HX and the tether; α_{PI} and α_{Si} are the liner CTE of the polyimide and silicon respectively; Δx_1 and Δx_2 are the elongation of the HX and the tether if the joint is not broken. Without failure or breaking happens, the force along the tether and the HX will be same, which gives the following equation:

$$F = E\varepsilon A = E\frac{\Delta x_1}{L_1'}A_1 = E\frac{\Delta x_2}{L_2'}A_2 \tag{3.11}$$

where L_1' and L_2' are the length of the HX and tether in the low temperature status and are given by

$$L_1' = L_1(1 - \alpha_{PI}\Delta T) \quad (3.12)$$

$$L_2' = L_2(1 - \alpha_{PI}\Delta T) \quad (3.13)$$

By using a tether size of 300 µm × 60 µm and HX size of10 mm × 3 mm respectively, with the PI-2574 material of which properties are given in Table 3.3, the stress on the tether ε_2 was calculated to be 434MPa which is too large for a material with ultimate strength of 130MPa. By using another material PI-2611 which has very low CTE (5 ppm/˚C) which is close to the CTE of Si for calculation, the maximum stress on the tether ε_2 is 33.9MPa. So the PI-2611 was preferred to be used to get larger design room.

Table 3.3 Material properties two different types of polyimide for failure calculation

	Si	***PI-2574***	***PI-2611***
CTE (**α**)	2.6ppm/C	40ppm/C	5ppm/C
Young's modulus		2.45GPa	8.5GPa
Ultimate Strength		130MPa	350MPa
Yield strength		About 80%*UTS	About 60%*UTS

More accurate analysis of this failure can be done by conducting numerical stress analysis and choosing a proper failure criterion**.** In general, solid materials are divided into brittle and ductile materials. The main difference between brittle and ductile fracture can be attributed to the amount of plastic deformation that the material undergoes before fracture occurs. Different

failure criteria have been developed to predict there fractures. Material with elongation value larger than 0.05 is considered as ductile material. Polyimide is pretty flexible at even very low temperature (4.2K) and we consider it to be ductile material even working under cryogenic condition [26]. For example, von Mises criterion can be used because it's convenient to get von Mises by using commercial FEA tools such as Coventorware. This theory proposes that the total strain energy can be separated into two components: the volumetric (hydrostatic) strain energy and the shape (distortion or shear) strain energy. It is proposed that yield occurs when the distortion component exceeds that at the yield point for a simple tensile test. This is generally referred to as the von Mises yield criterion and is expressed as:

$$\frac{1}{2}\left[(\sigma_1-\sigma_2)^2+(\sigma_2-\sigma_3)^2+(\sigma_3-\sigma_1)^2\right] \leq \ \sigma_y^2. \tag{3.14}$$

CHAPTER 4: FABRICATION AND ASSEMBLY OF THE POLYIMIDE-BASED MICRO CRYOGENIC COOLERS

4.1 Fabrication of polyimide heat exchanger

Properties of polyimide have been well studied at cryogenic temperature, and polyimide was proven to be a good candidate polymer for cryogenic applications. It has high stability even at cryogenic temperatures, e.g., with decreasing temperature from room temperature to 4.2 K, the failure strain of a typical polyimide continuously decrease by only 25%, and the fracture toughness increase continuously by 10% [27]. In addition, it has also been widely used in microelectronics due to their excellent planarizing and step coverage abilities [29] [31]. For a micro surface machining technology, electroplated copper has been used as a sacrificial layer to make suspended polyimide structures [31], [32]. In this project, we make the heat exchanger by using multiple suspended polyimide layers based on this technology and combine it with silicon bulk etching technology.

Figure 4.1 shows the cross-sectional view of the schematic of the HX (upper) and a picture of the HX (lower) while Figure 4.2 illustrates the major batch fabrication steps for the polyimide HX. The fabrication of the HX is based on the surface micro-machining technology using electroplated copper as the sacrificial layers and polyimide as the structural material. The process consists of multi-layers of metallization of copper, spin coating and curing of polyimide, and the patterning on each layer. As shown in Figure 4.2, after alternatively coated polyimide layers and electroplated copper layers, we performed reactive ion etchings (RIE) or deep reactive ion etching (DRIE) both from front side and back side of the wafer to make the openings on the ends of the channels and to expose the sacrificial layers (Cu). The metal layers were then etched

away to form the channels and a suspended polyimide structure. In this process, a particular releasing method has been designed to make the very long channel structure with micron gap releasable. A key aspect to accomplishing this is the design of lateral etching structures laid on top of the sealing edge of the channels (see Figure 4.1). In such a design, the etchant can keep diffusing inside from the sides of the channels instead of just going through holes on the two ends. To make the sealing of all the releasing holes, A special epoxy Stycast 2850 FT (Trade names are given here to clearly identify materials with unique characteristics used in the process, but it does not imply any endorsement or that they are necessarily the best materials for this application) which is well known for being good in cryogenic application, was used to fill them in after the device was released (see Figure 4.1). This method is also suitable for wafer-level manufacture requirements when using a silk-screen method by utilizing a shutter mask to just expose the releasing holes.

Due to the thermal mismatch between the polyimide layers and silicon substrate, all the tethers in this design were broken after the metal releasing. As shown in Figure 4.1, the heat exchanger warped and the cold-end is further distanced from the substrate. This heat exchanger still functions well, although it exhibits worse mechanical properties than designed. This thermal mismatch problem can be solved by designing the tethers to be of flexture structures (see Figure 4.1c) or replacing the PI-2574 with another type of polyimide which has a similar coefficient of thermal expansion to silicon. More details about using the new type of polyimide are to be introduced in Chapter 5. The process to make the polymer CFHX has an extensive application to make a variety of polymer based micro-fluid system or other polymer chamber structures.

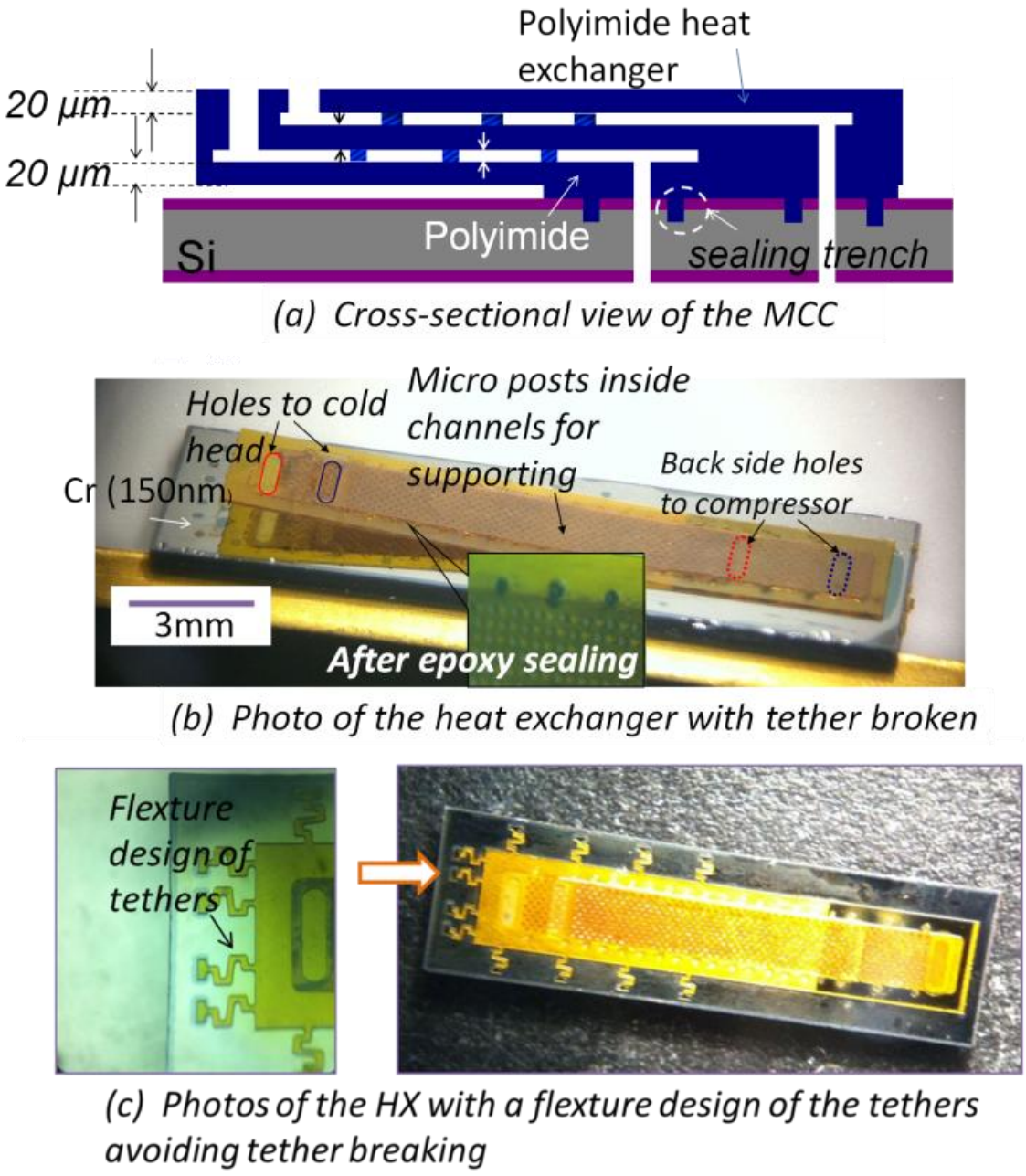

Figure 4.1: Cross-sectional view of the schematic of the heat exchanger (a), photo of the heat exchanger with tethers being broken due to the CTE mismatch (b) and photos of the heat exchanger with a flexture design to avoid the tether breaking.

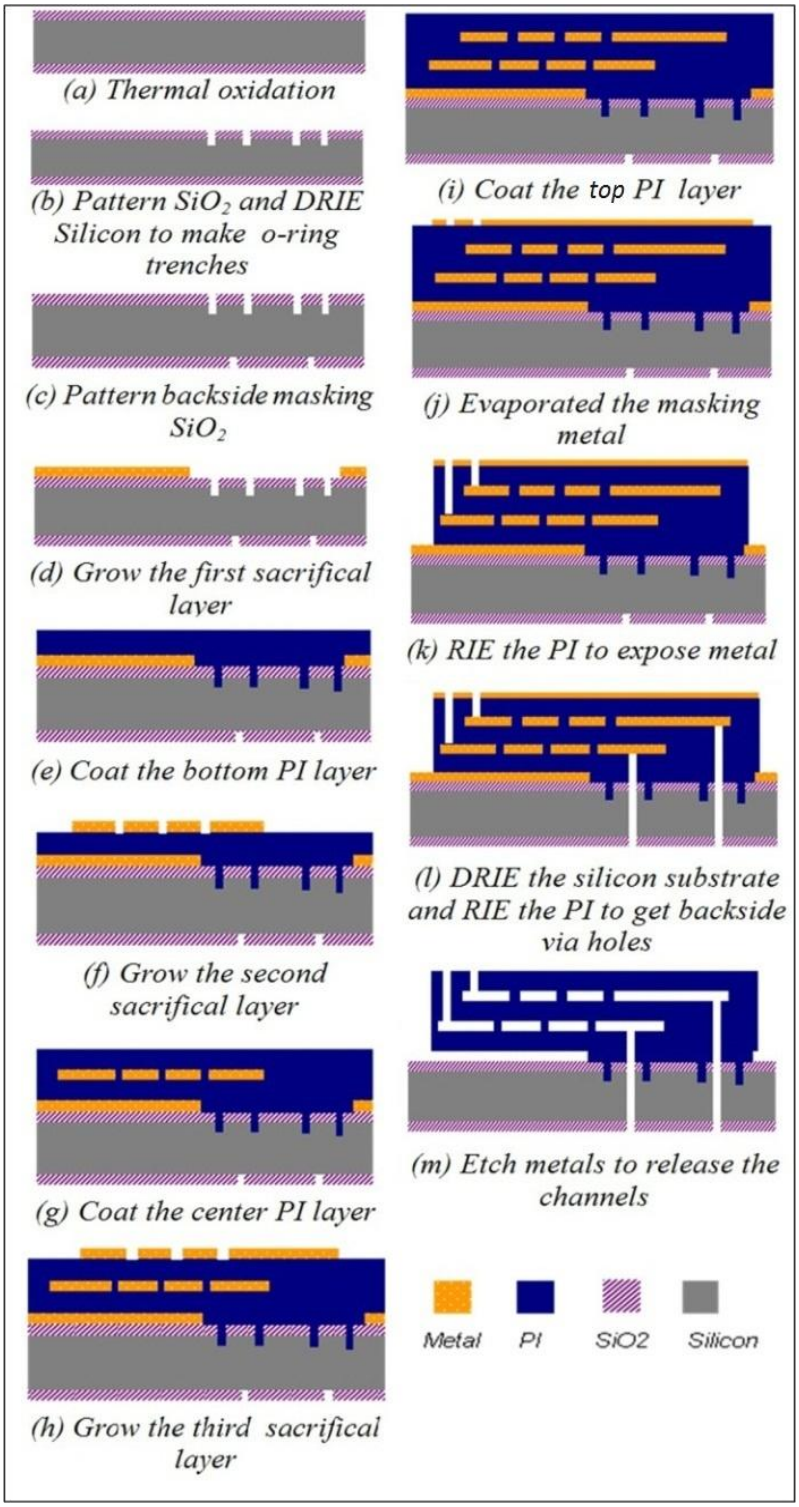

Figure 4.2: Fabrication process flow of the polyimide HX; all the conformal topography by PI coatings were drawn to be a planarized covering to make the fabrication process flow figures easier to read with more clarity.

The HX was fabricated using a 7 mask (see Figure 4.3) fabrication process on a 3 inches (76 mm) n-type <100> silicon wafer of 550 µm thickness. By carefully laying out, 25 units of HXs were fabricated at a 3 inch wafer (see Figure 4.4). The detailed steps and their explanations are as follows:

(a) A masking oxide approximately 1.8 µm thick was grown on both sides with wet thermal oxidation.

(b) O-ring shapes were patterned on the SiO_2 layer using reactive ion etching (RIE), followed by 5 µm deep reactive ion etching (DRIE) on silicon with silicon oxide as a mask. The trenches are to enhance the bonding and sealing between the interface of the polyimide layer and silicon substrate.

(c) Backside SiO_2 was patterned using RIE. This pattern is a masking preparation for later DRIE etching on the silicon to make entrance and exit holes.

(d) An adhesion layer of chromium 100 nm in thickness followed by an electroplating seed layer of copper 500 nm in thickness were evaporated onto the wafer using a thermal evaporator. Additional copper of 15 µm was then deposited using electroplating with a current density of approximate 5 mA/cm^2. The metals are then patterned using wet etching to complete the first sacrificial layer.

(e) Polyimide (DuPont PI-2574*) was then deposited onto the wafer in two spin coats of 2400 rpm for 30 seconds followed by a soft bake after each at 100 °C for 120 seconds. After all the spin coats, the polyimide was cured at 260 °C for 1 hour in nitrogen, arriving at an after- cure thickness of about 20 µm.

(f) Similar to (d) but using an adhesion layer of 30 nm thick titanium, instead of using chromium, followed by a 500 nm thick copper electroplating seed layer were deposited using a thermal

evaporator. Additional copper of 20 µm was then electroplated followed by patterning to the geometry as one of the later embedded micro channels in the HX. The patterning of copper and titanium were done by using wet etching and RIE in a plasma of CF_4:O_2 ratio at 4:16 respectively.

(g) A second polyimide (DuPont PI-2574*) layer was spin coated at 2400 rpm for 30 seconds followed by a soft bake at 100 °C for 120 seconds. Again, it was cured at 260 °C for 1 hour in nitrogen, yielding a thickness of about 10 µm.

(h) Same as (f), another 20 µm thick layer of copper plating and wet etching were done to form the geometry of the other embedded micro channel in the HX.

(i) The exact same process as described in (e) was done again to form another polyimide layer 20 µm in thickness.

(j) A hard metal mask of 30 nm of titanium (as the adhesion layer) and 2 µm of copper was evaporated on the polyimide layer from (i). It was then patterned to the geometry of the HX with alignment entrance and exit holes on the end and releasing holes along the sealing edge of the HX.

(k) The exposed polyimide was etched in a CF_4 and O_2 (CF_4:O_2= 6:10 sccm) plasma all the way down to the copper metal to expose all the three sacrificial layers, including the first sacrificial layer which is to suspend the whole HX structure and other two sacrificial layers which form the channels.

(l) By using the pre-defined SiO_2 mask in (c), backside entrance and exit holes were etched from the backside of the substrate using DRIE. Further RIE in a CF_4 and O_2 (CF_4:O_2= 6:10 sccm) plasma was then done to etch the polyimide making the entrance and exit holes go all the way to their channels filled with metal.

(m) The sacrificial layers of copper were etched away at the end in a standard copper etchant (Transene CE-100*) at 60°C to form the embedded micro channels in the HX and free the whole HX structure. The etch time to fully release the structure was approximately 48 hours.

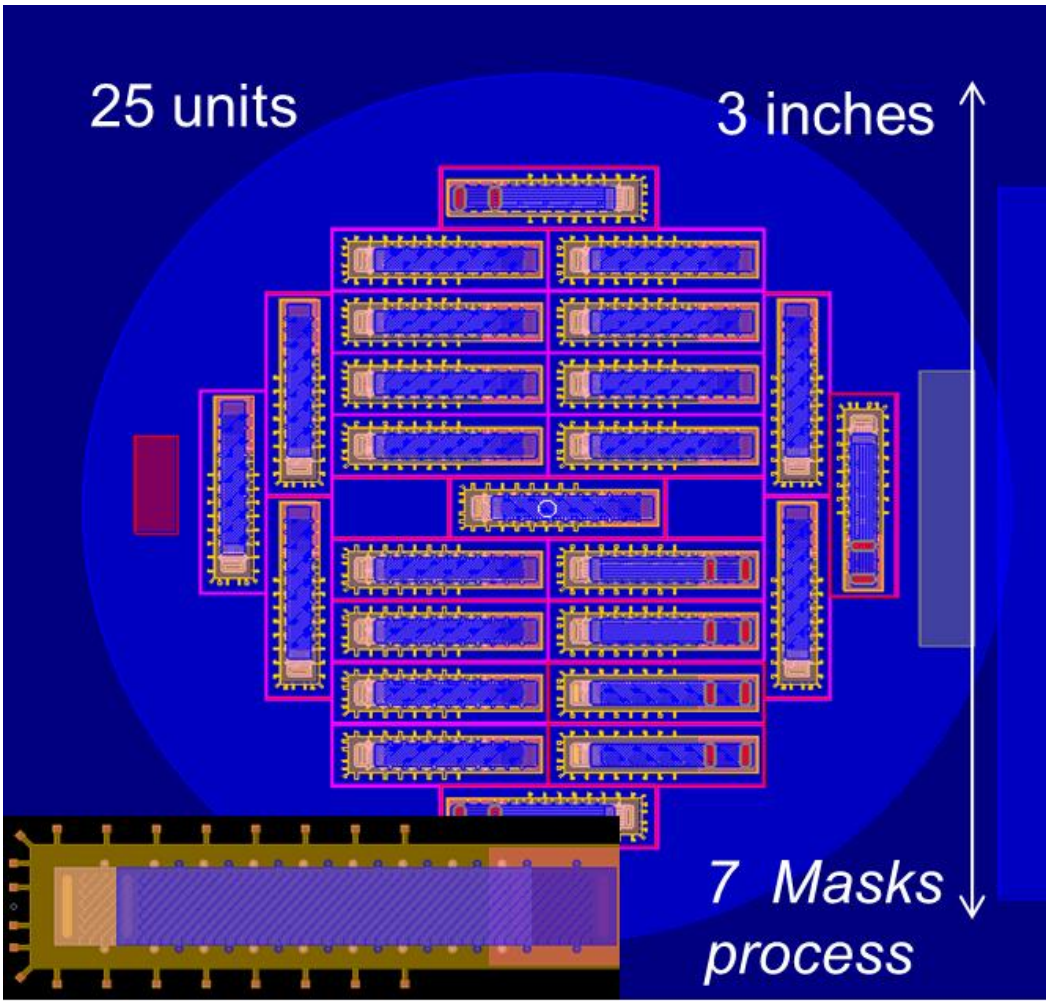

Figure 4.3: Layout of the heat exchanger on a 3 inches wafer. By carefully laying out, 25 units can be fabricated on one wafer.

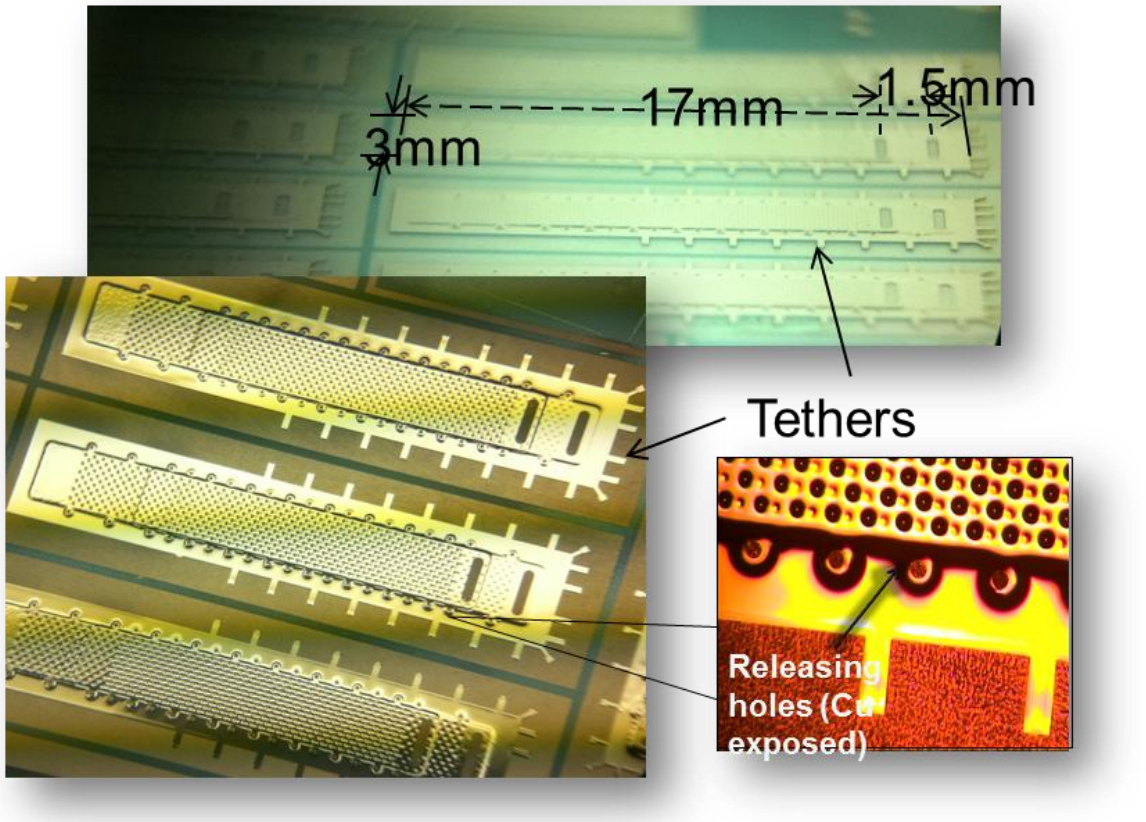

Figure 4.4: Picture of the fabricated polyimide based HX before released.

During the development of the fabrication, several challenges and interesting problems have been identified and solved including:

(1) Interesting electrochemical reaction phenomena when develop the selective etching method when there are different metals (Copper as sacrifical layer; Ti as adhesive layer; Cr as a shielding layer on Si). The details of the further discussion of problems and solution can be found in Appendix B.

(2) We always need to deal with a surface with large (>20um) vertical topology. This has always been inducing problem for MEMS fabrication. Details in order to solve this problem won't be addressed in this thesis. However, generally consideration was to use relative thick photo resist

and design with tolerance to solve problems such as step coverage, over etching and non-uniform etching rate on different area of the wafer.

(3) Releasing problem in order to release copper in long channel with a micro gap. We have figured out the strategy to etching the copper from the sides of the channel (see Figure 4.5). To fully release the metals which were defining the channels, the etchant would just go from the coupling holes on the two ends if there are no other available openings. For such long channels structures with only 10 or 20 μm gaps, exchanging of the etchant between inside and environmental was extremely difficult. Mass transferring of the etchant in the solvent can mainly based on diffusion mechanism which is a pretty low process. As a result, the etching took about one week to just etch about 3 mm into the channel in length and almost stopped there. For such a reason, lateral etching holes laid on top of the sealing edge of the channels were designed to accomplishing the releasing in a reasonable time, e.g. 2 days. In such a design, the etchant can keep diffusing inside from the sides of the channels instead of just going through holes on the two ends. To make the sealing of all the releasing holes, a special epoxy Stycast 2850 FT (see Figure 4.1) which is well known for being good in cryogenic application, was used to fill them in after the device was released. As seen in Figure 4.5, the releasing holes were designed with throttling features which can selectively allow the etchant and epoxy to get into the channels. Due to the large surface tension and viscosity, the epoxy was stuck in the throttle avoiding further flow into to the channels to block them.

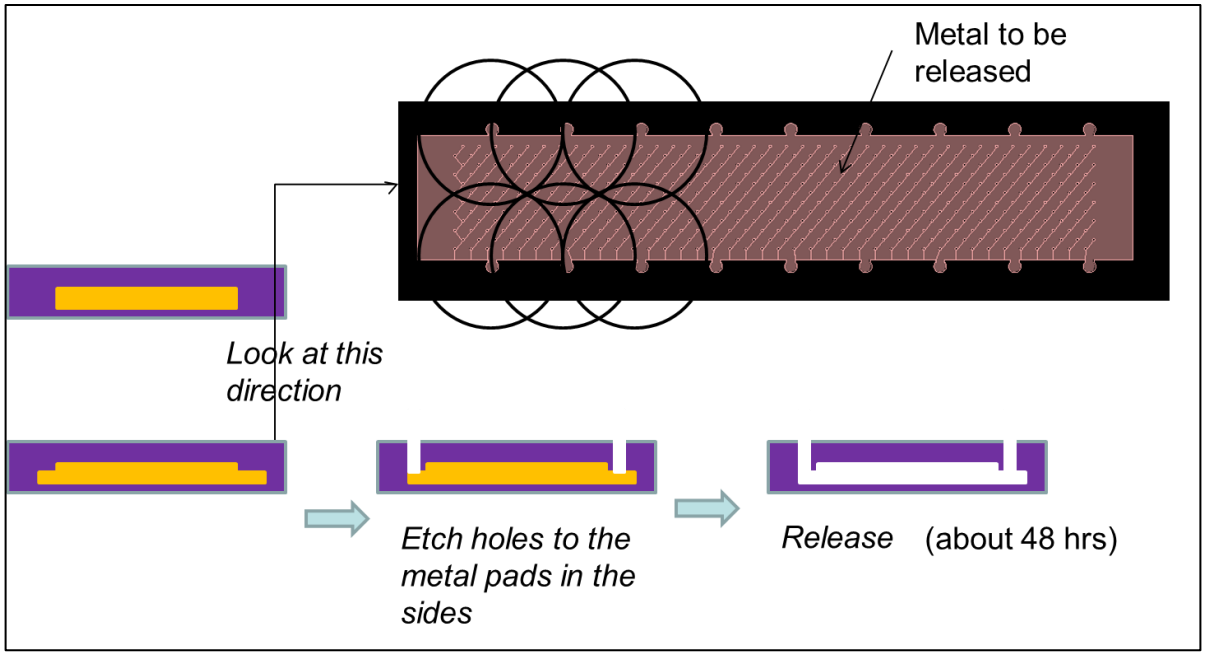

Figure 4.5: Illustration of the strategy of releasing from the sides of the channel.

4.2 Fabrication of Si/Glass cold head

The J-T valve has a footprint of 2.5 mm × 2.7 mm and is made up of a silicon/glass bonded stack which contains a micro gap (3 μm in height) to provide the gas restriction (see Figure 4.7). Features of the J-T valve include a "Lego" (or "plug-in slot") structure by multi-layer etching on silicon using deep reactive etching (DRIE) for better alignment and for avoidance of a solder bridging problem during the reflow process. The processes are illustrated in Figure 4.6.

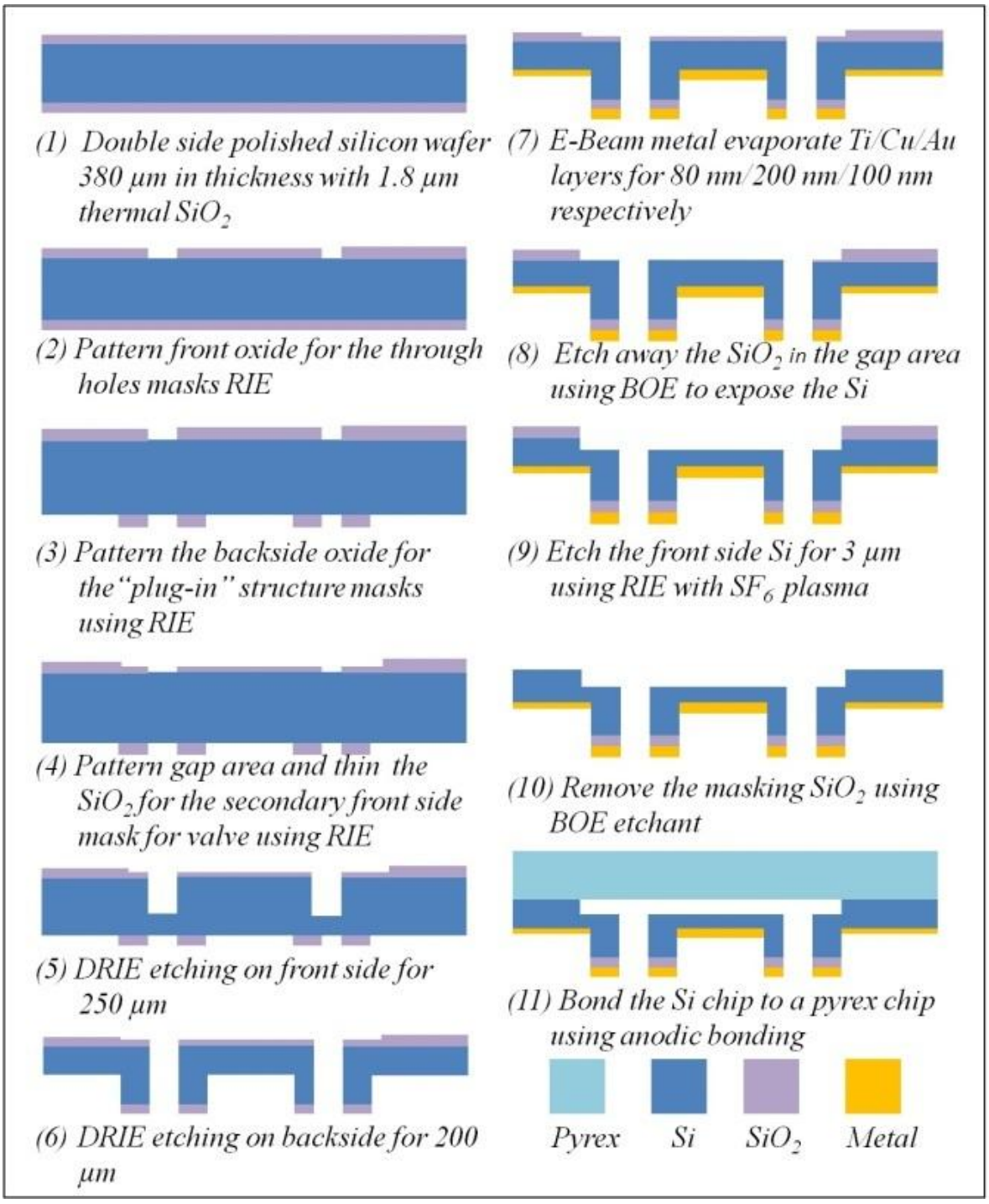

Figure 4.6: Fabrication process flow of the J-T valve chip.

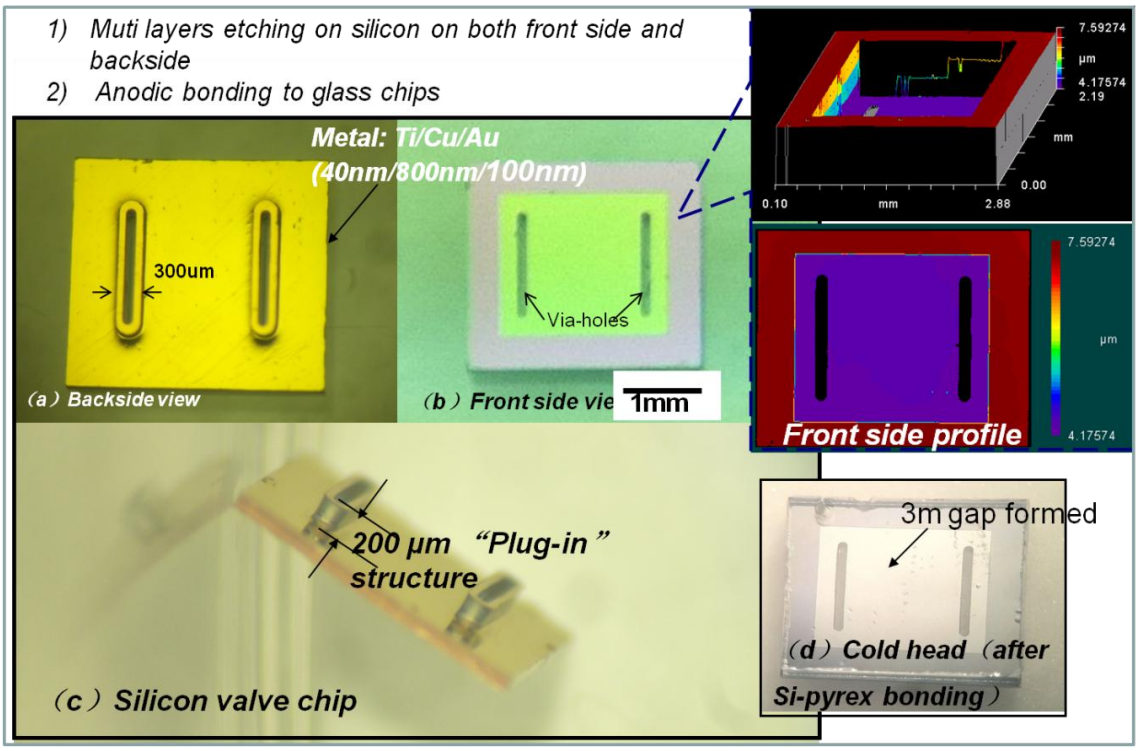

Figure 4.7: Backside (upper left), front side (upper right) and a perspective view (lower) of the silicon valve chip; the depth of cavity for the later gap were characterized using 3D optical surface profilers.

For silicon micro-machining, the number of structure layers is limited by the number of masks [7]. To fabricate the Si valve chip with a 3-layer structure, multiple SiO_2 mask patterns were pre-generated through controlling the etching time. First, SiO_2 was patterned to form the primary mask pattern, which was further patterned and etched, forming a thickness difference. During processing, etching proceeds with the primary mask first, and the thinner SiO_2 was selectively etched away by controlling etching time and etchant. The remaining SiO_2 served as a secondary mask for latter Si etching. After the etching, E-beam evaporation was used to deposit Ti as an adhesive layer, followed by Cu for soldering, and Au for oxidation protection. This metallization was to make a metal layer which is solderable for the following assembly. Finally, the Pyrex glass chip and the silicon valve chip were aligned and sandwiched by electrodes with cathode on silicon and anode on glass. The chips stack was then pre-heated at 400 °C for 10

minutes to stabilize ions in Pyrex glass and hence avoid arcing when voltage is applied. A 550 V voltage was applied across the chips for about 20 minutes to complete the boding. Figure 4.7 shows the pictures of the manufactured Si chip and J-T valve.

For the detailed steps and their explanations according to Figure 4.6, they are as explained as following:

(1) Thermal oxide the wafer with 1.8um masking SiO_2 .

(2) Using 10um photoresist AZ- 4620 as a mask, patterned the front side SiO2 with RIE of plasma of CF_4 and O_2. This pattern is to prepare the mask for the via holes DRIE etching.

(3) Patterned the backside oxide for a later backside DRIE etching mask.

(4) Patterned the front side SiO_2 for the secondary front side mask for gap area. Thinner the SiO_2 with 0.9 μm, instead of etching away all the SiO_2 of 1.8 um.

(5) Etched the Si using DRIE from the front side for 250 μm.

(6) Etched the Si using DRIE from the back side for 200 μm. After this step, the via-holes on the Si were etched through and meaning while, a so called "Lego" structure on the backside of the Si chip were formed. This structure played as a "plug-in" structure, which was important on alignment and avoiding the solder from bridging, in the later assembly procedure.

(7) Coat metal (Ti/Cu/Au of thickness of 40nm/800nm/100nm respectively) on the backside.

(8) Conducted BOE etching on front side to remove the thinner SiO_2 to expose the silicon of gap area.

(9) Etched the Si from the front side using RIE with a plasma of SF_6 for about 2-3 μm (the height can decide the flow impedance of the valve chip).

(10) Removed the reminding SiO_2 mask for a next anodic bonding requirement.

(11) Bonded the silicon chip to a pyrex with anodic bonding, under a bias voltage of 550V at 400 ˚C.

4.3 Assembly of MCC

To make the assembly of the cold head on the HX, soldering was chosen to make the sealing and connection since solder exhibits selective wetting to metal and other materials which makes the sealing and bonding controllable without inducing clogging problems as epoxy does. The first step was to metalize the cold end of the HX. A shutter mask made of aluminum was used to expose just the area on the cold end which is 2.7 mm × 2.5 mm followed by thermal evaporation of metal layers of Ti/Cu/Au in thickness of 40 nm/800 nm/100 nm, respectively (see Figure 4.8).

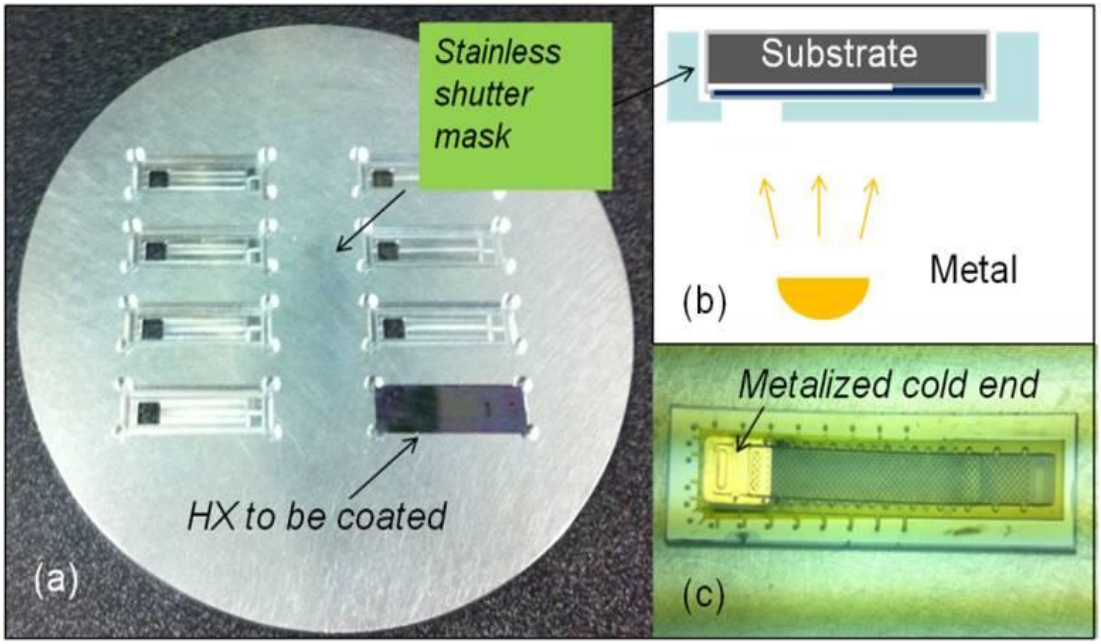

Figure 4.8: Metal coating on the cold end (a) stainless steel shutter mask; (b) evaporation on the cold end; (c) Metal coated HX.

A solder piece was then pre-molded to fit the shape of the metal pads and J-T valve for better wetting and reflow. Cold head, pre-molded solder and HX were then stacked as a

"sandwich" and then reflowed on a hot plate at 160 ˚C in a formic acid chamber. The "plug-in" structure on the cold head prevents the solder from bridging to clog the via-holes. As a result, the J-T valve and HX were bonded together (see Figure 4.9) and made a closed loop from one of the channel to the other.

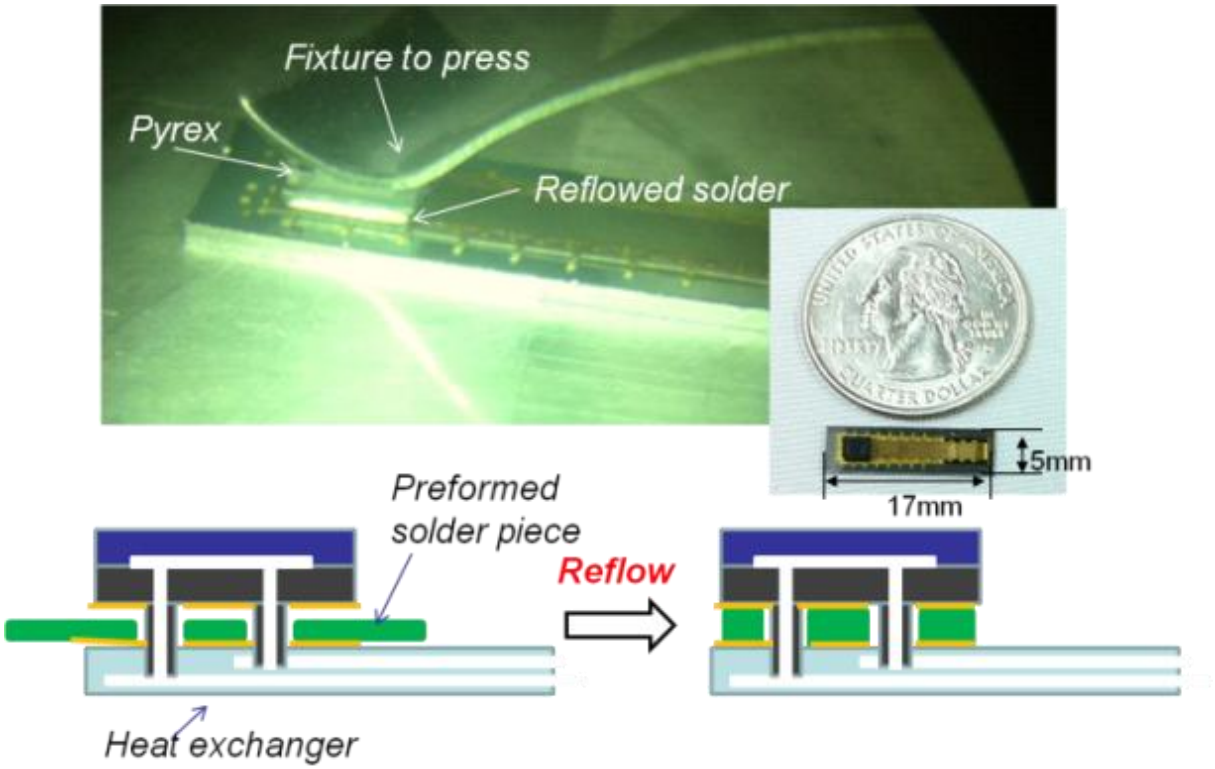

Figure 4.9: Solder reflowing method to make the connection and sealing of the cold head and the heat exchanger.

To make the connection of the macro facilities to the micro heat exchanger, two brass adaptors were used and glued with epoxy to connect the HX to the copper tubes to a stainless flange. The flange allowed O-ring connection to the macro measuring system so that the device was easily assembled and de-attached for repeating the test (see Figure 4.10).

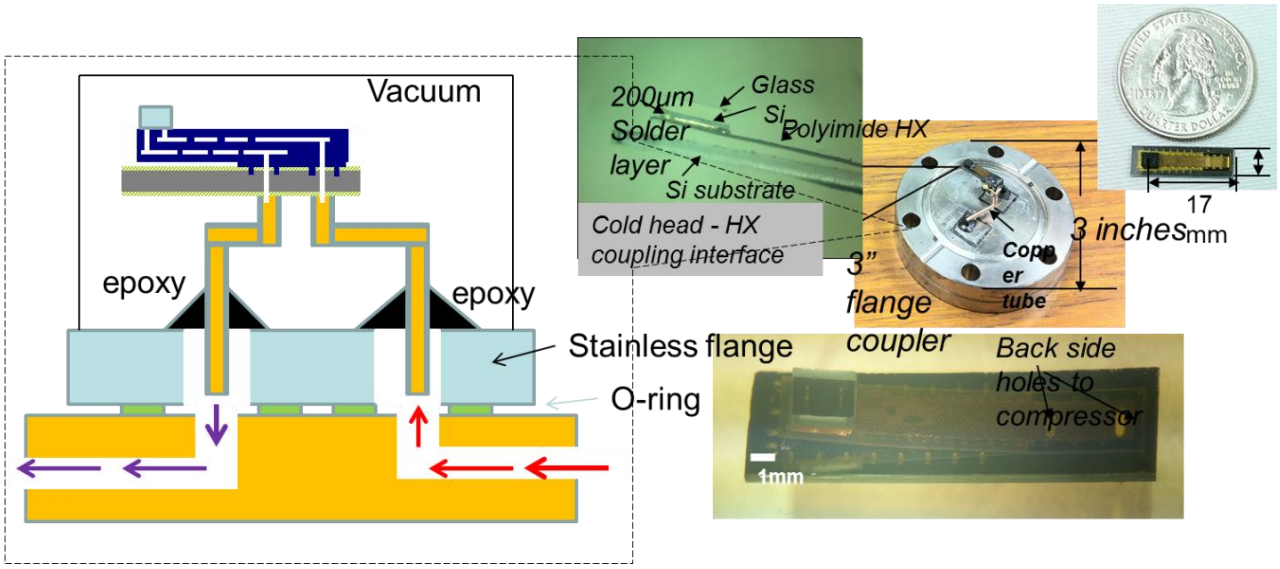

Figure 4.10 Assembled cold stage on a stainless flange.

CHAPTER 5: MONOLITHIC POLYIMIDE MCC - DESIGN AND FABRICATION

5.1 Motivations of the all polymer approach

In the last chapters, we presented the design and fabrication of a planar polymide-based MCC that consists of a micro machined polyimide counter flow heat exchanger (CFHX), and a silicon/glass based J-T expansion valve. Compared to the previous work based on the fiber-based heat exchangers, most of the fabrication processes for the planar MCC are achieved on wafer-level that substantially enhances the manufacturability and scalability. The scalable configuration enabled a designer to choose a fluid channel width for a specific heat lift with the same vertical layers. In addition, polyimide can maintain ductility at cryogenic temperatures, and it minimizes the material failure due to crack propagation in brittle materials during vibration, shock, or impact.

However, in such an assembly, the J-T valve and the heat changer have been made separately to achieve the 3-D micro fluid system, which was soldered and epoxy-bonded to make 3-D connections between the channels of the heat exchanger and the J-T valve. This assembly challenge affects the manufacturability and yield of the device due to the complicated connection process. For example, a mechanical leakage problem (see Figure 5.1) has been identified in the bonding interface of the device, which will be explained in details in Chapter 6 that covers the test results of the polyimide-based MCC.

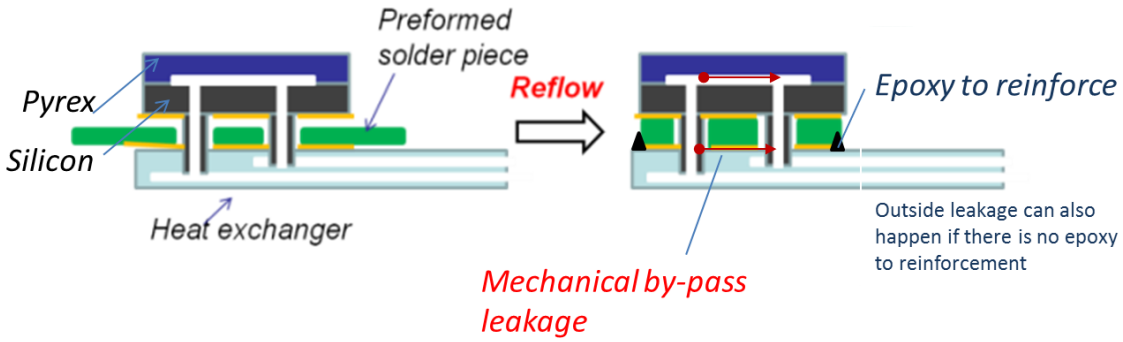

Figure 5.1: Potential mechanical by-pass leakage in the interface to cold head.

In this Chapter, the MCC assembly method has been replaced by a fairly new approach by making monolithic polyimide MCCs as presented in Figure 5.2. The new MCC cold stage including a heat exchanger and a J-T valve are all fabricated monolithically on a wafer using polyimide. Compared to the old assembly approach, such an all-wafer-level processing successfully avoided the mechanical leakage problem by making the cold stage a whole piece out of same material. It also further enhanced the manufacturability and scalability. The scalable configuration enables a designer to choose a fluid channel width for a specific heat lift with the same vertical layers. One of the major problems solved for this novel approach is the development of the wafer-level 3-D interconnect for making high pressure, e.g. 10 atm, gas channels.

The design, optimization, fabrication of the MCC manufactured with the monolithic polyimide approach are to be presented in the following sections.

5.2 Design of the monolithic MCC

Functionally, similar to the polyimide-based MCC, the monolithic MCC still have to consist of a micro machined polyimide heat exchanger and Joule-Thomason (J-T) expansion valve. The heat exchanger had a structure consisting of two parallel rectangular polyimide

channels stacked on top of each other. On the cold end, the two heat exchanger channels were interconnected with a polyimide gap of 3.4 μm, while on the worm end they are connected to the fluid via holes on the silicon substrate going to compressors thereby forming a Joule-Thomason loop. Polyimide posts were used to strengthen the polyimide fluid channels that have been proven reliable for a 10-atm gas flow. The polyimide MCC's dimensions are 15 mm × 3 mm × 90 μm with one of the ends tethered for both excellent thermal isolation and good mechanical properties (see Figure 5.2).

For the system and device design of the monolithic MCC, all the heat exchanger optimization and device thermal and mechanical analysis of the polyimide-based MCC are directly applicable here. In such a case, the typical dimensions of the monolithic MCC were same to that in Table 2.1. The only difference was that the silicon/glass valve was replaced with a polyimide valve integrated with the heat exchanger, this can make the cold head becomes a cold tip which was even so that the radiation loss was also improved.

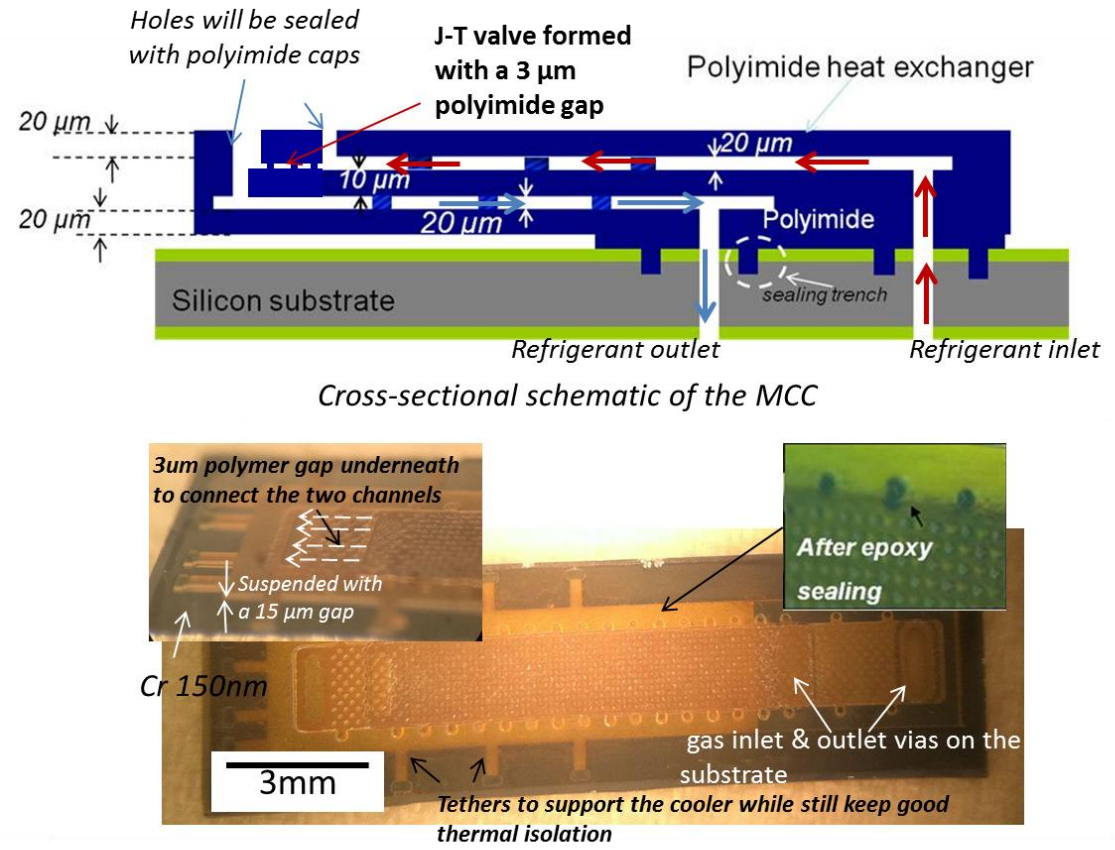

Figure 5.2: Schematics of the operation principle of the J-T micro cryocooler system with top and cross-sectional views of the planar polymer-based MCC.

5.3 Fabrication of the all polymer MCC

Similar to method for the polyimide based MCC heat exchanger, the fabrication process for the all polymer MCC consists of multi-layers of metallization of copper, spin coating and curing of polyimide, and the patterning on each layer. The J-T valve can be integrated in the heat exchanger process in which copper was also used to sever as a sacrificial layer to make the small gap J-T valve. With proper alignment and over lapping of the different channels sacrificial layers, a through etching 3-dimensionally connected all the channels to form the J-T loop. The detailed steps and their explanations are as follows and illustrated in Figure 5.3:

(1) A masking oxide approximately 1.5 μm thick was grown on both sides with wet thermal oxidation.

(2) O-ring shapes trenches were patterned on the SiO_2 layer using reactive ion etching (RIE), followed by 7 μm deep reactive ion etching (DRIE) on silicon with silicon oxide as a mask. The trenches were to enhance the bonding and sealing between the interface of the polyimide layer and silicon substrate.

(3) Backside SiO_2 was patterned utilizing RIE. This patterning was to prepare oxide mask for later DRIE etching from the backside of the silicon substrate.

(4) An adhesion layer of chromium 100 nm in thickness followed by an electroplating seed layer of copper 500 nm in thickness were evaporated onto the wafer using a thermal evaporator. Additional copper of 15 μm was then deposited using electroplating with a current density of approximately 10 mA/cm2. The metals were then patterned with wet etching serving as the first sacrificial layer.

(5) Polyimide (DuPont PI-2611*) was then deposited onto the wafer in two spin coats of 2000 rpm for 30 seconds followed by a soft bake after each at 100 ℃ for 120 seconds. After all the spin coats, the polyimide was cured at 260 ℃ for 1 hour in nitrogen, arriving at an after- cure thickness of about 20 μm.

(6) Similar to (4) but using an adhesion layer of 10nm thick titanium, instead of using chromium, followed by a 400 nm thick copper electroplating seed layer were deposited using a thermal evaporator. Additional copper of 20 μm was then electroplated followed by patterning to the geometry as one of the later embedded micro channels in the HX. The patterning of copper and titanium were done by using wet etching and RIE in a plasma of CF_4:O_2 ratio at 4:16 respectively.

(7) A second polyimide (DuPont PI-2611*) layer was spin coated at 2000 rpm for 30 seconds followed by a soft bake at 100 ℃ for 120 seconds and cured at 260 ℃ for 1 hour in nitrogen, yielding a thickness of about 10 μm.

(8) Same to (6), another 20 μm thick layer of copper plating and wet etching were done to form the geometry of the other embedded micro channel in the HX.

(9) Photoresist of 10 μm thick was deposited on to the wafer and patterned to expose the J-T valve area followed by thermally evaporating 10 nm Ti and 3 μm thick copper. The metal layers were then patterned with lift-off by the photoresist serving as a sacrificial layer for forming the J-T valve.

(10) The exact same process as described in (5) was done again to form another polyimide layer 20 μm in thickness.

(11) A hard metal mask of 10 nm of titanium (as the adhesion layer) and 2.5 μm of copper was evaporated on the polyimide layer. It was then patterned to the geometry of the HX with alignment entrance and exit holes on the end and releasing holes along the sealing edge of the HX.

(12) The exposed polyimide was etched in a CF_4 and O_2 (CF_4:O_2= 6:10 sccm) plasma until down to the copper metal to expose all the sacrificial layers, including the bottom sacrificial layer, lower channel sacrificial layer and the J-T valve sacrificial. At this situation, the lower channel was then connected to the J-T valve. Because, the metal defining the J-T valve is already connected to the upper channel sacrificial layer, three of them should be able to be connected together after releasing.

(13) Backside entrance and exit holes were etched from the backside of the substrate using DRIE. Further RIE in a CF4 and O_2 (CF_4:O_2= 6:10 sccm) plasma was then done to etch the polyimide making the entrance and exit holes go all the way to their channels filled with metal.

(14) The sacrificial layers of copper were etched away at the end in a standard copper etchant (Transene CE-100) at 60°C forming the embedded micro channels in the MCC and free the whole MCC structure. The etch time to fully release the structure was approximately 48 hours.

(15) A Kapton film was used as a cap and was epoxy-bonded to seal the top etching holes on the cold tip.

In the previous polymer-based MCC design introduced in the above Chapters. DuPont PI-2574 was used as the structure material. Because of the thermal mismatch between the polyimide layers and silicon substrate, all the tethers in this design were broken after the metal releasing. In order to solve the problem, DuPont PI-2611 which has a similar coefficient of thermal expansion to silicon was chose to making this device. No tether breaking was found after the copper releasing of the device as can be seen in Figure 5.4.

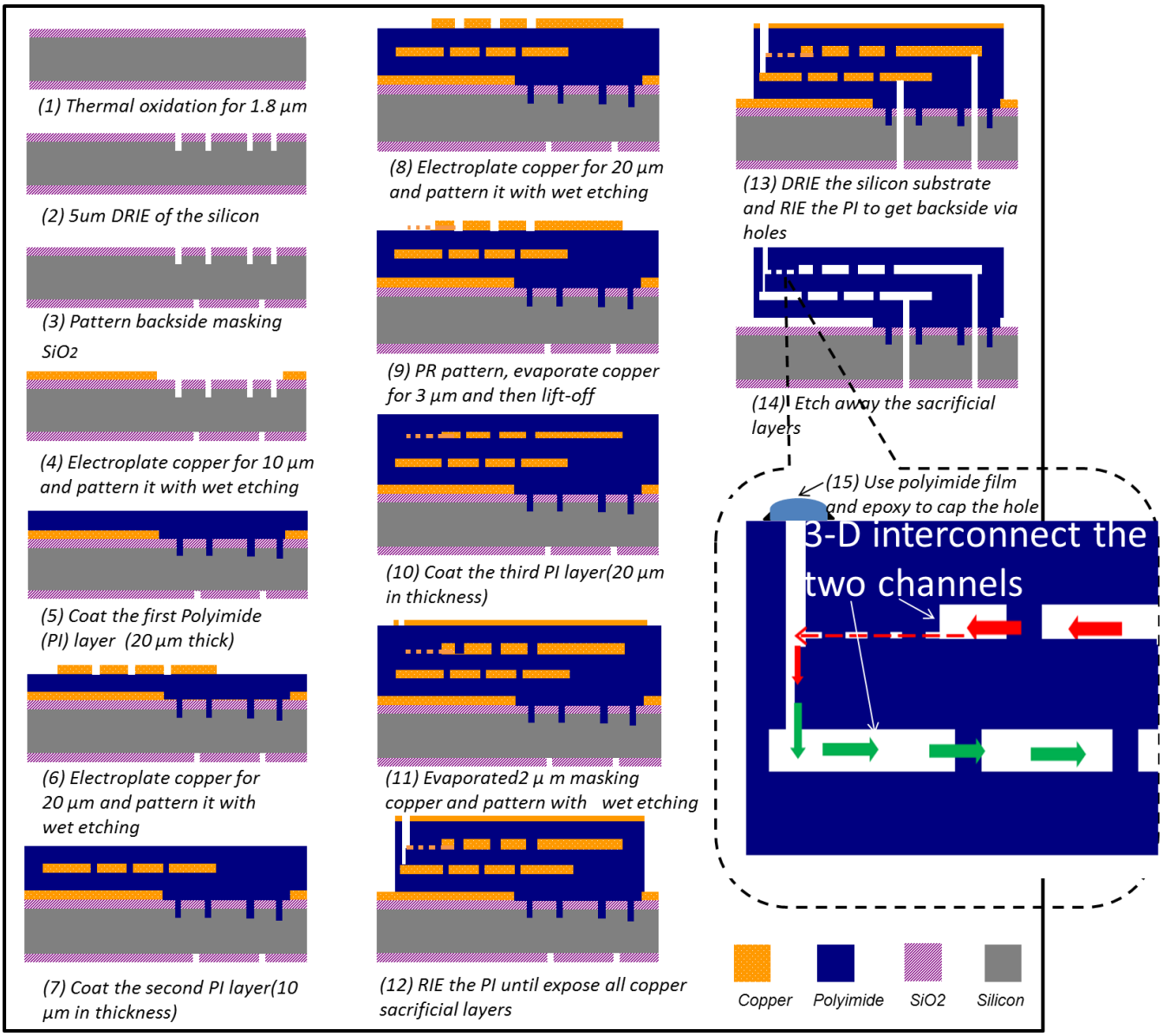

Figure 5.3: Fabrication process flow of the polyimide HX; all the conformal topography by PI coatings were drawn to be a planarized covering to make the fabrication process flow figures easier to read with more clarity.

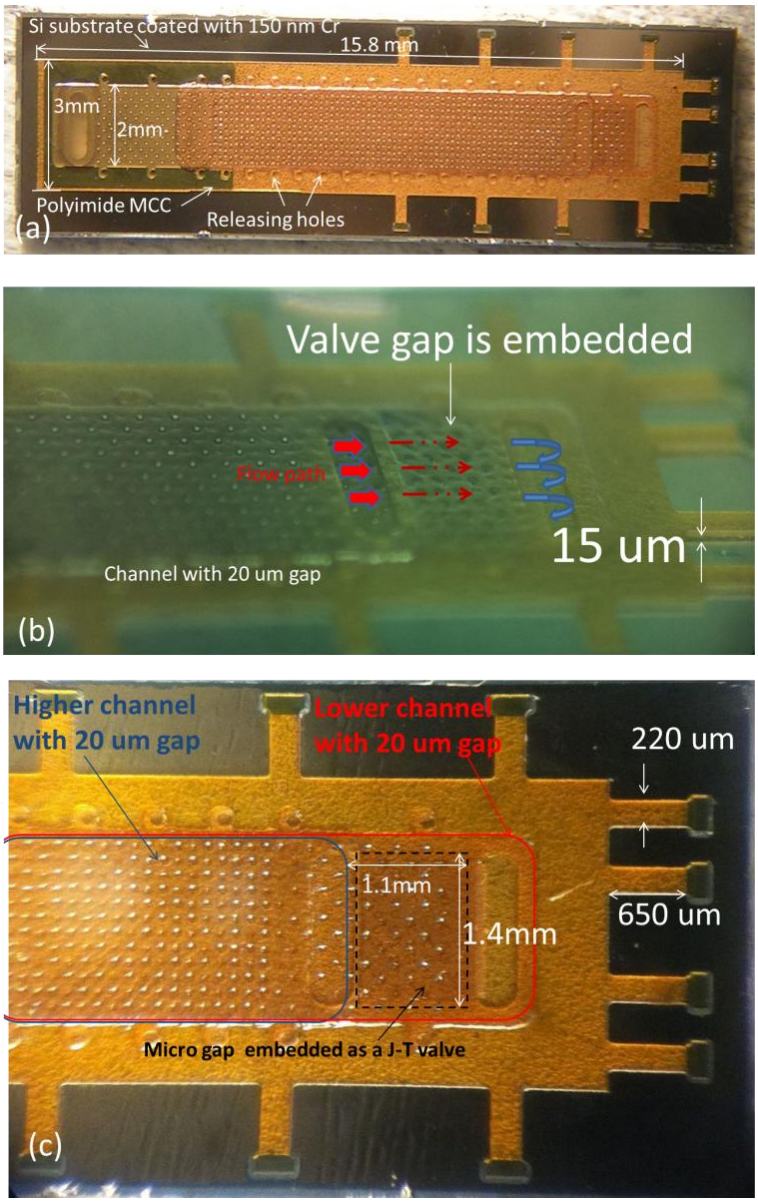

Figure 5.4: Cross-sectional view of the schematic of the heat exchanger (a), photo of the heat exchanger with tethers being broken due to the CTE mismatch (b) and photos of the heat exchanger with a flexture design to avoid the tether breaking.

CHAPTER 6: TEST OF THE POLYIMIDE-BASED MCC AND ALL POLYIMIDE MCC

6.1 Mechanical test of the polyimide heat exchanger

Before conducting the cooling test of the MCC, it is good to conduct a study on the mechanical integrity of the HX. This will tell us how much pressure the heat exchanger can survive and what's the flow resistance generated by the heat exchanger's channel.

In the experimental study, two mechanical tests were conducted on the HX to be used in a Joule- Thomason micro cryogenic system later. The first test was to estimate the pressure drop of fluid in the HX. One of the energy losses in HX is the pressure drop along the flow channels. Slip flow will begin to occur in nitrogen with channel diameters smaller than about 66 μm when Knudsen number K_n in regime of 10^{-3} to 10^{-1} for room temperature and atmospheric pressure and this critical number could be smaller at cryogenic conditions [15]. However, for K_n less than 10^{-2} (in our case, the $K_n = \lambda_{N2}/D_n$= 66nm/36 μm=0.00183, where λ_{N2} is the molecular mean free path of standard nitrogen gas and D_h is the hydraulic diameter of the channels and has a relationship to the channel gaps of D_h= 2 × gap), the effects on friction factors and Nusselt numbers can be ignored [15]. In this case, the pressure drop in a flow channel is where the flow density can be considered as a constant value is given by in [15].

$$dp = \frac{2f_r(\dot{m}/A_g)^2}{\rho D_h} dl, \tag{6.1}$$

In equation (6.1) f_r is the Fanning friction factor, $\dot{m}$ is the mass flow rate in the flow channel, ρ is the density of the gas, and A_g is the cross-sectional area of the flow channel. For a plate form where the width of the channel is much larger than the gap, f_r is given by

$$f_r = \frac{24}{N_{re}}, \tag{6.2}$$

where the Reynolds number Nre can be expressed as

$$N_{re} = \frac{D_h}{\mu(A_g/\dot{m})}, \tag{6.3}$$

where μ is the viscosity of the fluid. By using nitrogen gas for example, at room temperature, the viscosity can be approximated as a constant for pressures less than 1 MPa. For a flow-rate of nitrogen of 100 sccm, which is the largest flow-rate in the interested range, the number N_{re} is calculated to be 109 with the density of nitrogen gas given as 1.165g/ in standard condition indicating that the flow is laminar in the interested range.

The density in (6.1) is varying along the channel because gases are compressible, which give a relationship between it and the pressure as

$$\rho = \rho_0 \frac{P}{P_0}, \tag{6.4}$$

where the ρ_0 is the density of nitrogen gas at standard condition and the P0 is the standard atmosphere pressure. By combining the equations (6.1), (6.2) and (6.3), and doing the integration along the channel, the pressure across the channel and the standard volume flow-rate has a relationship of

$$\int_{P_L}^{P} P\,dp = \int_0^L \frac{48\mu\dot{V}\,P_0}{D_h^2 A_g}\,dl, \tag{6.5}$$

and (6.5) can be further simplified as

$$\Delta P = P - P_L = \sqrt{\frac{96\mu \dot{V} P_0}{D_h^2 A_g} L + P_L^2} - P_L \qquad (6.6)$$

By using a nitrogen viscosity of 1.78 Pa·s and P_L of 0.081 MPa, the theoretical relationship between the volume flow-rate and the pressure drop for rectangular channels without posts inside but with the same dimensions is shown in Figure 6.3.

However, in our device, many micro posts were placed inside the channel for supporting and increasing the heat exchanging surface, which can introduce an extra pressure drop along the flow channels. To estimate the how much the posts can affect the pressure loss of the fabricated HX, an experimental study with the test facility schematically shown in Figure 6.1 was done. Nitrogen is fed from the substrate end to one of the channels and goes across to the atmosphere from the freestanding end.

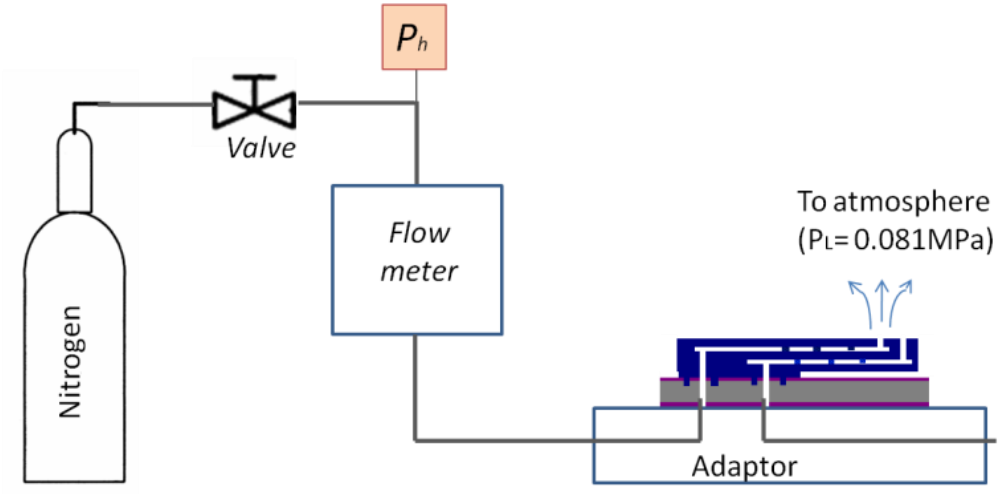

Figure 6.1: Schematic of the pressure drop test setup.

To make the connection of the macro facilities to the micro heat exchanger, two brass adaptors were used and glued with epoxy to connect the HX to the copper tubes to a stainless flange (see Figure 6.2). The flange allowed O-ring connection to the macro measuring system such the device was easily assembled and de-attached for repeating the test (see Figure 6.2).

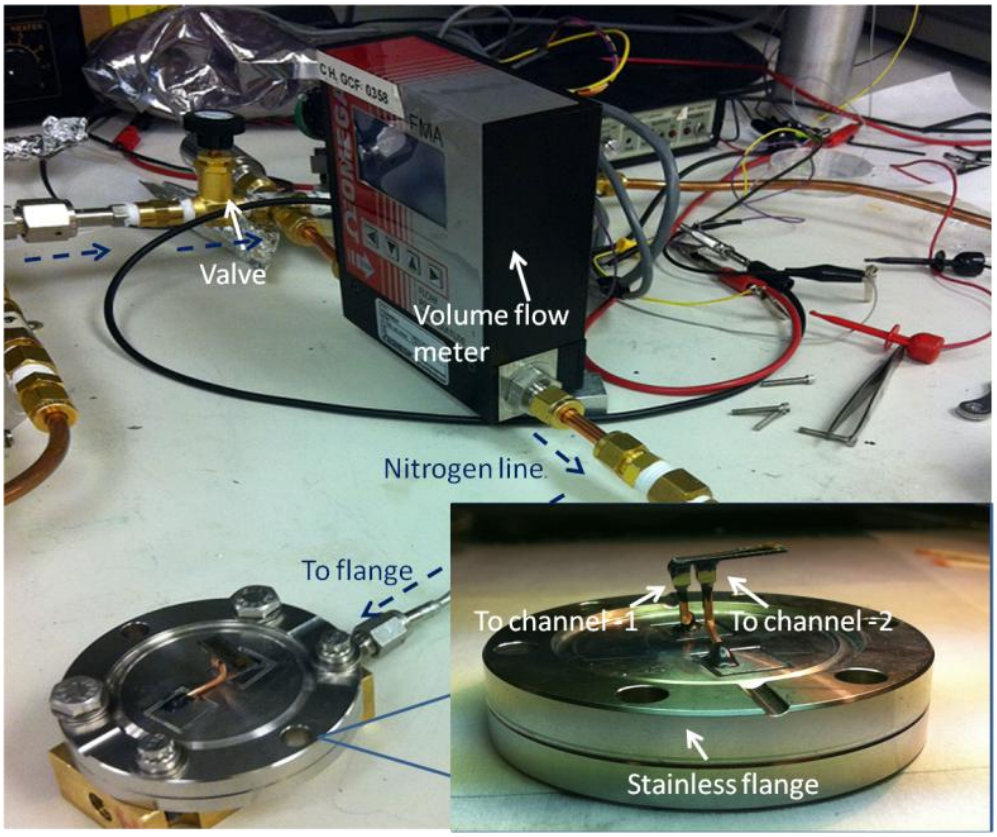

Figure 6.2: Picture of the pressure drop test setup.

By controlling the valve to adjust the inlet pressure and measuring the flow-rate, flow-rate v.s. ΔP curves for each channel on a same HX were measured (see Figure 6.3). The pressure drop across a channel was found to increase linearly in a large range with the flow-rate through it which is according to the theoretical calculation, as assessed with standard nitrogen in room temperature (see Figure 6.3). From the comparison of the testing result for channels with posts

and the analytical result for channels without posts for a same device, the affection on the pressure drop brought by the posts design was tolerated in our device. The pressure drop was ignorable in a Joule - Thomason micro cryogenic cooler aiming at an operation pressure ratio of around 4:1 (0.4 MPa : 0.1 MPa). However, one should not simply make a conclusion that the difference of pressure drop is due to adding posts. Other the process deviations such as that from the thickness controlling of the metal sacrificial layers and over etching on metals could also affect the flow resistance.

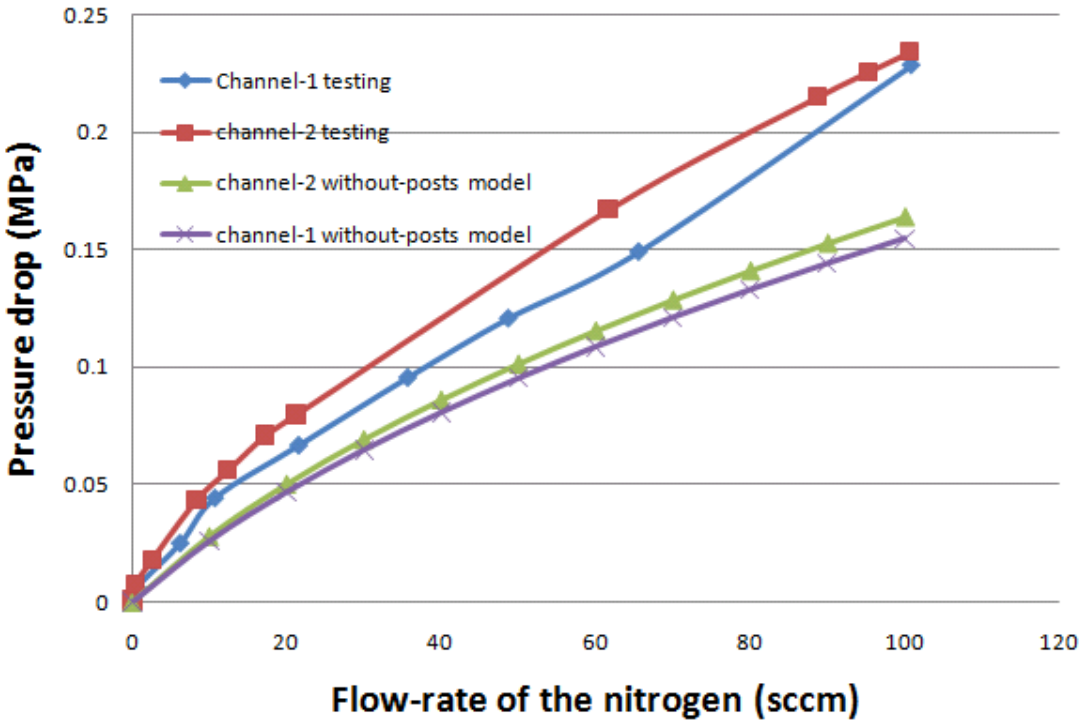

Figure 6.3: Experimental pressure drop v.s. flow-rate across the channels when using nitrogen gas at room temperature compared with analytical result for channels without posts.

The other test was to assess the over pressure withstanding capability of the HX. Each channel was tested by sealing one of its ends with epoxy while feeding nitrogen gas from the other end. The result showed that the channel structure was able to hold a pressure of at least up

to 1 MPa. Such a high pressure was good enough for an application of a Joule-Thomason micro cryogenic cooler aiming at an operation pressure ratio of 4:1 (0.4 MPa : 0.1 MPa). No bulging or leakage was observed. To verify the quality of this heat exchanger in cryogenic environment, same sealing testing was conducted after applying thermal shock by cycling the temperature between 77 K and room temperature multiple times. The results showed that the polyimide heat exchanger could sustain a cryogenic temperature down to at least 77 K, without de-bonding or cracking. .

6.2 Cooling test setup

To evaluate and measure the performance of the MCC, we have constructed a measurement apparatus as shown by the schematic in Figure 6.4 and by photo in Figure 6.5. The MCC cold stage was epoxy-bonded to copper tubes and then connected to a stainless coupler. The coupler was compatible with a cooling test setup which includes a miniature compressor composed of a miniature piston oscillator and micro-machined check valve assembly [17]. The MCC was held in a vacuum of $<10^{-4}$ Torr during the cooling tests, to minimize heat loads associated with conduction through air. Icing has been noted as a problem in MCCs [17], so to ensure that any trace amount of water in the refrigerant was removed, 1 g of 3 Å molecular sieve was placed in the test loop. A 15 μm particulates filter was installed between the molecular sieve and the MCC to prevent any particulate build-up in the micro-channels. Before running any tests, the lines were evacuated to a pressure of $<10^{-4}$ Torr, then charged with refrigerant from a low-pressure supply cylinder. A temperature sensor (Omega platinum resistance thermometer), with a footprint of 2 mm × 2 mm which allowed good thermal contact was attached to the cold head using small amount of wax. The resistance was monitored by applying a small voltage and

measuring the current-draw. Heating can also be applied to learn the heat lift by operating the temperature sensor at a higher voltage. Temperature started to drop once the compressor was turned on.

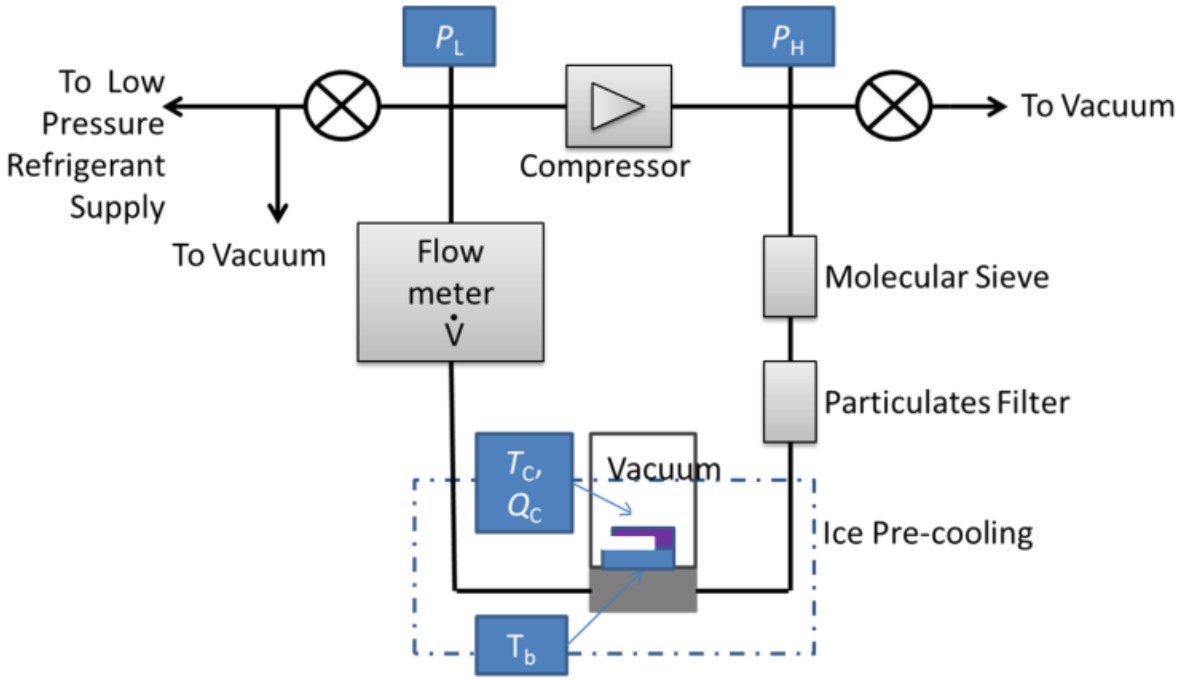

Figure 6.4: Schematic of the setup for cooling test.

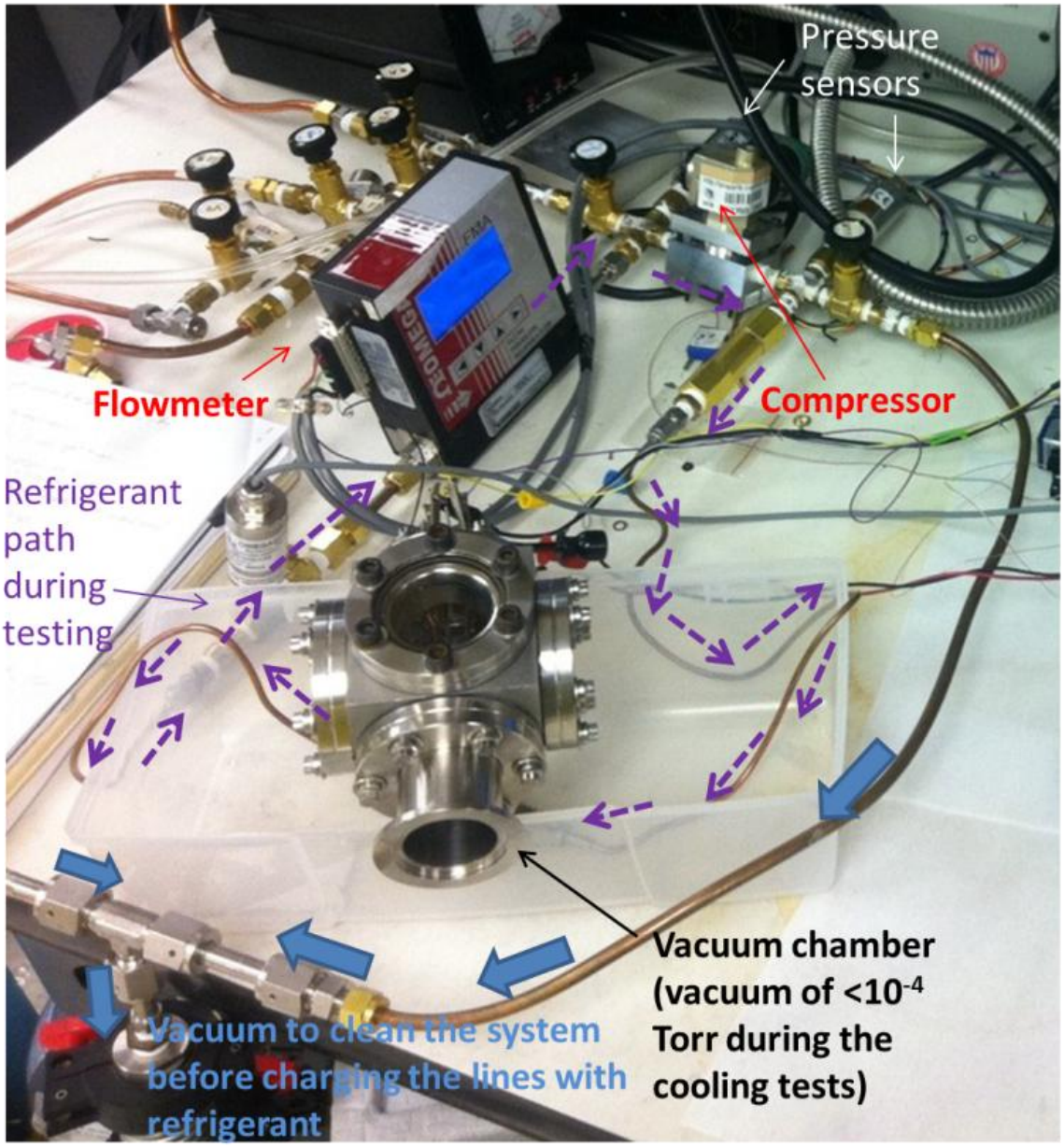

Figure 6.5: Photo of the setup for cooling test.

6.3 Cooling test of polymide-based MCC

6.3.1 Results

In macro-scaled Joule-Thomson refrigeration systems, mixed refrigerants have been widely applied to enhance the efficiency and refrigeration power. Radebaugh [11], Missimer [34], and Boiarski [35] reviewed recent developments and history of mixed refrigerants. Fuderer and

Andrija [36] first used mixed gases in a single stream without phase separators in 1969. They found that the mixtures experienced mostly two-phase flow in the heat exchanger. As a result, boiling and condensing heat transfer of two-phase flow greatly enhanced cooling efficiency.

The composition (8% methane, 46% ethane, 14% propane, 4% butane, 26% pentane) we used was optimized by the program NIST4 [16] to maximize $(\Delta h|T)_{min}$ in the range of 300 K to 200 K with a high pressure of 4.0 bar and a low pressure of 1.0 bar. The enthalpy difference curve is shown in Figure 6.6. The minimum isothermal enthalpy difference is 4.09 kJ/mol in the temperature range from 300 K to 200 K. During the test, the base and inlet of the cold stage was pre-cooled in the ice and water bath to cool the inlet mixture to cooler than a standard room temperature, which ensured the temperature to be lower than 300 K.

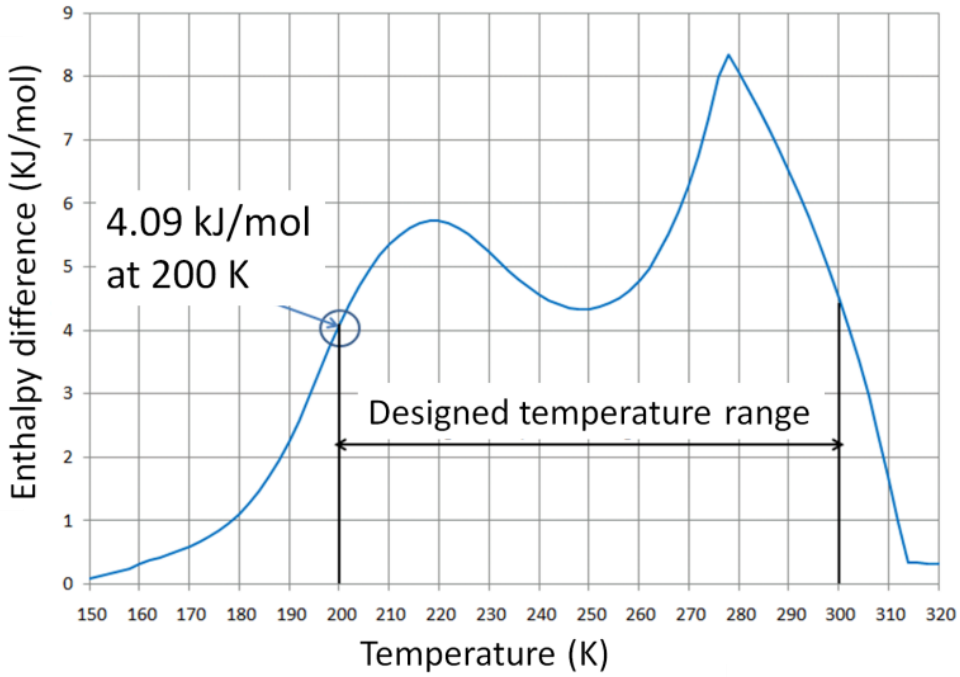

Figure 6.6: Curve of isothermal enthalpy difference for a 5 component mixture with a high pressure of 4 bar and a low pressure of 1 bar. The minimum isothermal enthalpy difference is 4.09 kJ/mol in the temperature range 300 K to 200 K.

The cooling test result is shown in Figure 6.7. The cold tip was able to reach to a stable temperature of about 233±2 K. The compressor pressure and the flow rate are shown in Figure 6.8 and 6.9 respectively. The low side pressures were adjusted by using regulation of the refrigerant supply, and the high side pressures increased according to the increasing of the low side pressures. Flow-rate kept increasing during the test procedure until the flow-rate meter was saturated. Increasing of the flow-rate is both due to the increase of pressure difference between the two sides and a drop of the temperature of the J-T valve and resulting gas liquefaction. Two-phase flow and periodical phase change of the refrigerant have been observed when the flow-rate is higher than 100 sccm. Figure 5.10 shows pictures of the cold head taken with a high speed camera, showing a cycle of the phase changes. This periodic phase change was accompanied by the flow rate oscillations shown in Figure 14 after 3000 s. More interesting phenomena between two-phase flow patterns and cooling power of mixed refrigerant in MCC is being reported in [38].

As a result, the flow rate of the mixture is more than 200 sccm under the pressure ratio of 7:1.5 bar giving a stable tip temperature of about 233 K.

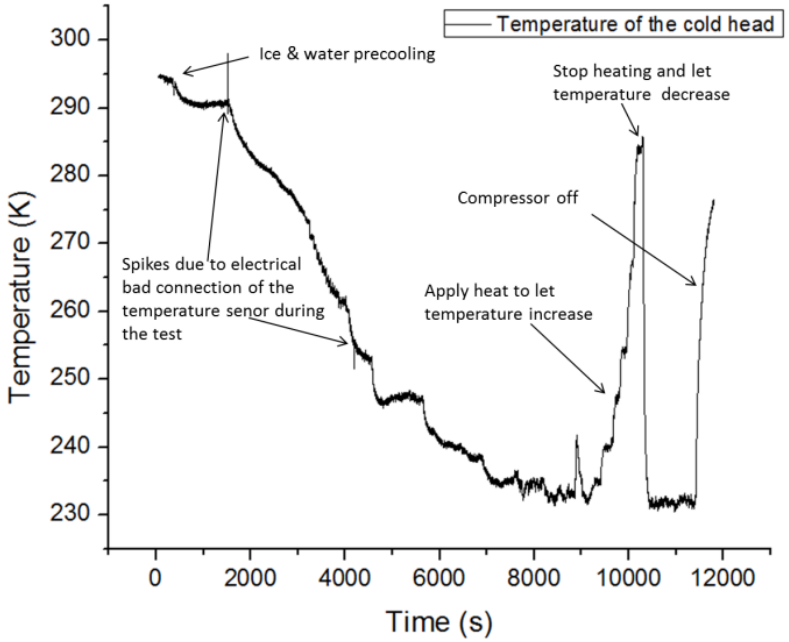

Figure 6.7: Curves of cooling result. The cold tip was able to reach to a stable temperature of about 233±2 K.

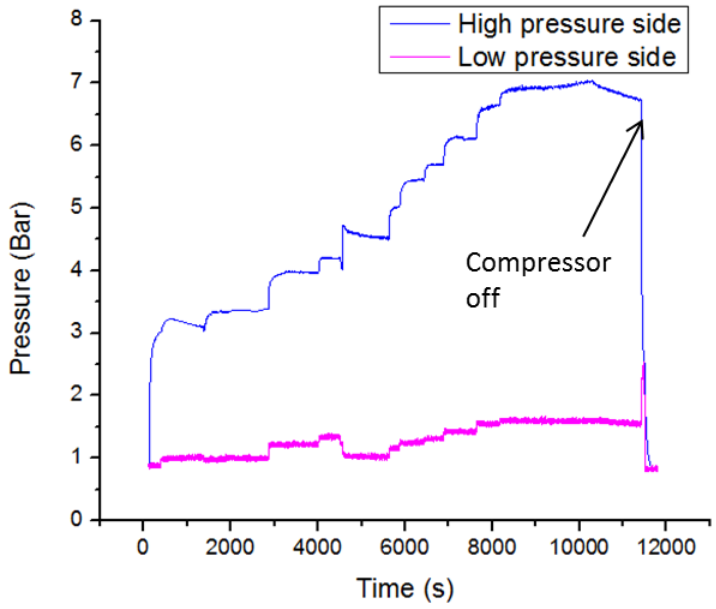

Figure 6.8: Curves of pressure of each side of the compressor, the highest compression ratio reached is about 7:1.5 bar.

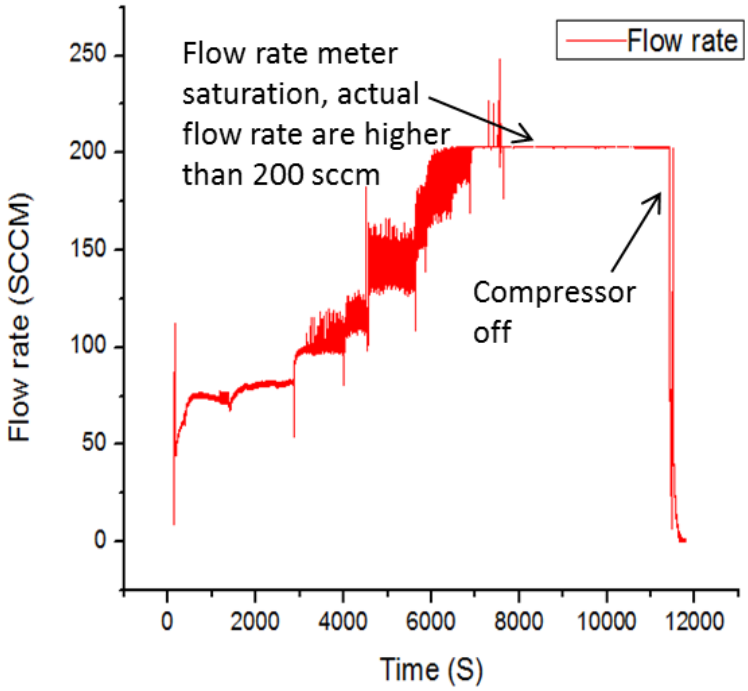

Figure 6.9: Curve of the flow rate vs. time; flow rate kept increasing during the test procedure until the flow rate meter was saturated.

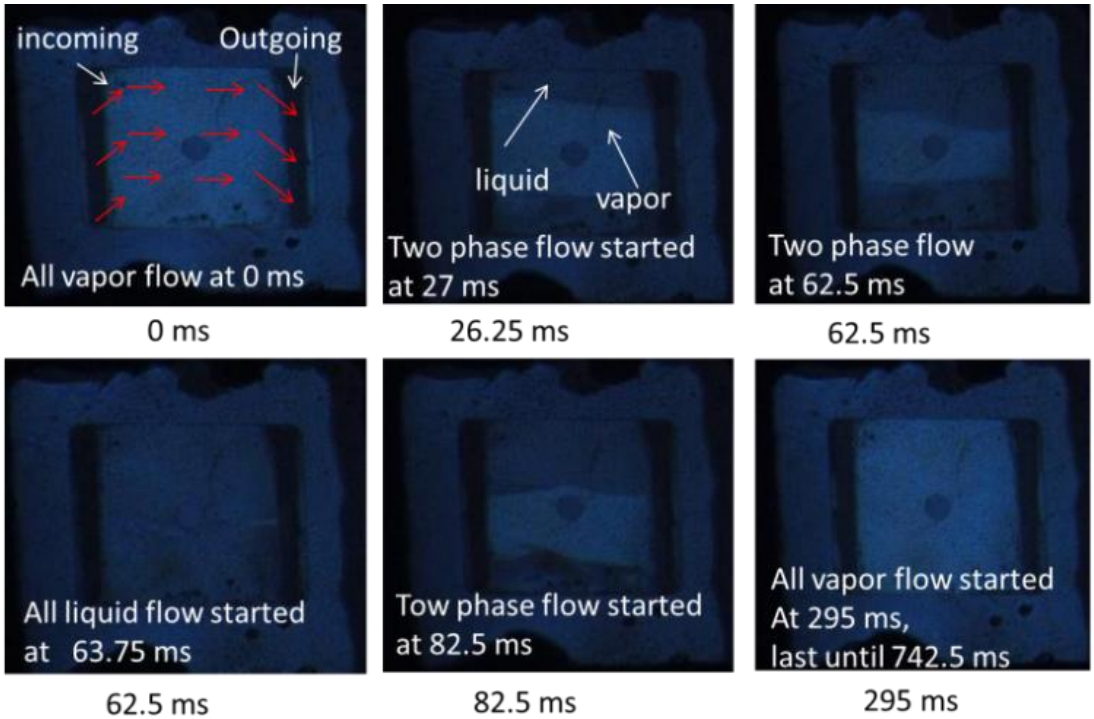

Figure 6.10: Pictures of the cold head taken with high speed camera, showing a cycle of the two –phase flow pattern change in the cold head. The camera used is an

Olympus i-speed visible-light camera with no filters. The light source was a white LED.

6.3.2 Problems and discussions

During the testing, we were able to intentionally adjust the high-pressure to make the high side pressure go up in order to get lower temperature. For example, we increased the high side pressures by just increasing the low side pressures a little with charging more gases from the mixture cylinder. We can also increase the frequency of the piston of compressor from 8 Hz to 50Hz to increase the pressure ratio.

The demonstrated 233K result by using the 5 components mixture is still higher than the targeted optimized temperature which was 200K. The reason is because the mixture was not working under the optimized conditions. The flow-rate is much higher than 10 sccm which was the design flow. This is because the flow restriction of the valve was not large enough. Under this condition, since the flow-rate is too high, the pressure loss along the channel can increased which made the actual pressure drop across the valve became smaller than 4:1 even when the total pressures were at 7:1.5 bar. Besides this, the velocity of the flow was much higher than the design velocity therefore a poor heat transfer occurred between the two lines (incoming channel and outgoing channel) which decreased the effectiveness of the HX. The valve was easily detached from the cold end after the testing, and external leakage sometimes happened on the solder bonding interface between the cold head and heat exchanger, so a mechanical by-pass leakage was also believed to happen in the solder interface between the J-T valve and heat exchanger to create the non-enough resistance problem.

To improve the cooing ability of the device, the assembly method has been replaced by a fairly new approach by making monolithic MCCs. The new MCCs were fabricated monolithically on a wafer all using polyimide which avoided the potential by-pass leakage

problem. Preliminary test results of the new coolers reached a 190 K stable temperature by using the same refrigerant and this will be seen in Section 6.4.

The MCC took much longer than what expected to cool down to 233K by considering the quite small thermal mass. The potential reason was that for the big system, it took long time to be stabilized. Some component, e.g. pentane, is supposed to be liquefied at room temperature at high pressure, e.g. 5.5 bar, and will condense and then be held in the large tube of the system, in that case the actual mixture to passed the cooler had been changed to that has a much lower enthalpy difference (as much as 10× lower). This can happen until the condensed liquid amount reached to a certain level thus the system reached to the equilibrium. A further study by compactly integrating a micro compressor and the cold stage is ongoing in our group to solve the large tube liquid condensing problem to improve the cooling time. However, it is outside of the coverage of this thesis.

6.4 Cooling test of the monolithic polyimide MCC

6.4.1 Results

Same to the procedure of testing the polyimide-based MCC, The composition (8% methane, 46% ethane, 14% propane, 4% butane, 26% pentane) was also used here to test the all polymer based MCC Same to the reason in testing polyimide-based cooler, the base and inlet of the cold stage was pre-cooled in the ice and water bath in order to enable a fast reaching of the equilibrium of the mixture.

The cooling result is shown in Figure 6.11. The cold tip was able to reach to a stable temperature of about 190±10 K while the compressor is operated at a pressure ratio of 6.2 bar : 1 bar. Curves of the flow-rate and the compressor low and high sides pressures are shown in

Figure 12 and 13 respectively. We also applied switched heating to control the temperature expecting to see more stable temperature, specifically, we were able to program the temperature sensor so that it applied 20 mW heat when the temperature is below 200K and switched off once the temperature once it reached 200 K. The temperate was then stabilized at about 200 K. The average heat applied is about 5.2 mW indicating the heat lift is 5.2 mW at 200 K. After applying heat, the flow rate decreased according to the changing of the viscosity and density of the mixture components.

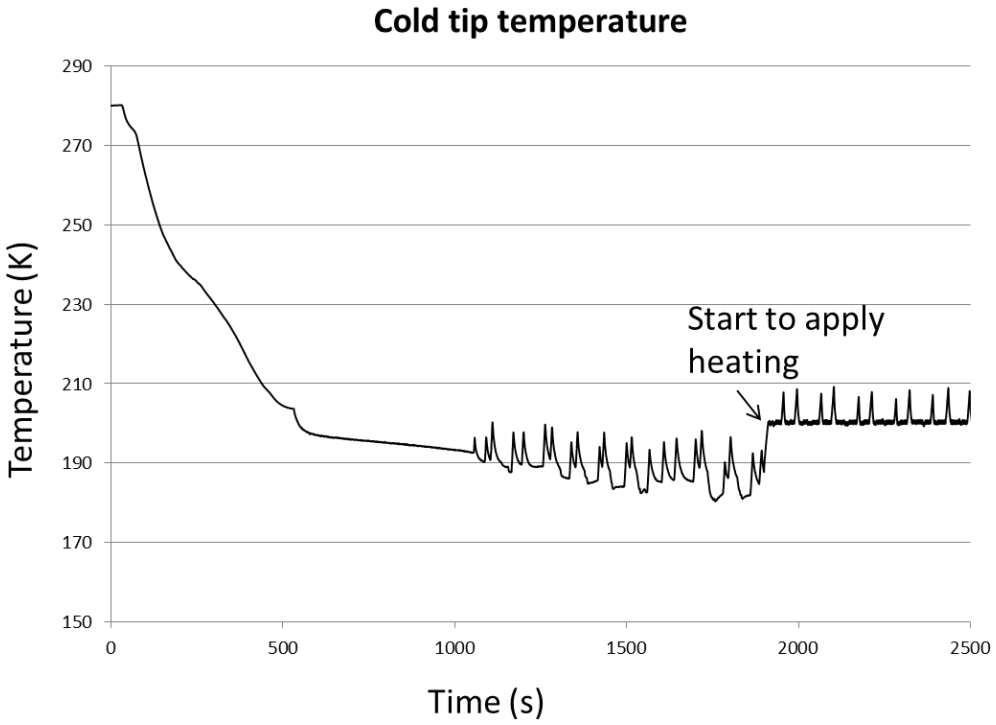

Figure 6.11: Curves of cooling result. The cold tip was able to reach to a stable temperature of about 190±10 K.

Flow-rate and pressures are fluctuating when the cold tip get cooling (see Figure 6.12 and Figure 6.13), this is believed due to the liquid holding and sending issue. More details on study and improvement according to the study of the mixture can be found in [39].

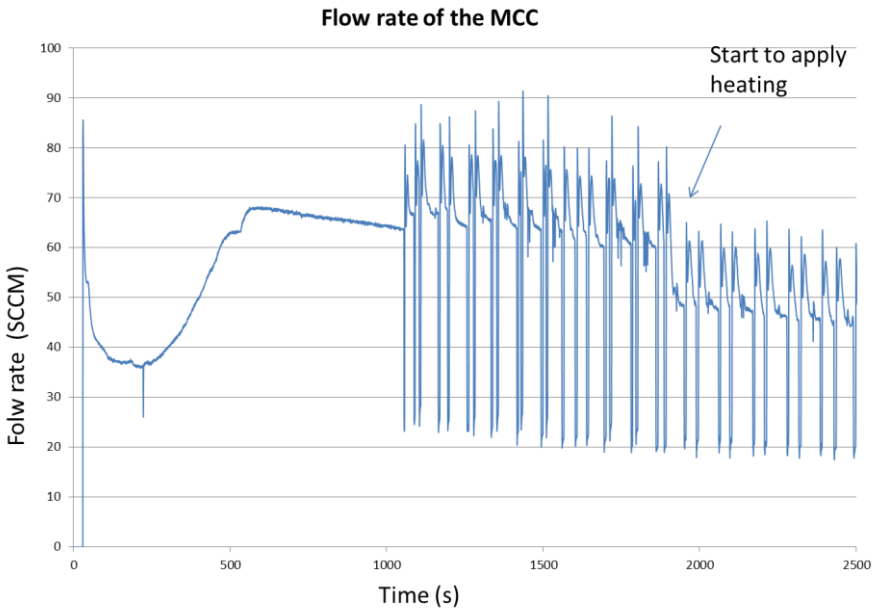

Figure 6.12: Curve of the flow rate vs. time; flow rate kept increasing when the temperature is decreasing; the flow rate start to fluctuate when the temperature reached the 190 K.

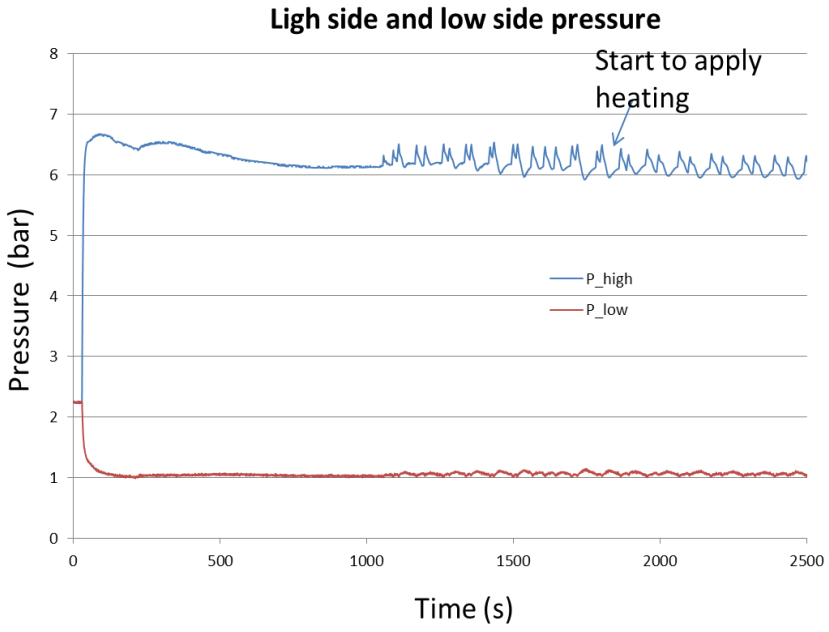

Figure 6.13: Curves of pressure of each side of the compressor, the highest compression ratio reached is about 6.2:1bar. Pressures fluctuate according to the flow rate.

6.4.2 Problems and discussions

The cooling temperature demonstrated by using the 300 K - 200 K mixture successfully reached the optimized temperature. However, the net heat lift was still lower than what we had expected which was about 12 mW. The flow rate was higher than that designed (actual: 60 sccm; designed: 10 sccm). The higher flow-rate provided higher gross refrigeration, however, the heat exchanger efficiency was thus degraded due to a large flow-rate. Another potential problem was that the enthalpy difference of the mixture in the optimization was under the assumption of a thoroughly mixed refrigerant. However, due to the liquid vapor separation issue, the enthalpy difference was smaller than the one calculated that also contributed to the reduced refrigeration. In addition, the heat exchanger tested had no metal shielding to cover its top surface. Without this additional radiation shielding, the thermal load was higher than what we had expected.

It is essential to reach the designed flow-rate with the correct gap of the J-T valve. It is the main reason we decided to conduct a detailed study to character the J-T valve gap. This study will be reported in Chapter 7. In summary, we have developed the amonolithic polymide MCC with five components mixture and successfully demonstrated the 200 K cooling with a 5.2 mW heat lift The MCC can be further improved.

CHAPTER 7 STUDY OF THE POLYMER J-T VALVE

7.1 J-T valve and previous work on pressure drop prediction of two phase flow

The function of J-T valve in Joule-Thomson cryogenic cooler is to: (1) enable a significant pressure drop along with a large temperature drop in temperature [40]; (2) regulate the cryogenic fluid in order to achieve the desired flow-rate though the MCC. In other words, to achieve the optimization condition at which we aimed, and to provide required refrigeration, this valve regulate the flow-rate for a given pressure drop. In the MCC system, mixtures of two-phase flow are required to achieve high enthalpy difference for effective refrigeration, we need sound knowledge of the two-phase frictional characteristics in order to improve the accuracy of the design of the J-T valve.

Typically, there are two different approaches to predict the frictional pressure drop of a two phase flow: the homogeneous model and the separated flow model. For the homogenous model, the two-phase flow is assumed thoroughly mixed and can be treated as a single-phase flow so that the slip ratio equals to 1. The pressure drop is computed as if the flow is a single phase with some properties modified. Details of using the homogeneous model will be given in Section 7.3.5 in this chapter. In the separated flow model, the two phases of the flow are considered separately and their velocities may differ [41].

There are lots of works been done on precisely prediction of two phase flow based on comparison of experimental data and theoretical correlations in order to improve the design accuracy of systems such as steam-power and petrochemical plants, refrigeration and air-conditioning systems. Most of the frequently used correlations to predict the two-phase frictional pressure gradient take the form of two-phase frictional multipliers. This concept was first introduced by Lockhart and Martinelli 1949 [42]. In their formulation, the multipliers were a

function of the Martinelli parameter. Detailed formula and definition of the multipliers was introduced by Lockhart and Martinelli in [43]. In 1979, Friedel improved the prediction by proposing correlations based on a bank of 25,000 data and the multiplier is given in [44]. However, these correlations were found to be limited to specific range of flow conditions as surface tension of the flow, fraction of the vapor and dimensions and geometry of the channel. For example, it was found that the Friedel correlation significantly over-predict the data having smaller liquid mass flux while under-predict the data of higher liquid mass flux of air–water in capillary tubes [45] [46]. On the other hand, interestingly, it can fairly predict the refrigerant data in a 3-mm diameter tube which has been proved by Yang et al [47]. Due to the limitation of existing correlations, there are more works kept being done to enlarge the data base and generating more accurate correlations. In 1992, an experimental study was conducted by Souza et al [41] to provide the local pressure drop during two-phase flow of R-134a and R-12 inside smooth tubes. A correlation was developed based on theoretical pressure drop modeling. The ranges studied were those utilized in residential and automobile air conditioning evaporators. In 2002, Chen et al [42] developed an appropriate correlation to predict the two-phase pressure drop in small tubes, $D < 10$ mm, based on the relevant database.

However, despite these progress made to predict pressure drop both experimentally and theoretically, it seems that the applicability of these correlations for refrigerants for even smaller channels, such as a micro gap is still not clear. Furthermore, most of the two-phase flow studies were focusing either on air-water mixture or commercial refrigeration making their results hard to be confidently applied to our specific case of the MCC valve design due to that all these correlation limitations to specific range of flow types and conditions

In this chapter, a study on the polymer J-T valve will be conducted in order to experimentally study the pressure drop of the customized mixture for micro gaps with the dimension of interest for the MCC design. In this study, the polyimide valve was fabricated and tested to simulate the real case in the monolithic polyimide MCC. An apparatus was built to test the pressure drop v.s. flow-rate with different fluids. Pressure drop data for micro gaps with nitrogen and a five components mixture were obtained. Because of the reason that even would be just valid for the bubbly flow, homogeneous model was reported to give comparatively accurate predictions in smaller tubes for various flow conditions [41] [45], it was chosen as a comparison to the test date of the valve. The calculation using homogeneous was assisted with NIST-REFPRO to generate the flow properties under different pressure and temperature conditions.

It was indicated that prediction method using the homogenous model assisted NIST-REFPRO has a good predictive ability (a mean deviation < 10%) for a five component mixture through the valve of typical dimensions in the MCC. Details of the study are to be introduced in the following sections.

7.2 Problems of the current polyimide J-T valve design

The all polyimide approach to make the MCC as mentioned in Chapter 5, demands an accurate design of the polyimide gap for the J-T valve .However, for the current design of the valve, due to the reason discussed above in Section 7.1, the J-T valve dimensions were obtained by trials and errors. What's more, polyimide gap structure was very compliant without any stiffness design, making the flow restriction sensitive to pressure as what is shown schematically in Figure 7.1 (a). This deflection under pressure will add a nonlinear effect making it difficult to predict the restriction of the valve.

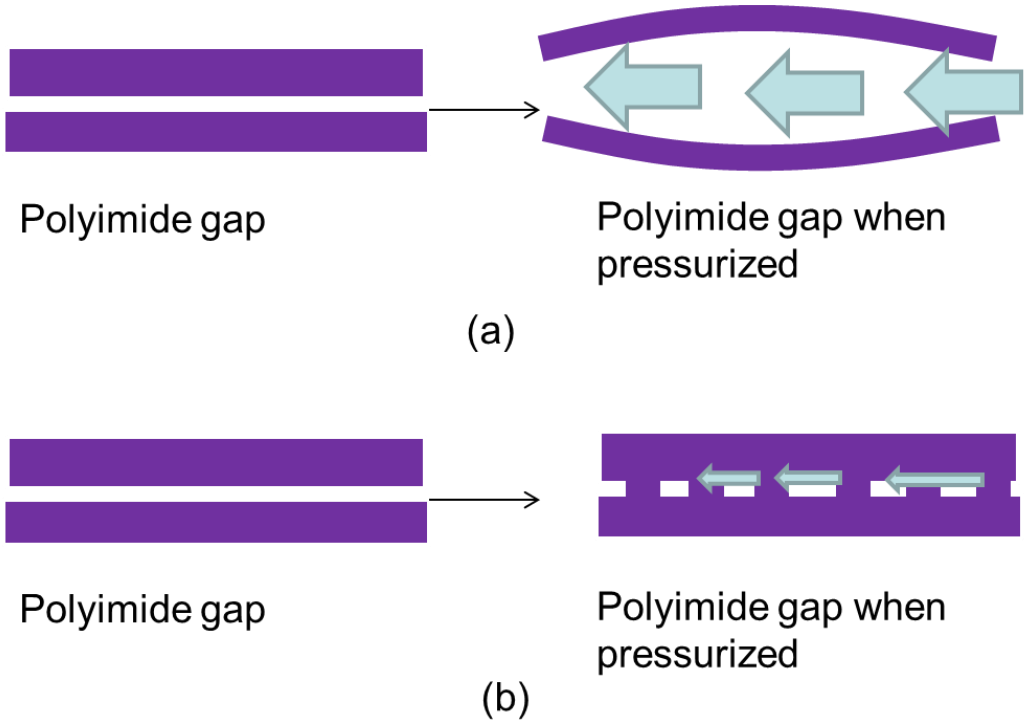

Figure 7.1 Schematics of the deformation of the polyimide gap (a) without any stiffness design and (b) with stiffness design.

As a result, it is desirable to understand more on how to predict the polyimide J-T valve restriction. This chapter will propose and verify an effective analytical design method.

7.3 Experimental study of the J-T valve

7.3.1 Study method

In order to propose a design reference, a systematic testing of J-T valve resistance needed to be tested under different temperatures. For this reason, we decoupled the testing of the valve from the MCC, which meant we fabricated and tested valves in different dimension separately. The test can be conducted with any flow that are interested and the study were limited to a dimension range interested according to the interested flow-rates and pressures for the polymer-based MCC.

After the test, the results were compared to calculation results by using homogenous model in order to understand how good it is effectively to predict the valve flow resistance. The processes and methods developed in this study can also be references for engineers who work on the similar cooler design to follow to understand the flow resistance under similar conditions.

7.3.2 Design of the test vehicles

Stiffness design of the polyimide gap

As mentioned in above, since polyimide (for PI-2611, Young's modulus is 8.5 GPa) is compliant material making the flow restriction sensitive to pressure, a induce a nonlinear effect which makes it difficult to predict the restriction of the valve see (Figure 7.1 a). In order to reduce the nonlinear effect, supporting structures were designed to make the gap to be rigid avoiding large deflection under internal pressure (see Figure 7.1 b).

Numerical study in Conventorware was used in order to understand the deformation of the polyimide gap deformation under internal high pressures. For example, in Figure 7.2, for a given valve with a 3 μm gap and a deformable layer in thickness of 20 μm which similar to the conditions in the current demonstration of MCC, by choosing posts diameter of 100 μm and space between each post to be 100 μm either, the maximal deformation is only 66 nm under an internal pressure of 4 bar. This deformation is considered to be negligible for a 3 um gap. To understand this, by doing a simple calculation, when a gap change from 3 μm to 3.066 μm, based on equation (7.1) the flow rate will become $(3.066/3)^3$ =1.07 times for a given pressure drop and fixed other conditions of the valve and flow properties. This posts design parameters were chosen to make all the test vehicles discussed in this chapter.

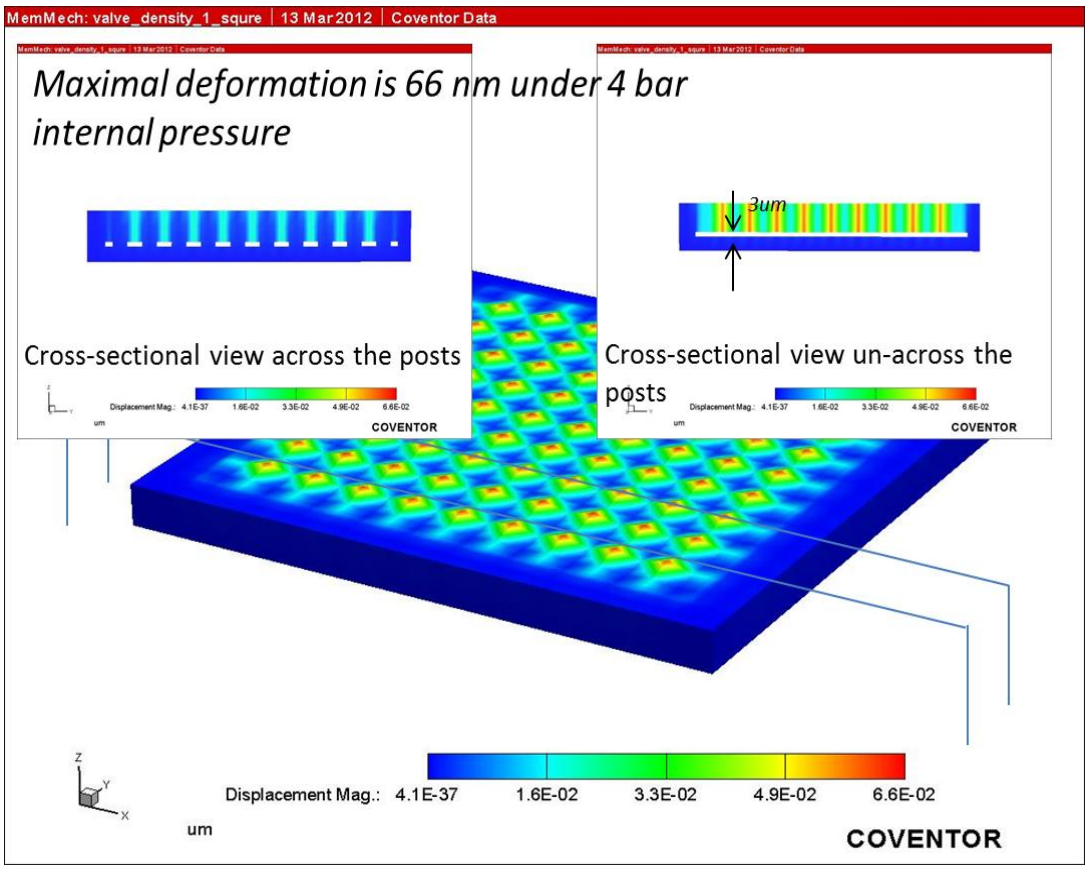

Figure 7.2 Simulation of the deformation of the valve for a typical posts design.

Flow resistance calculation and dimension design of the test vehicles

In this study, due to the fabrication requirement of the planar polymer-based MCC, the interested structure of the J-T valve here was nothing but a gap. In order to fabricate the valve together with the heat exchanger, the evaporated copper was used as the sacrificial layer to make the polymer gap that serves as a pressure drop restriction. In this case, the gap height interested was confined to be from one to several micron (e.g. 1 - 4 μm). Smaller gap could make the releasing substantially difficult and could also make valves to be too sensitive to any deformation under high pressures condition. For example, by using equation (7.1), if the gap g varies from 1 μm to 1.066 μm, the flow rate will become $(1.066/1)^3$ =1.2 times for a given pressure drop and

fixed other conditions of the valve and flow properties. In our study, 3.2 μm was chosen as the valve gap by having the concerns discussed above. Under confinement, we designed several different dimensions of valves in our interested flow restriction range. The dimension was decided based on experience. For a motivation to make the device small, the valve can be scaled down by making both the length and width smaller while still keeping a same restriction. However, when the width and length becomes too small, any small contamination introduced from the system can risk the valve to be totally clogged. Furthermore, the restriction of the valve can also become too sensitive to the deviation the fabrication. Based on these considerations, typical dimensions of the valve in this study have been chosen are shown in Table 7.1.

Table 7.1 Dimensions of the studied test vehicles

	Set-1	**Set-2**	**Set-3**	**Set-4**
Length (L)	1.5mm	3mm	4mm	1.5mm
Width (W)	2mm	2mm	2mm	6mm
Gap (g)	3.2 um	3.2um	3.2um	3.2um

7.3.3 Fabrication and assembly of the test vehicles

The valves were fabricated on a 3 inch (76 mm) n-type <100> silicon wafer of 380 μm thickness. Evaporated copper were used as the sacrificial layer and polyimide was used as the structural material to simulate the real situation for the valve in the polyimide MCC. Figure 7.3 illustrates the major batch fabrication steps for the polyimide J-T valve. The detailed steps and their explanations are:

(1) Polyimide (DuPont PI-2611) was deposited on to the wafer in spin coat of 2000 rmp for 30 second followed by a soft bake at 100 °C for 120 seconds. After all the spin coats, the polyimide was cured at 260 °C for 1 hour in nitrogen, coming with an after- cure thickness of about 10 µm.

(2) An adhesion layer of 20 nm thick chromium followed by a 3.2 µm thick copper layer were deposited using thermal evaporator.

(3) The copper and chromium were then patterned using CE-100 (Transene) etchant and 30% HCl solution respectively.

(4) Another Polyimide (DuPont PI-2611) layer was deposited on to the wafer in two spin coats of 2000 rmp for 30 second followed by a soft bake after each at 100 °C for 120seconds. After all the spin coats, the polyimide was cured at 260 °C for 1 hour in nitrogen, coming with an after-cure thickness of about 20 µm.

(5) Proper dicing was conducted to achieve the right dimensions of the valves (length) and to expose the metal layer.

(6) Etched away copper layer to release the device using copper etchant (Transene CE-100).

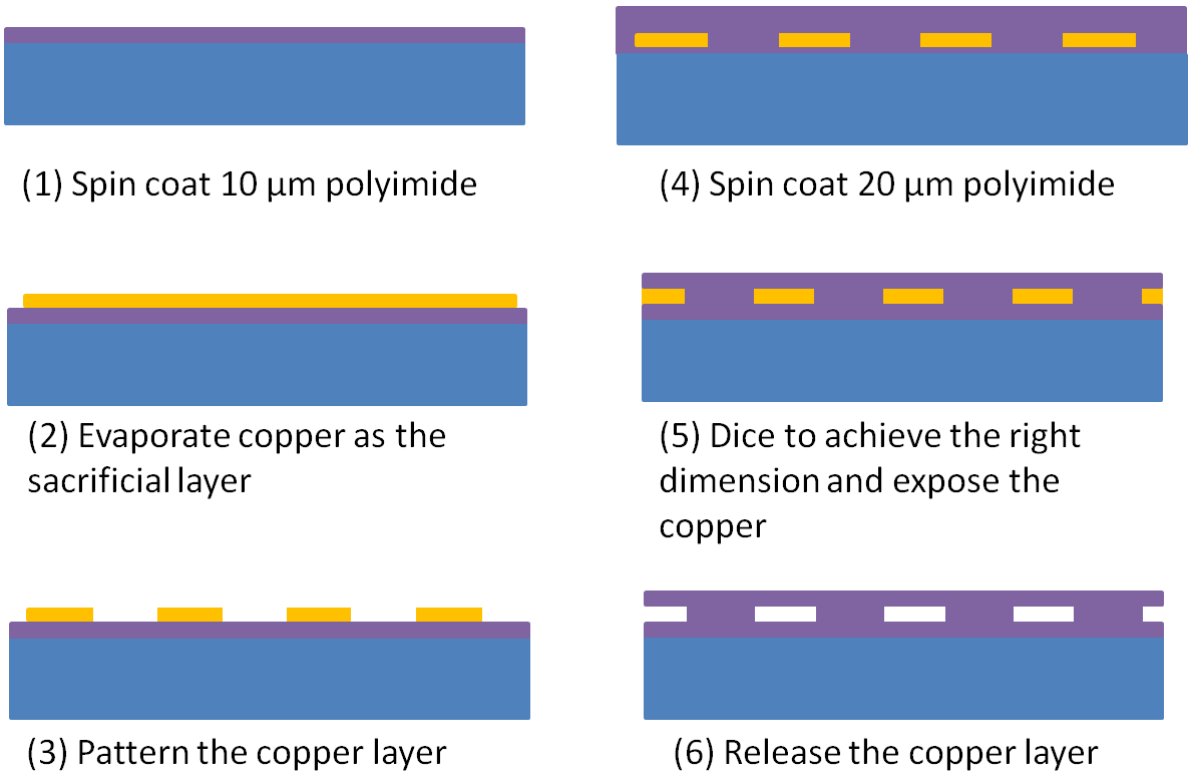

Figure 7.3: The fabrication steps of the J-T valve test vehicles.

Figure 7.4 shows the picture of a fabricated J-T valve, a fabricated valve is a polyimide gap on top to silicon substrate, the top layer of polyimide is about 20 µm thick. To couple out the gap to the test setup, the gap was then epoxy-bonded to an aluminum fixture, and then with stainless tube connection, the gap was connected to the 3" flange which was compatible with the fluids test setup mentioned in Chapter 6.

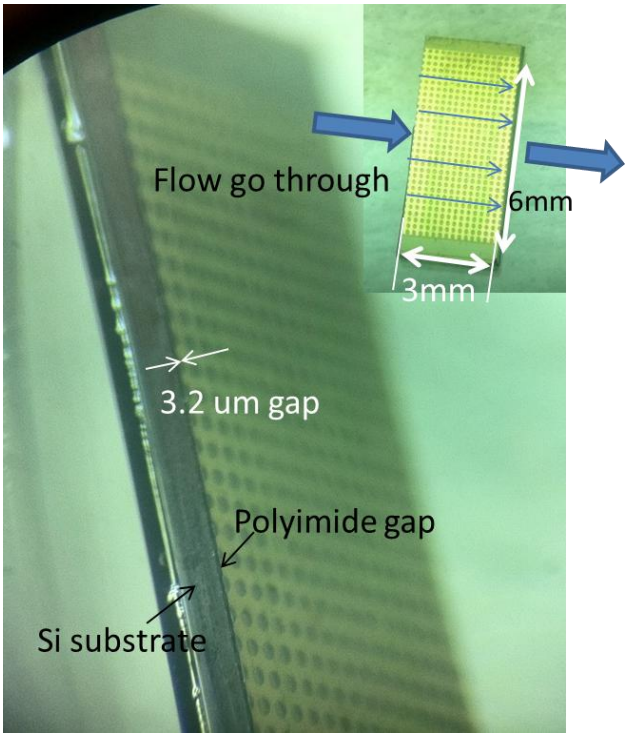

Figure 7.4: Photos of a typical J-T valve test vehicle, the valve is a polyimide gap on top of the surface.

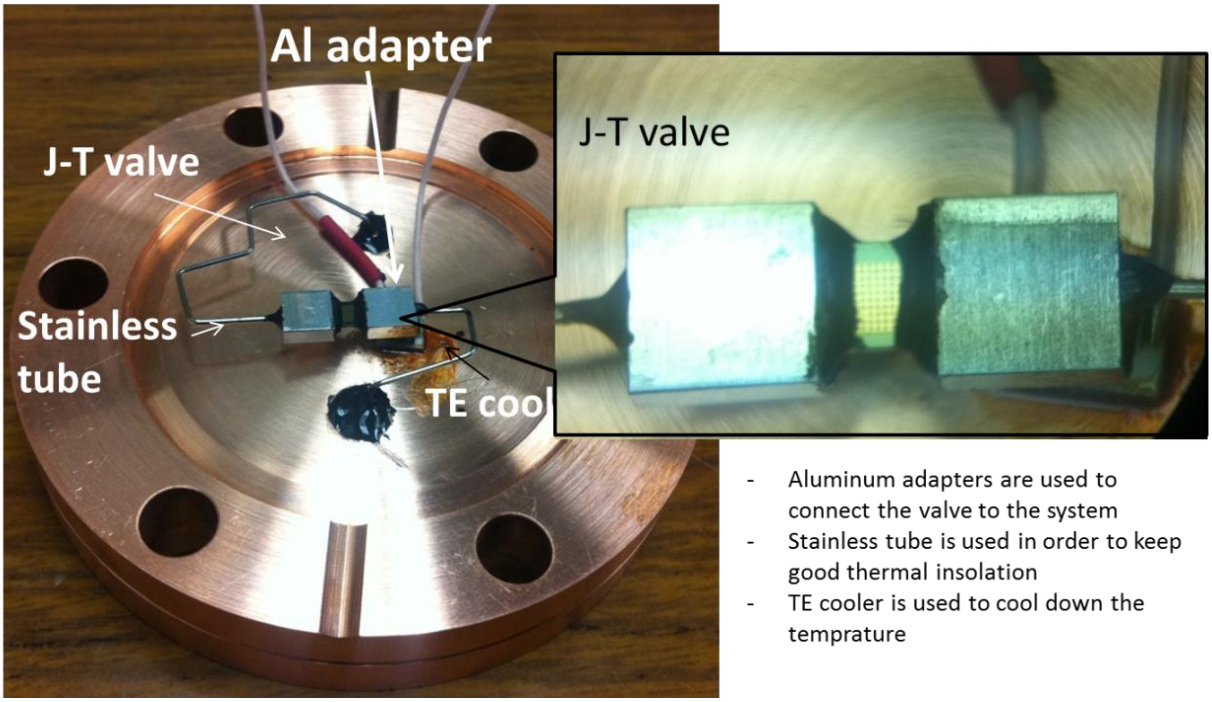

Figure 7.5: Schematic of the assembly of the test vehicle for connecting the valve to the system.

7.3.4 Test setup

To measure the pressure drop v.s. the flow rate of polyimide valve, we constructed a measurement apparatus as shown by the schematic in Figure 7.6. The valve was connected and epoxy-sealed to aluminum and then connected to a copper flange with stainless tube. The flange is compatible with our cooling test setup as described in Chapter 6, which includes a miniature compressor composed of a miniature piston oscillator and micro-machined check valve assembly [16]. A TE cooler was then placed under the test valve assembly so that the valve can be tested under different temperatures. The MCC was held in a vacuum of $<10^{-4}$ Torr during the cooling tests, to minimize heat loads associated with conduction through air. The lowest temperature reached is 252K by using a TE cooler with 100 mW heat lift for maximum cooling temperature of 60 °C (dT_{max}). A valve at the high pressure side of the J-T valve was used to adjust the pressure (see Figure 6.4).

A temperature sensor is epoxy-bonded on top of the assembly to test the temperatures, since the thin gap (g=3.2 μm) severed as a very good "heat exchanger", the average fluid temperature inside the valve was considered to be same to the temperature measured on the assembly. The actual temperature difference of the fluids going through and the solid part can be calculated using [48]

$$\Delta T = (T_{in} - T_{TE})\, e^{\frac{-\pi \times 3.66 \times k \times W \times L}{g C_p \dot{n}}} \tag{7.1}$$

where T_{in} is the inlet fluid temperature, T_{TE} is the temperature of the wall of the channel, which is considered to be same to the measured temperature due to a good thermal conductivity of the aluminum and silicon; L is the length of the channel and W is the width of the channel, g is

height of the gap, C_p is the average specific heat of the mixture for a given pressure and temperature range. $\dot{n}$ is the flow-rate in mole/s.

To understand that ΔT is negligible in our interested flow and temperature range, we can take a calculation for a specific case. For example, for a conservative assumption, even when the inlet mixture will be precooled with the aluminum fixture, we still assume it is 295 K as a worst case. In this case, by using equation (6.3), ΔT is only 1.4 K when choosing a T_{TE} of 252 K which was the lowest temperature in our experiment and a flow-rate of 40 sccm which was the largest number in our experiment, 150 μm of the channel is good to make the ΔT to be about 1.4 K. The calculation suggests that in our tests which are to be reported in the following sections, it is okay to assume that the temperature of the fluid is same to that we are measuring.

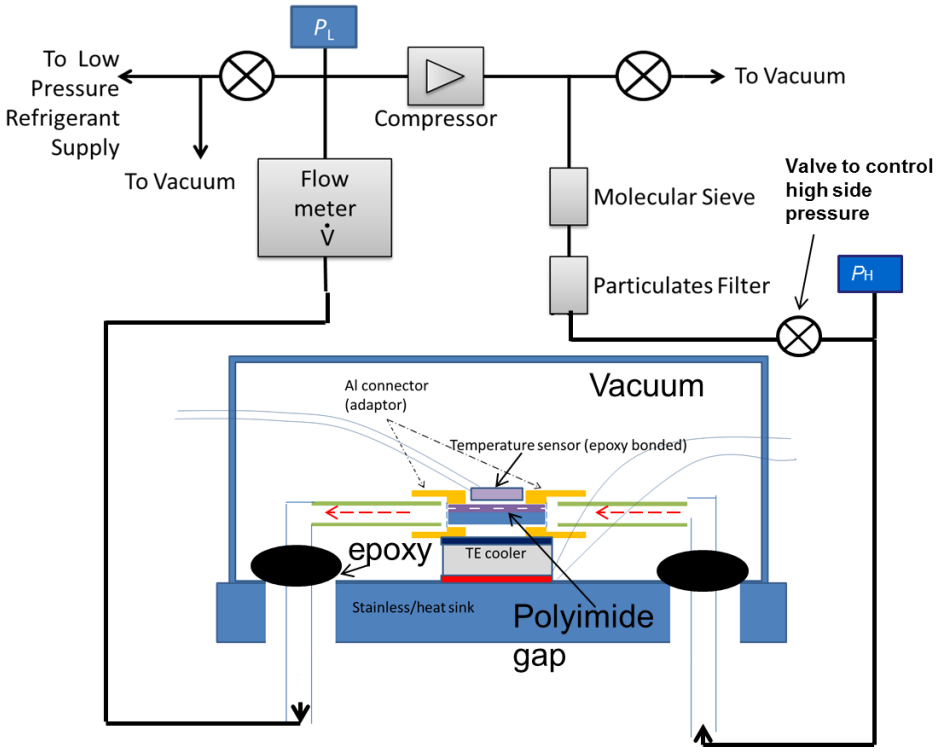

Figure 7.6: Schematic of the measurement apparatus to test the valve restriction under different temperature. By making a good thermal isolation design, TE cooler

can be used to enable a low cost system to test the valve restriction at low temperature.

7.3.5 Models for flow restriction

To calculate the flow restriction of the pressure drop in a flow channel where the flow can be considered as laminar flow is given in [15],

$$dp = \frac{2f_r(\dot{m}/A_g)^2}{\rho D_h} dl, \tag{7.2}$$

where f_r is the Fanning friction factor, $\dot{m}$ is the mass flow rate in the flow channel, ρ is the density of the fluid, and A_g is the cross-sectional area of the flow channel. For a plate form where the width of the channel is much larger than the gap, f_r is given by

$$f_r = \frac{24}{N_{re}}, \tag{7.3}$$

where the Reynolds number N_{re} can be expressed as

$$N_{re} = \frac{D_h}{\mu(A_g/\dot{m})}, \tag{7.4}$$

and μ is the viscosity of the fluid. By using nitrogen gas to estimate, at room temperature, the viscosity can be approximated as a constant for pressures less than 1 MPa (about 10 bar). In such a case, equation (7.2) can be simplified to be

$$dp = \frac{48\dot{m}\mu}{A_g D h^2 \rho} dl \tag{7.5}$$

The high side pressure then can be calculated using

$$\int_{P_L}^{P} P\,dp = \int_{0}^{L} \frac{48\dot{m}\mu}{A_g D h^2 \rho}\,dl, \tag{7.6}$$

However, to use the equation, the flow has to be laminar flow which is the situation in our study. For a flow-rate of nitrogen of 100 sccm, which is even more than largest flow-rate (40 sccm) in the interested range, the number N_{re} is calculated to be 109 with the density of nitrogen gas given as 1.165g/L in standard condition indicating that the nitrogen flow is laminar in the interested range. For the mixtures in our study, the standard densities of mixtures are usually similar to it of the nitrogen, which means that mass flow-rate $\dot{m}$ of the mixture for a same volume flow-rate (40 sccm as the largest interested) is similar to that of nitrogen, on the other hand, viscosity of mixture μ is always large than that of nitrogen indicating that the mixture can also be treated as laminar flow here.

For mixture flow under low temperature, the flow becomes two-phase. The homogeneous model is the simplest approach to the prediction of two-phase flows is to assume that the phases are thoroughly mixed and can be treated as a single-phase flow so that equation 7.6 is still applicable. For the homogeneous model, the bulky density and viscosity were given in [50]:

$$\rho_H = \frac{\rho_G \rho_L}{x\rho_L + (1-x)\rho_G}, \tag{7.7}$$

$$\frac{1}{\eta_{hp}} = \frac{x}{\eta_G} + \frac{(1-x)}{\eta_L} \tag{7.8}$$

where ρ_G and ρ_L are the gas and liquid densities and x is the quality (fraction of the total mass flow which is vapor). η_G and η_L are the gas and liquid viscosities respectively. The liquid and vapor properties of the mixture under different pressures and temperatures can be generated

using NIST- REFPRO. For example, under temperature of 252K, the properties of the five components mixture optimized for 275K-160K under different pressures are shown in Table 7.1.

Table 7.2 The liquid and vapor properties of the 275 - 160 K mixture (34% ethane, 22% ethane propane, 22% ethylene, 12% isobutane, 12% isopentane) generated using NIST-REFPRO.

Temperature (K)	Pressure (MPa)	Density (kg/m³)	Quality (kg/kg)	Liquid Phase Viscosity (µPa-s)	Vapor Phase Viscosity (µPa-s)
252.00	0.10000	1.6404	0.96329	333.37	8.1810
252.00	0.11000	1.8363	0.92977	330.22	8.2243
252.00	0.12000	2.0340	0.90162	327.18	8.2616
252.00	0.13000	2.2334	0.87749	324.24	8.2942
252.00	0.14000	2.4345	0.85647	321.40	8.3232
252.00	0.15000	2.6372	0.83789	318.66	8.3492
252.00	0.16000	2.8415	0.82129	316.00	8.3727
252.00	0.17000	3.0474	0.80632	313.44	8.3941
252.00	0.18000	3.2549	0.79270	310.96	8.4138
252.00	0.19000	3.4639	0.78022	308.56	8.4321
252.00	0.20000	3.6743	0.76873	306.23	8.4490
252.00	0.21000	3.8863	0.75808	303.97	8.4649
252.00	0.22000	4.0996	0.74818	301.78	8.4797
252.00	0.23000	4.3144	0.73893	299.65	8.4937
252.00	0.24000	4.5305	0.73026	297.58	8.5069
252.00	0.25000	4.7479	0.72211	295.56	8.5194
252.00	0.26000	4.9666	0.71442	293.60	8.5313
252.00	0.27000	5.1867	0.70715	291.68	8.5426
252.00	0.28000	5.4080	0.70026	289.81	8.5534
252.00	0.29000	5.6306	0.69371	287.98	8.5637
252.00	0.30000	5.8544	0.68748	286.19	8.5737
252.00	0.31000	6.0794	0.68154	284.44	8.5835
252.00	0.32000	6.3056	0.67587	282.73	8.5930
252.00	0.33000	6.5330	0.67044	281.05	8.6022
252.00	0.34000	6.7616	0.66523	279.40	8.6110
252.00	0.35000	6.9914	0.66023	277.78	8.6196
252.00	0.36000	7.2223	0.65542	276.19	8.6278
252.00	0.37000	7.4544	0.65080	274.63	8.6359
252.00	0.38000	7.6877	0.64634	273.09	8.6437
252.00	0.39000	7.9221	0.64203	271.58	8.6512
252.00	0.40000	8.1576	0.63787	270.09	8.6586

7.3.6 Test and discussions

Valve restriction using nitrogen

N_2 gas was first used to check error of the system and tested as a simple reference. 4 different kinds of test vehicles in different dimensions have been tested. The result is shown in Figure 7.5. Testing results are presented as the spots while the calculation results are presented as curves in the graph. The results suggest that the testing is generally according well to the modeling. However, in the lower flow rate range, discrepancy of the pressure drop are of larger numbers, this is because that in the low flow rate range, the pressure is more sensitive to flow rate, in this case, any small error in reading the flow rate will induce relative larger error of pressure discrepancy. For the device of set-4, we have repeated the tests for 6 times and error bars are present in figure, the result shows that the repeatability of one device is good.

In Figure 7.5, one can find that the device of set-4 shows a large discrepancy between test and calculation to that of other sets. This is because of the propagation of uncertainties. Specifically, for a comparison between set-1 and set-4, the only difference is that the width of set-4 is 3 times of that of set-1. In the valve restriction equation (7.1), $\dot{m}$ is proportional to the Ag if other parameters are fixed, so for a specific valve, e.g. of set-1, if the flow-rate under a certain pressure is $\dot{m}_1$, the flow rate $\dot{m}_2$ under same pressure for set-4 should satisfy:

$$\dot{m}_2 = 3 \times \dot{m}_1 \tag{7.9}$$

In this case, according to the theory of propagation of uncertainties [49], if $\delta\dot{m}1$ if the uncertainty of measuring of $\dot{m}_1$, the uncertainty of for flow-rate $\dot{m}_2$ is:

$$\delta\dot{m}_2 = 3 \times \delta\dot{m}_1 \tag{7.10}$$

which suggest that in Figure 7.7, the obvious larger discrepancy between test and calculation for set-4 compared to other set is reasonable.

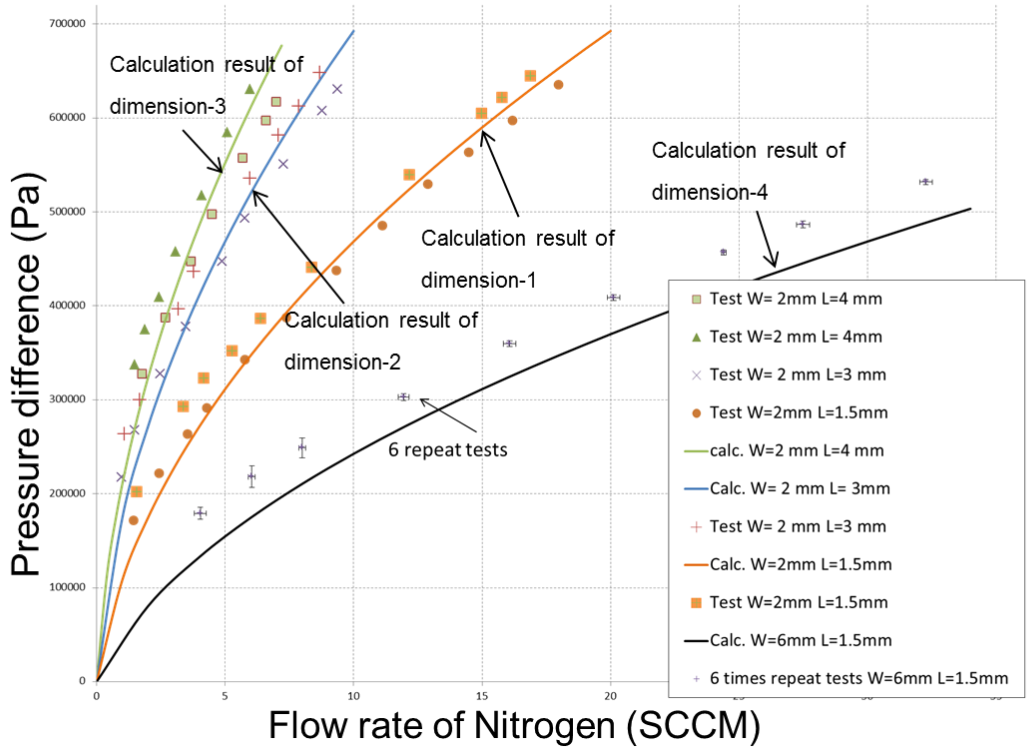

Figure 7.7: Calculation and measurement result of the valves' restriction using nitrogen as the flow.

Valve restriction test of a five components mixture

In order to understand the performance of the valve for a complicated cryogenic fluid, a mixture of 5 components (34% ethane, 22% ethane propane, 22% ethylene, 12% isobutane, 12% isopentane in mass fraction) which optimized by the program NIST4 [5] to maximize $(\Delta h|T)_{min}$ in the range of 275 K to 160 K with a high pressure of 4.0 bar and a low pressure of 1.0 bar was also used to conduct the flow resistance measurements. There were several reasons for choosing this mixture as a candidate for this study. Firstly, the components of this mixture using was similar to the one used for the 200 K demonstration in Chapter 6. Secondly, the mixture itself was designed for a 275 K-160 K cooling which is being used in the future cooling demonstration

in this project therefore measured results can directly benefit the future work. Thirdly, compared to the other similar mixtures, this mixture won't be liquefied at room temperature for relatively higher pressure, e.g. up to 5 atm. This can make the testing go up for comparatively higher pressure range (up to 5.5 atm compared to only 2 atm with the 300-200 K mixture mentioned in Chapter 6) by avoiding the condensing and liquid hold-up problem. Figure 7.8 illustrates the condensation and liquid hold-up problem of the mixture. Some components could be liquefied even at room temperature when the pressure is high, e.g. pentane at 5.5 atm. These liquid components were held in the large tube in the high pressure side of the testing setup. Once the liquid hold-up happened, the actual components went through the valve were changed from that of the original mixture. This could result a changing of the mixture we measured when the pressures were changed and the changed mixture components are not accurately predictable making us had no idea what we were testing.

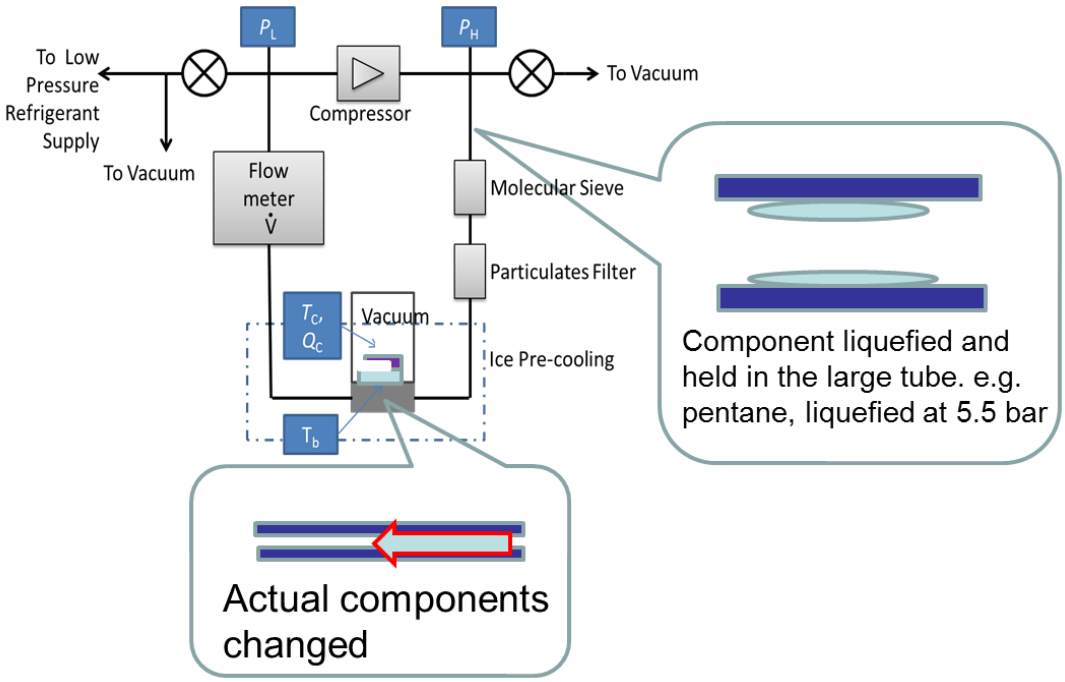

Figure 7.8: Illustration of the condensing and liquid hold-up problem of the 300-200K mixture.

Even used the 275 K-160 K mixture which can avoid the large tube liquid hold-up problem, one thing needs to be noticed is that when the temperature went down liquefaction could still happen in the valve assembly's small cold volume. However, since the cold volume was is very small, we expected that the liquid accumulation can reach to a certain level quickly and be sent through the valve finally. To verify that condensing and liquid hold-up in the small cold volume won't induce the components changing problem, samples of mixture after going through different temperatures were collected and analyzed. The components analysis results are shown in Figure 7.8. The results indicated that there was no major permanent components change after the mixture went through a valve at both room temperature and 256K. The result confirmed our assumptions discussed above making us believe the components kept consistence for the test conducted at three different temperatures of 295 K, 265 K, and 252 K.

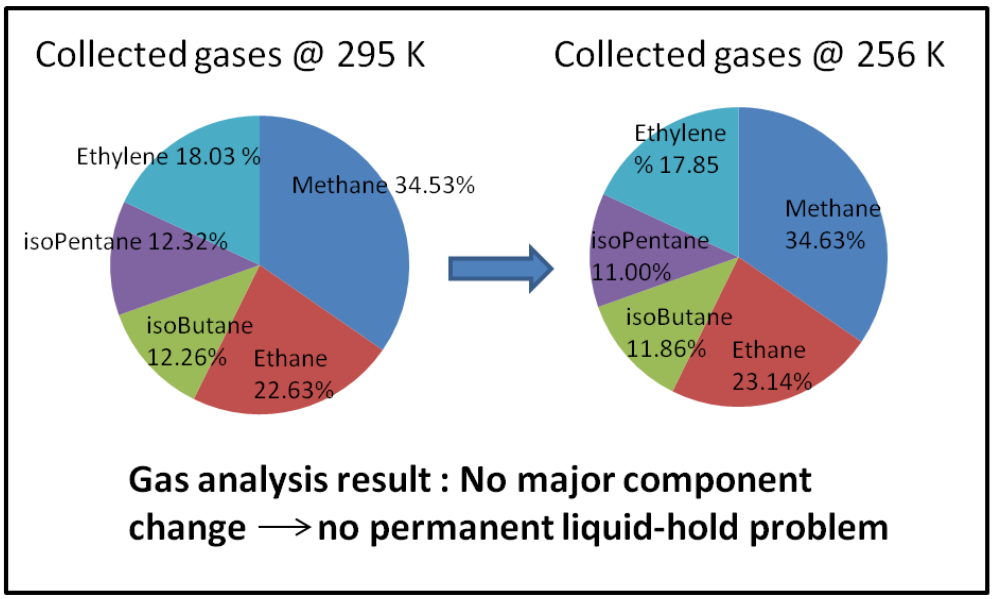

Figure 7.8: Comparison of components analysis of the 275-160 K mixture between experiment conducted under 295K and 256K.

As can be seen in Table 7.2, at 252 K, the vapor quality was about 64% before it gets into the valve when it is under 4 bar pressure which indicate that there were enough liquid existing in the system. Figure 7.9 shows the tested valve restriction for the 275 -160 K mixture (34% ethane, 22% ethane propane, 22% ethylene, 12% isobutane, 12% isopentane in mass fraction) under three different temperatures of 295 K, 265 K and 252 K.

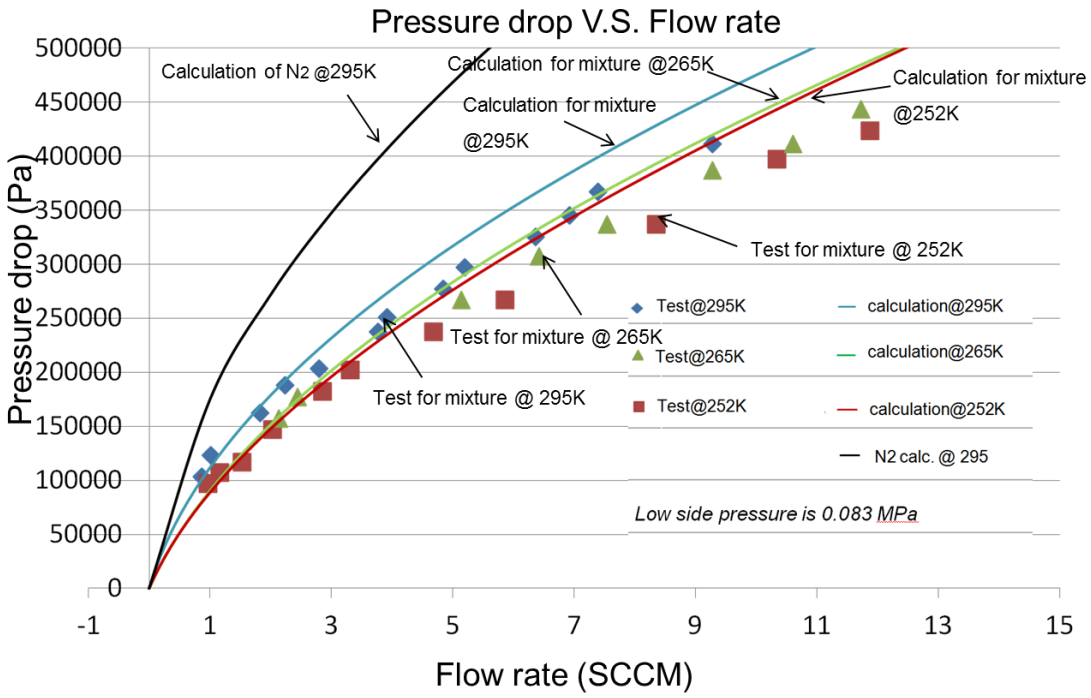

Figure 7.9: Calculation and measurement result of the valves restriction for 275-160 K mixture under different temperature; the tested valve was of set-2 in Table 7.1.

In Figure 7.9 we also compared the test results (dots in the figure) to the result calculated with homogeneous model assistant with NIST-REFPRO introduced in Section 7.3.5, the result

has suggested a good match between them for different temperature. A calculation of the restriction of nitrogen at room temperature was also plotted in the figure as a reference.

By playing with a calibration factor, specifically, in equation (7.5), if we introduce a calibration factor K_c and choose the right number, we can fit the calculation curve to the measurement very well. K_c shown in the figures are 0.91, 0.91 and 0.88, however, they are all treated as 0.9 since the data were not good enough to us the accuracy down to 0.01) (see Figure 7.10, 7.11 and 7.12).

$$K_c \times d_p = \frac{48\dot{m}\mu}{A_g D h^2 \rho} dl \tag{7.12}$$

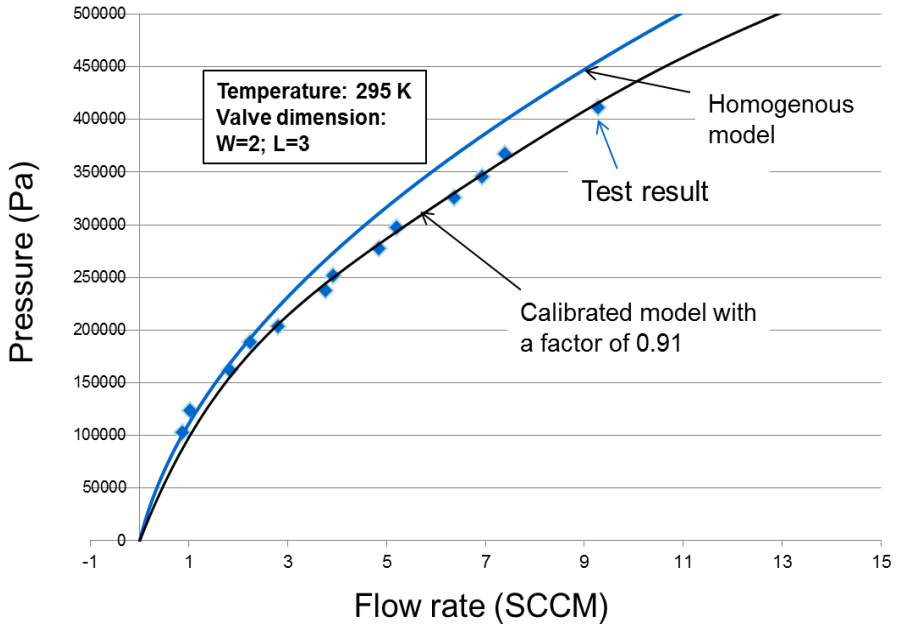

Figure 7.10: Calculation, calibrated calculation and 6 times repeat measurement results of the valves restriction for 275-160 K mixture under 295 K; the valve tested was of set-2 in Table 7.1.

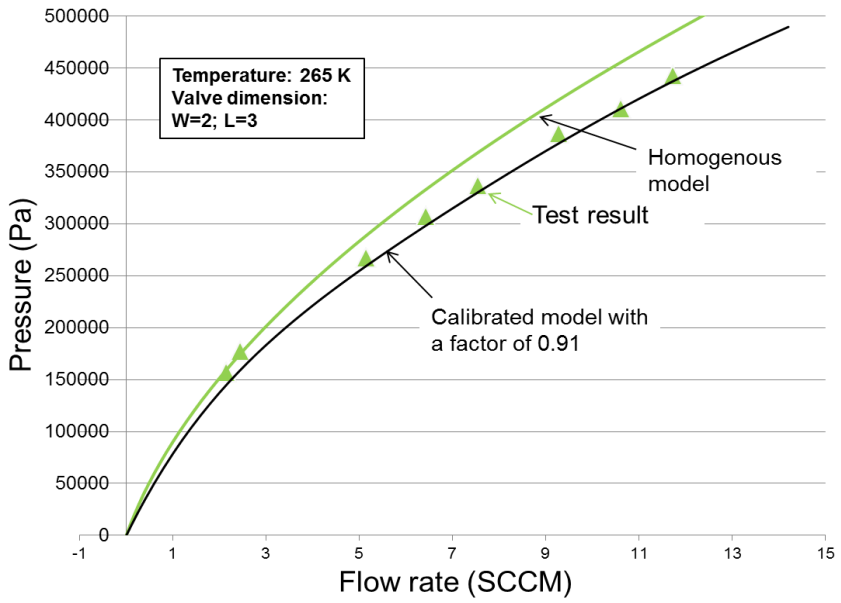

Figure 7.11: Calculation, calibrated calculation and measurement result of the valves restriction for 275- 160 K mixture under 265 K; the valve tested was of set-2 in Table 7.1.

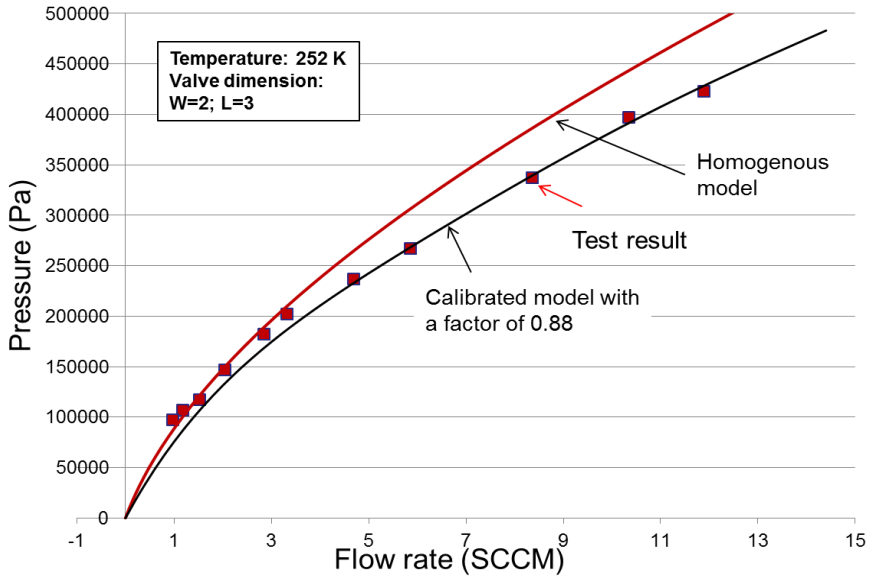

Figure 7.12 Calculation, calibrated calculation and measurement result of the valves restriction for 275- 160 K under 252 K; the dimension of the tested valve was of set-2 in Table 7.1.

In Figure 7.9, for the condition under 295 K, since the mixture were all gases, the test result should fit better to the single model (for the same valve tested with N_2 only 5% discrepancy was estimated). However, there was still a 0.9 discrepancy between the prediction and measurement. This is partially because of a calibration gap of the flow meter itself for testing mixture. In the flow meter, there is an internal built calibration coefficient for testing different gases. This coefficient could induce a 10% error when tested mixture, which suggested that our test results could have up to 10% errors to the real flow-rate numbers. The results of Figure 7.10 and Figure 7.11 suggest that when the temperature goes down and start to have two-phase flow, e.g. 252K, according a mass fraction of liquid in the inlet end of 36%, the homogenous model was still good to predict the flow resistance.

In Figure 7.13, there are the 6 times repeating test results and according calculations and calibrations for the same dimension of the valve discussed in Figure 7.9 to Figure 7.12. The results suggested that the repeatability of the tests were good. The raw data of the repeated tests can be found in appendix E.

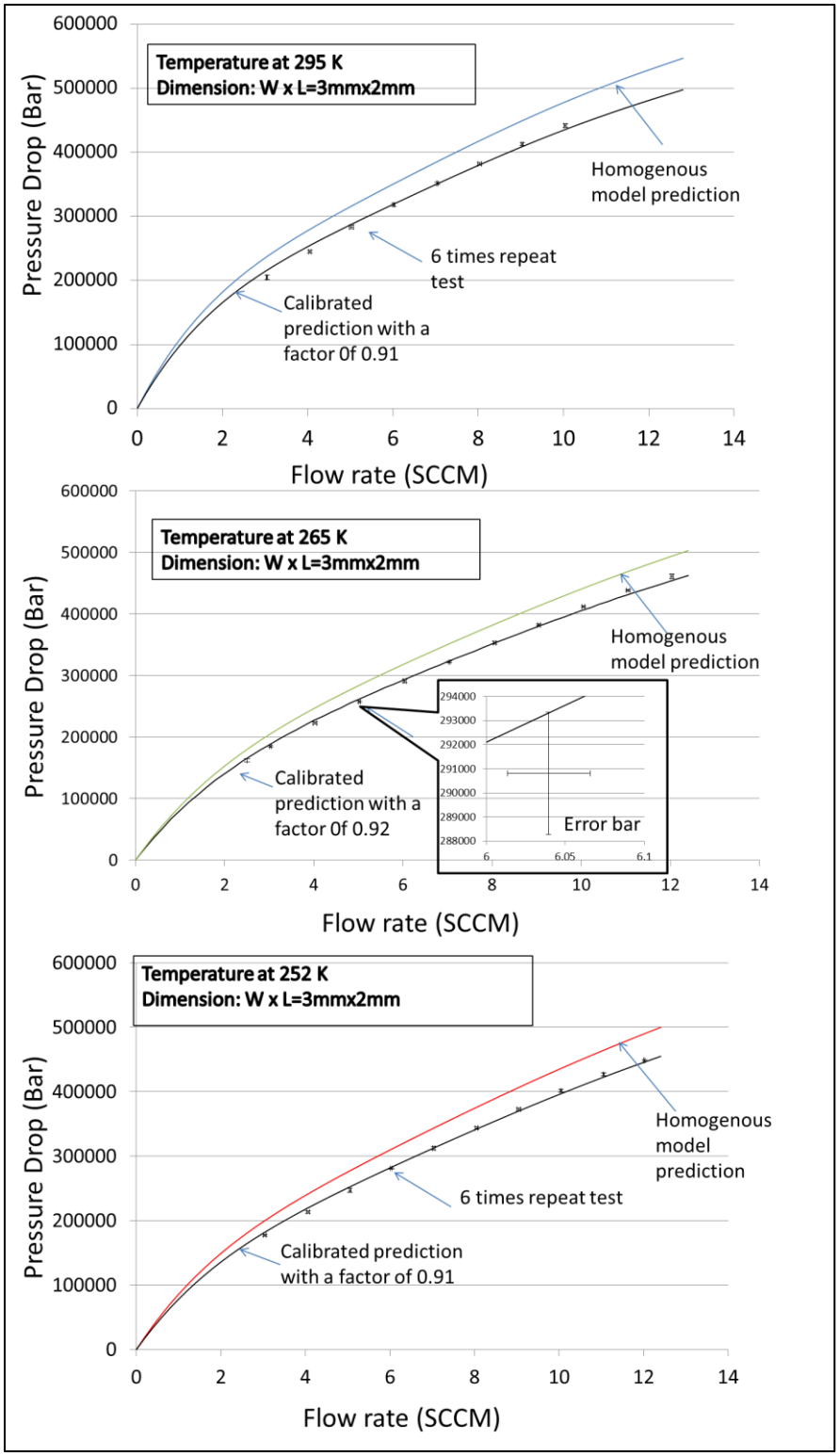

Figure 7.13 Calculation, calibrated calculation and measurement result of 6 times of the valves restriction for 275- 160 K mixture under 3 different temperatures; the dimension of the tested valve was of set-2 in Table 7.1.

Based on the above discussion, there are several J-T valve design suggestions generated as following:

(1) For mixture without liquid hold up issue and under similar liquid fraction condition, one can directly use the developed homogenous model to predict the flow restriction for valve in such a small dimension (micro gap).

(2) For mixture without liquid hold up issue and with larger liquid fraction condition. One can still use the developed homogenous model to predict the flow restriction, however, one should notice that larger error by using the model could happen due to more contribution to potential two phase separation, in that case, a different calibration number may be need, to estimate the number, one can follow the process develop in the study.

(3) For mixture with different components designed for different temperature range which could has the liquid condensing and hold-up issue, one can calculate the real components going through the valve after it reach to an equilibrium situation and then apply the developed homogenous model to predict the flow restriction. The calculation method of the varied components after condensing and reach to equilibrium is elaborated in [37]. After the calculation of the real components getting through the valve, the method can be applied by considering the suggestions (1) and (2).

7.4 Conclusion

In this study, we have designed and conducted an experimental test to study the valve flow restriction under different temperatures with limited thermoelectric (TE) cooling. Test vehicles with micro gaps have been designed and fabricated to simulate the polyimide J-T valve used in MCC. The restrictions of the valve have been tested with a N_2 gas and a five components

mixture. The measured results match well to the calculated ones resulting from the use of a homogenous two phase flow model with properties estimated using NIST-REFPRO software. A calibration constant of 0.9 was found to be needed when use the homogenous model to predict the flow resistance. The 0.9 calibration number was partially contributed by a calibration gap of the flow meter itself when test mixtures beside for that by the process variation. The model verified can be used to predict the flow resistance for a micro gap valve under certain temperatures and flow types conditions. Several design suggestions have been developed based on the results and discussions. The model and the method developed are important to design future micro-scaled J-T valves for the polyimide MCC.

CHAPTER 8: SUMMERY AND FUTURE WORKS

8.1 Summery

In this thesis, we present the fabrication and test of a novel polymide-based Joule-Thomson (J-T) micro cryogenic cooler (MCC). Monolithic fabrication processes for high pressure polymer channels and 3-D interconnects for fluid channels including a valve have been developed for a planar MCC. In general, an MCC consists of a cold stage and a compressor. However, MCC has been used to represent the planar cold stage in this thesis work. This representation may not be accurate; however, it is has been used by most of previous publications related to MCC. In addition, the planar processes can be used to fabricate future compressors compatible with the planar cold stage. The MCC, i.e. the planar cold stage, consists of a polymer heat exchanger (HX) and a silicon/glass J-T valve. The cooling temperature reachable was around 233 K under an operation pressure ratio of 0.7:0.15 MPa by using a custom-designed mixed refrigerant. It is the first demonstration ever reported for the J-T MCC fabricated and assembled based on wafer-level, planar thin-film processes.

After the demonstration of the first polyimide-based MCC, we identified a mechanical by-pass leakage problem. And, we improved the fabrication method by designing a monolithic polyimide MCC. The fabrication is based on surface micro-machining technology using electroplated copper as the sacrificial layers and polyimide as the structural material. The process includes multi-layers of metallization of copper, spin coating and curing of polyimide, and patterning on each layer. One of the techniques enabling this novel approach is the development of the wafer-level 3-D interconnect for making high pressure, (e.g. 10 atm) polymer fluid micro channels. To evaluate the performance of MCC, a five-component fluid mixture was used as a refrigerant. The cold tip was able to reach to about 190 K under a refrigerant pressure ratio of

only 5.5 : 1.1 bar. In addition to the monolithic wafer-level processing capability, this approach is also scalable to meet different refrigeration requirements.

The J-T valve in the all-polymer MCC is an essential part therefore we have studied the valve in details. We have developed a model to predict the flow rate and pressure drop for a given gap; the model was verified by the experimental data for the cases with pure nitrogen and the 5-component mixture. Several design suggestions have been developed based on the modeling results and discussions. This model can be used to design the optimum J-T valve for MCC.

Major contributions of this work are summarized below:

(1) Developed the world's first polymer-based micro cryogenic cooler, which was the also the smallest MCC at the time of publication. It should be noted that MCC is used to represent the cold stage of a cryocooler in this thesis work and in most of previous studies.

(2) Developed a monolithic fabrication method for 3-D interconnection of a multi-channel structure. The method allows us to selectively interconnect horizontal channels in different layers.

(3) Achieved a high thermal isolation design for MCC to minimize the refrigeration losses.

(4) Developed a process to study the flow restriction in a J-T valve with mixtures at different temperatures.

(5) Developed and verified an effective model to predict the flow behavior of the J-T valve under certain limitations assumed.

8.2 Future Work

8.2.1 Hermetic sealing for packaging

Hermetic sealing is important to ensure a vacuum package for MCC. It is essential to maintain a reliable vacuum environment for closed MCC with negligible refrigerant losses for years.

Diffusion rates through polymer are generally much more worse than those through inorganic materials , e.g. silicon, metal. The polyimide-based MCC and epoxy-bonded seal and interfaces are not acceptable for hermetic seal. Atomic Layer Deposition (ALD)-based moisture barrier coatings can provide a nanoscale, conformal, pinhole-free, hermetic alumina coating on the polymer substrate [51] [52] [53] [54]. Since the coating is at nanoscale, the induced thermal conduction loss and mechanical effect will be negligible. Because of its conformal coating and low temperature process, e.g. 100 ℃ to 150 ℃, the fabricated polyimide MCC package can be encapsualated at the end of the manufacturing process and transformed from non-hermetic to hermetic ones.

However, defects of the barrier coating can be generated during the deposition process or operation resulting from strains. Further understanding of these potential challenges is important to apply this technology for the hermetic sealing of the polymer-based MCC.

8.2.2 Fully integration of MCC

For a portable system consideration, the MCC is going to be integrated with miniature or micro compressors, thermal electrical cooler, vacuum packaging, pressure sensors, temperature sensors, getter, functional sensor, control electronics, and power electronics [10].

MEMS-enabled micro compressor, with pressure ratios above 4:1 bar, has been demonstrated by other team members of the MCC project at the University of Colorado – Boulder (CU-Boulder). Such pressure ratios are high enough to drive vapor-compression and

Joule-Thomson refrigeration systems [55]. Meanwhile, MEMS compressor can improve these microcompressor with additional size reductions of 10 × or 100 ×. Such a compressor is also being studied here at CU-Boulder [6].

Figure 8.1 illustrates the schematic of a future fully integrated MCC with a MEMS compressor and a sensor to be cooled. It is always a challenge to design and fabricate such complicated micro fluid systems [10]. This thesis has integrated the heat exchanger, cold heat including the J-T valve with wafer-level processes. Naturally, we should extend the integration to cover the MEMS compressor and the fluid couplings between the heat exchanger and the compressor.

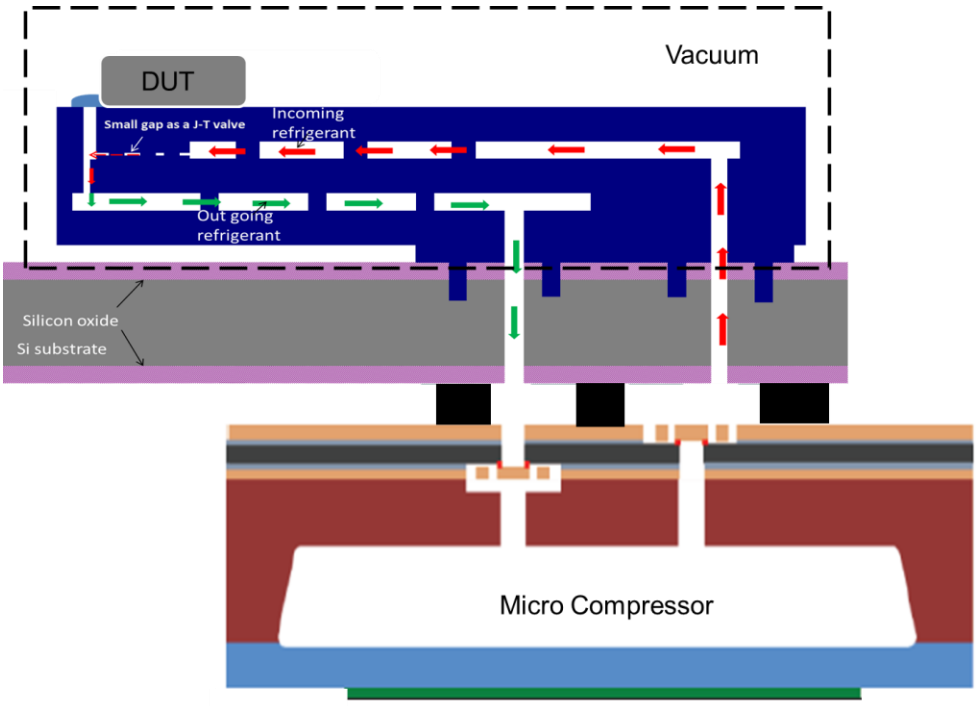

Figure 8.1: Schematic of a fully integrated MCC with a MEMS compressor and a sensor to be cooled.

APPENDICES

Appendix A: List publications related to this dissertation

Related works can be found in:

[1] **Yunda Wang**, Ryan Lewis, M.-H. Lin, Ray Radebaugh and Y.C. Lee "The Development of Polymer-Based Planar Micro Cryogenic Coolers" IEEE/ASME J. of MEMS, 2012, in press.

[2] **Yunda Wang**, Ryan Lewis, M.-H. Lin, Ray Radebaugh and Y.C. Lee "Wafer-level Processing for Polymer –based Planar Micro Cryogenic Coolers", Proc. of IEEE MEMS'12, Paris, France, Jan. 29 - Feb. 2, 2012 pp.341-344

[3] **Yunda Wang**, Ryan Lewis, M.-H. Lin, Yiwei Yan, Ray Radebaugh Peter Bradley and Y.C. Lee "A Monolithic Polyimide Micro Heat Exchanger with a Suspended 3D Parallel Channels Structure for Cryogenic Application," Proc. IMECE2011, Denver, CO, Nov. 11-17, 2011.

[4] Ryan Lewis, **Yunda Wang**, Mu-Hong Lin, Marcia L. Huber, Ray Radebaugh, Y.C. Lee, "Enthalpy Change Measurements of a Mixed Refrigerant in a Micro Cryogenic Cooler in Steady and Pulsating Flow Regimes" *Cryogenics*, in press

[5] Ryan Lewis, **Yunda Wang**, Jill Cooper, M.-H Lin., Victor Bright, Y.C. Lee, Peter Bradley, Ray Radebauth, and Marcia Huber "Micro Cryogenic Coolers for IR Imaging", SPIE 2011., 2011, pp 8012-75

[6] Ryan Lewis, Hayley Schneider, **Yunda Wang**, Ray Radebaugh, Y.C. Lee, "Two-phase Flow Patterns and Cooling Power of Mixed Refrigerant in Micro Cryogenic Coolers" ASME ICNMM2012, July 8-12, 2012.

[7] Ryan Lewis, M.-H. Lin, Jill Cooper, **Yunda Wang**, Marcia Huber, Peter Bradley, Ray Radebaugh and Y.C. Lee "Demonstration of an Integrated Micro Cryogenic Cooler and Miniature Compressor for Cooling to 200K," Proc. IMECE2011, Denver, CO, Nov. 11-17, 2011.

Potential future publications are:

[8] **Yunda Wang**, Ryan Lewis, M.-H. Lin, Ray Radebaugh and Y.C. Lee "Design and Fabrication of All-Polymer Planar Micro Cryogenic Coolers" being prepared for IEEE/ASME J. of MEMS, 2013

[9] Ryan Lewis, **Yunda Wang**, Peter E. Bradley, Marcia L. Huber, Ray Radebaugh, Y.C. Lee, "Experimental Investigation of Low-pressure Refrigerant Mixtures for Micro Cryogenic Coolers" submitted to Cryogenics, 2012

[10] Ryan Lewis, M.-H. Lin, Jill Cooper, **Yunda Wang**, Marcia Huber, Peter Bradley, Ray Radebaugh and Y.C. Lee "Demonstration of an Integrated Micro Cryogenic Cooler and Miniature Compressor for Cooling to 200K," Accepted at Journal of Thermal Science and Engineering Applications, Sept 2012.

[11] Ryan Lewis, **Yunda Wang**, Ray Radebaugh, Marcia L. Huber, "Study of Mixed Refrigerant Undergoing Pulsating Flow in Micro Coolers with Pre-cooling," being prepared for Cryogenics, October 2012.

Appendix B: Standard operation of procedure of fabrication of the silicon valve chip of for polyimide-based MCC

The following steps numbers are according to that in Figure 4.6.

(1) Thermal oxidation.

- Prepare double side polished (DSP) 3 inch (76 mm) n-type <100> silicon wafer of 380 μm in thickness
- Wet thermal oxide use CNL standard oxidation Instruction on CNL's Lindberg Diffusion/oxidation/annealing furnace 85304
- Wet oxidation of 1.8 μm SiO_2 for about 7 hrs

(2) Pattern front side for the through holes.

- Spin coat photoresist AZ- 4620 on front side at 1600rmp for 60 s
- Prebake on hotplate @ 110 °C for 4 minutes
- Expose using CNL Karl Suss MJB3 Mask aligner-I to expose for 3'15'' @ 195W (using CH Mask-1)
- Develop in developer (AZ400K:H_2O=1:2.5) for 5-10 minutes (inspection under micro scope is need to make sure the photoresist are properly developed)
- O_2 plasma for 1 minute (repeat if required)
- Post bake the wafer for 2 minutes @ 110 °C
- Do RIE etching on the front side of the wafer using CNL Plasmatherm 540/540 Dual Chamber RIE system: etch for 25 minutes for Silicon oxide (4 sccm O2 + 16 sccm CF4 @ 150W); rotate the wafer and etch for another 25 minutes
- Clean off the photoresist use the standard acetone + IPA procedure in CNL

(3) Backside SiO_2 was patterned using RIE.

- Spin coat photoresist AZ- 4620 on back side at 1600rmp for 60 s

- Prebake on hotplate @ 110 °C for 4 minutes
- Expose using CNL Karl Suss MJB3 Mask aligner-II (front-to-back alignment) to expose for 2'15'' @ 275 W (using CH Mask-2)
- Develop in developer (AZ400K:H_2O=1:2.5) for 5-10 minutes (inspection under micro scope is need to make sure the photoresist are properly developed)
- O_2 plasma for 1 minute (repeat if required)
- Post bake the wafer for 2 minutes @ 110 °C
- Do RIE etching on the back side of the wafer using CNL Plasmatherm 540/540 Dual Chamber RIE system: etch for 25 minutes for Silicon oxide (4 sccm O_2 + 16 sccm CF4 @ 150W); rotate the wafer and etch for another 25 minutes

(4) Pattern the front side gap area and thinner the SiO_2 for secondary mask.

- Spin coat photoresist AZ- 4620 on front side at 1600rmp for 60 s
- Prebake on hotplate @ 110 °C for 4 minutes
- Expose using CNL Karl Suss MJB3 Mask aligner-I to expose for 3'15'' @ 195W (using CH Mask-3)
- Develop in developer (AZ400K:H_2O=1:2.5) for 5-10 minutes (inspection under micro scope is need to make sure the photoresist are properly developed)
- O_2 plasma for 1 minute (repeat if required)
- Post bake the wafer for 2 minutes @ 110 °C
- Do RIE etching on the front side of the wafer using CNL Plasmatherm 540/540 Dual Chamber RIE system: etch for 20 minutes for Silicon oxide (4 sccm O_2+ 16 sccm CF_4 @ 150W
- Clean off the photoresist use the standard acetone + IPA procedure in CNL

(5) DRIE to etching on front side.

- Distribute crystal bond 555 on a bare silicon wafer (as a backup wafer) under hotplate of 95 ℃
- Bond the backside of the wafer under processing to the backup wafer and make the front side exposed
- Do DRIE etching using NIST STS DRIE using standard silicon etching recipe at an etching rate about 1.1 μm/cycle
- Etching for 227 cycles for about 250 μm
- Take off the wafer on hot plate set @ 95 ℃
- Clean off the crystal bond residue using the standard acetone + IPA procedure in CNL

(6) DRIE to etching on back side to make the "lego".

- Distribute crystal bond 555 on a bare silicon wafer (as a backup wafer) under hotplate of 95 ℃
- Bond the fronside of the wafer under processing to the backup wafer and make the backside exposed
- Do DRIE etching using NIST 3'' DRIE using standard silicon etching recipe: "specnod"
- Etching until the holes are etched through and the backup wafer will been seen (usually take 200 cycles)
- Take off the chips on hot plate set @ 95 ℃
- Clean off the crystal bond residue using the standard acetone + IPA procedure in CNL 5mins ultrasonic respectively

(7) Metalize the silicon valve chip for soldering

- Spin coat photoresist AZ- 4620 on a 3" bare wafer at 1600rmp for 60 s
- Place the silicon valve chips on the wafer while making the front side of chips to upside.
- Bake the wafer on hotplate @ 110 ℃ for 4 minutes
- Evaporate Ti/Cu/Au for 40nm/1um/100nm respectively (with a standard fast vacuum plasma for 5mins)
- Take off and clean chips using the standard acetone + IPA procedure in CNL 5mins ultrasonic respectively

(8) Etch away the silicon oxide of the gap area using BOE

- Spin coat photoresist AZ- 4620 on a 3 glass slide at 1600rmp for 60 s
- Place the silicon valve chips on the glass slide while making the front side of chips to upside.
- Bake the glass slide on hotplate @ 110 ℃ for 4 minutes
- Etch away the gap area SiO_2 for about 12 minutes (don't depends on the time, check frequently to inspect until the silicon substrate is exposed)
- Immerse the glass slide in DI water for 5 minutes and dry up with N_2 gun.

(9) Etch the silicon valve

- O_2 plasma the chips on glass slide for 5 minute
- Do RIE etching on the front side of the wafer using CNL Plasmatherm 540/540 Dual Chamber RIE system: etch for the demanded depth (5 sccm SF_6 @ 150W; 1.17 μm for 1 mintutes)
- Measure and verify the depth using profilometer in CNL and Zygo in MEMS lab

- Add more time of RIE etching if needed

(10) Remove the masking silicon oxide using BOE

- Etching the chips on slides in BOE for 10 minutes (increase the etching time if the silicon oxide is still exist) to totally remove the silicon mask left.
- Immerse in DI water for 5 minutes
- Take of the chips and clean using the standard acetone + IPA cleanness procedure in CNL
- Dry up the chips using N_2

(11) Anodic bonding

- Clean the silicon chips and Pyrex chips in ultrasonic with acetone for 5 minutes, then with IPA in ultrasonic for another 5 minutes
- Dry up the chips and do O_2 plasma in Fab Lab for 5 minutes to clean the surface of the silicon chips and Pyrex chip.
- Flip the glass and place it on silicon chips
- Place the stack on the anodic bonding hot plate, lower the bonding tip until touch the silicon/glass stacks
- Increase the temperature until 400°C
- Once the temperature reached 400°C, apply 550 V voltage for 20 minutes.
- Stop the voltage applying and stop the heating , wait the hotplate to cool down until temperature lower than 100 °C

(Now the cold head is ready for assembly)

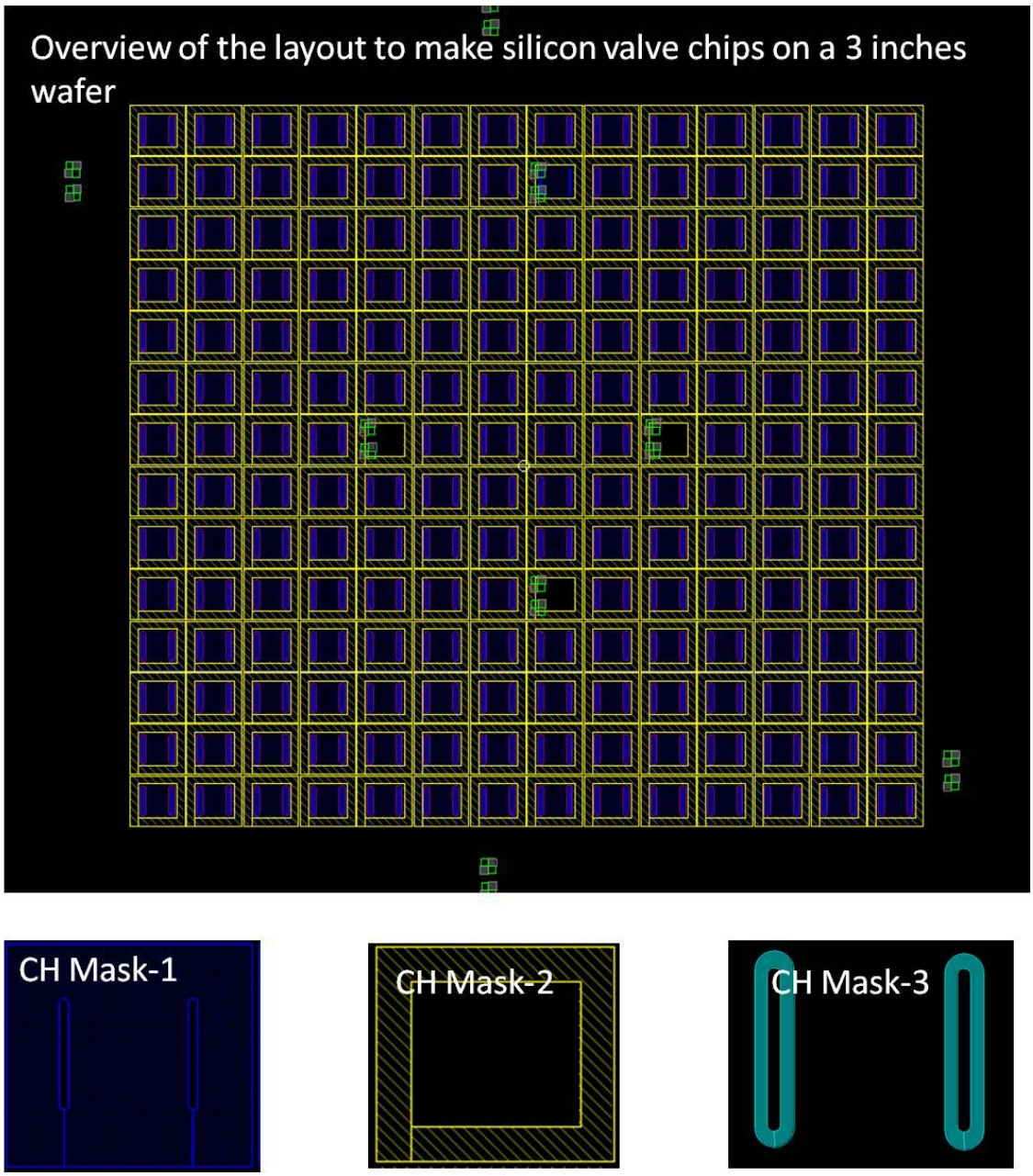

Figure A.1: Overview of the layout to make silicon valve chips on a 3 inches wafer and the layouts for different mask layers of one unit.

Appendix C: Standard operation of procedure of fabrication of the polyimide heat exchanger

(a) Thermal oxidation.

- Prepare double side polished (DSP) 3 inch (76 mm) n-type <100> silicon wafer of 550 μm in thickness
- Wet thermal oxide use CNL standard oxidation Instruction on CNL's Lindberg Diffusion/oxidation/annealing furnace 85304
- Wet oxidation of 1.8 μm SiO_2 for about 7 hrs

(b) O-ring shapes trench making.

- Spin coat photoresist AZ- 4620 on front side at 1600 rmp for 60 s
- Prebake on hotplate @ 110 °C for 4 minutes
- Expose using CNL Karl Suss MJB3 Mask aligner-I to expose for 3'15'' @ 195W (using HX Mask-1)
- Develop in developer (AZ400K:H_2O=1:2.5) for 5-10 minutes (inspection under micro scope is needed to make sure the photoresist are properly developed)
- O_2 plasma for 1 minute to clean (repeat if required)
- Post bake the wafer for 2 minutes @ 110 °C
- Conduct RIE on the front side of the wafer using CNL Plasmatherm 540/540 Dual Chamber RIE system: etch for 20 minutes for Silicon oxide (4 sccm O_2 + 16 sccm CF_4 @ 150W); rotate the wafer and etch for another 20 minutes
- Do RIE etching on the front side of the wafer using CNL Plasmatherm 540/540 Dual Chamber RIE system: etch for 4 minutes for silicon (5 sccm SF_6 @ 150W)
- Strip off the photoresist use the standard acetone + IPA procedure in CNL

(c) Backside SiO_2 was patterned using RIE.

- Spin coat photoresist AZ- 4620 on back side at 1600rmp for 60 s
- Prebake on hotplate @ 110 °C for 4 minutes
- Expose using CNL Karl Suss MJB3 Mask aligner-II (front-to-back alignment) to expose for 2'15'' @ 275 W (using HX Mask-2)
- Develop in developer ($AZ400K:H_2O=1:2.5$) for 5-10 minutes (inspection under micro scope is need to make sure the photoresist are properly developed)
- O_2 plasma for 1 minute (repeat if required)
- Post bake the wafer for 2 minutes @ 110 °C
- Do RIE etching on the back side of the wafer using CNL Plasmatherm 540/540 Dual Chamber RIE system: etch for 20 minutes for silicon oxide (4 sccm O_2 + 16 sccm CF_4 @ 150W); rotate the wafer and etch for another 20 minutes
- Strip off the photoresist use the standard acetone + IPA procedure in CNL

(d) Plate and pattern the first sacrificial layer

- Do E-beam evaporation to coat chromium 100 nm in thickness followed by an electroplating seed layer of copper 500 nm in thickness using Thermal evaporator CNL
- Copper of 15 μm was electroplated with a current density of approximate 5 mA/cm^2 in CU MEMS lab, thickness is monitored using profilometer
- Spin coat photoresist AZ- 4620 on front side at 1600rmp for 60 s
- Prebake on hotplate @ 110 °C for 4 minutes

- Expose using CNL Karl Suss MJB3 Mask aligner-I to expose for 3’15’’ @ 195W (using HX Mask-3)
- Develop in developer (AZ400K:H_2O=1:2.5) for 5-10 minutes (inspection under micro scope is needed to make sure the photoresist are properly developed)
- Do O_2 plasma for 1 minute to remove the photo resist residue (add more time if required)
- Post bake the wafer for 2 minutes @ 110 °C
- Do wet etching of the copper using Transene CE-100, the etching can be conducted both at room temperature or up to 40 °C giving different etching rate.
- Dip the wafer in to DI water for 5 minute and then dry it with N_2 gun
- Do wet etching of the chromium using 30% HCl solution (HCl is supposed not to etch chromium Cr, however, there could be some electrochemical reaction when there are both Cr and Cu that enable the etching of Cr)
- Dip the wafer in to DI water for 5 minute and then dry it with N_2 gun
- Strip off the photoresist use the standard acetone + IPA procedure in CNL

(e) Coat the bottom PI layer

- Polyimide (DuPont PI-2574*) was deposited onto the wafer in two spin coats of 2400 rpm for 30 seconds followed by a soft bake after each at 100 °C for 120 seconds.
- After all the spin coats, the polyimide was cured at 260 °C for 1 hour in nitrogen use the hotplate in fab lab arriving at an after- cure thickness of about 20 µm. When doing the curing, use the fixture with clampers to keep the wafer flat. Increase and decreasing the temperature very slowly to reduce thermal shock or thermal stress.

(f) Plate and pattern the second sacrificial layer

- Do E-beam evaporation to coat titanium of 30 nm in thickness followed by an electroplating seed layer of copper 500 nm in thickness using Egun-2 evaporator in NIST BMF cleanroom
- Copper of 20 μm was electroplated with a current density of approximate 5 mA/cm^2 in CU MEMS lab, thickness is monitored using profilometer
- Spin coat photoresist AZ- 4620 on front side at 1600rmp for 60 s
- Prebake on hotplate @ 110 °C for 4 minutes
- Expose using CNL Karl Suss MJB3 Mask aligner-I to expose for 3'15'' @ 195 W (using HX Mask-4)
- Develop in developer ($AZ400K:H_2O=1:2.5$) for 5-10 minutes (inspection under micro scope is needed to make sure the photoresist are properly developed)
- Do O_2 plasma for 1 minute to remove the photo resist residue (add more time if required)
- Post bake the wafer for 2 minutes @ 110 °C
- Do wet etching of the copper using Transene CE-100, the etching can be conducted both at room temperature or up to 40 °C giving different etching rate.
- Dip the wafer in to DI water for 5 minute and then dry it with N_2 gun
- Do wet etching of the chromium using 30% HCl solution (HCl is supposed not to etch chromium Cr, however, there could be some electrochemical reaction when there are both Cr and Cu that enable the etching of Cr)
- Dip the wafer in to DI water for 5 minute and then dry it with N_2 gun

- Conduct RIE etching on the front side of the wafer to etch Ti using CNL Plasmatherm 540/540 Dual Chamber RIE system: etch for 10 minutes with 4 sccm O_2 + 16 sccm CF_4 @ 150W, more time can be added when needed
- Strip off the photoresist use the standard acetone + IPA procedure in CNL

(g) Coat the center (second) PI layer

- Polyimide (DuPont PI-2574*) was deposited onto the wafer in spin coat of 2400 rpm for 30 seconds followed by a soft bake after each at 100 °C for 120 seconds.
- After all the spin coats, the polyimide was cured at 260 °C for 1 hour in nitrogen use the hotplate in fab lab arriving at an after- cure thickness of about 20 µm. When doing the curing, use the fixture with clampers to keep the wafer flat. Increase and decreasing the temperature very slowly to reduce thermal shock or thermal stress.

(h) Plate and pattern the third sacrificial layer

- Do E-beam evaporation to coat titanium of 30 nm in thickness followed by an electroplating seed layer of copper 500 nm in thickness using Egun-2 evaporator in NIST BMF cleanroom
- Copper of 20 µm was electroplated with a current density of approximate 5 mA/cm^2 in CU MEMS lab, thickness is monitored using profilometer in CNL
- Spin coat photoresist AZ- 4620 on front side at 1600rmp for 60 s
- Prebake on hotplate @ 110 °C for 4 minutes
- Expose using CNL Karl Suss MJB3 Mask aligner-I to expose for 3’15’’ @ 195 W (using HX Mask-5)

- Develop in developer (AZ400K:H_2O=1:2.5) for 5-10 minutes (inspection under micro scope is needed to make sure the photoresist are properly developed)
- Do O_2 plasma for 1 minute to remove the photo resist residue (add more time if required)
- Post bake the wafer for 2 minutes @ 110 °C
- Do wet etching of the copper using Transene CE-100, the etching can be conducted both at room temperature or up to 40 °C giving different etching rate.
- Conduct RIE etching on the front side of the wafer to etch Ti using CNL Plasmatherm 540/540 Dual Chamber RIE system: etch for 10 minutes with 4 sccm O_2 + 16 sccm CF_4 @ 150W, more time can be added when needed

- Bath the wafer in to DI water for 5 minute and then dry it with N_2 gun
- Strip off the photoresist use the standard acetone + IPA procedure in CNL

(i) Coat the top PI layer

- Polyimide (DuPont PI-2574*) was deposited onto the wafer in two spin coats of 2400 rpm for 30 seconds followed by a soft bake after each at 100 °C for 120 seconds
- After all the spin coats, the polyimide was cured at 260 °C for 1 hour in nitrogen use the hotplate in fab lab arriving at an after- cure thickness of about 20 µm. When doing the curing, use the fixture with clampers to keep the wafer flat. Increase and decreasing the temperature very slowly to reduce thermal shock or thermal stress

(j) Coat and pattern final mask layer

- E-beam evaporation to coat chromium 100 nm in thickness followed by an electroplating seed layer of copper 500 nm in thickness using Thermal evaporator CNL
- Spin coat photoresist AZ- 4620 on front side at 1600rmp for 60 s
- Prebake in oven @ 110 ℃ for 4 minutes
- Expose using CNL Karl Suss MJB3 Mask aligner-I to expose for 3’15’’ @ 195W (using HX Mask-6)
- Develop in developer (AZ400K:H_2O=1:2.5) for 5-10 minutes (inspection under micro scope is needed to make sure the photoresist are properly developed)
- Do O_2 plasma for 1 minute to remove the photo resist residue (add more time if required)
- Post bake the wafer for 2 minutes @ 110 °C
- Do wet etching of the copper using Transene CE-100 at room temperature
- Dip the wafer in to DI water for 5 minute and then dry it with N_2 gun
- Conduct RIE etching on the front side of the wafer to etch Ti using CNL Plasmatherm 540/540 Dual Chamber RIE system: etch for 10 minutes with 4 sccm O_2 + 16 sccm CF_4 @ 150W, more time can be added when needed
- Strip off the photoresist use the standard acetone + IPA procedure in CNL

(k) RIE etch to expose the sacrificial layers and define the shape of the heat exchanger

- Do RIE on the front side of the wafer using CNL Plasmatherm 540/540 Dual Chamber RIE system: etch for 30 minutes using parameter of: 4 sccm O_2 + 16 sccm CF_4 @ 150W
- Rote the wafer for 45° and repeat the previous etching step

- Repeat the previous rotation and etching for about 8 times until the first layer of the sacrificial metal to be exposed which is looks shiny (this rotation and etching is to keep a good uniformity of the whole etching in order to keep the under cutting of the polyimide to be uniform, more or less of this etching might required depending the variation of the etching rate)

(l) Etch the backside via holes

- Apply the Crystalbond™ 555 on a silicon wafer when heat it up to 95 °C with a hotplate; disperse the Crystalbond™ even onto the wafer, this wafer is a backup wafer for doing the later DRIE
- Place the wafer processed to the backup wafer (backside up) when keep the heating, press gently to make a better contact and shut done the hotplate, let the wafer cool down to room temperature
- Do DRIE in NIST cleanroom using standard silicon process setup for a etching rate of silicon of about 1.1 um/cycle, etch for about 3hrs until it etch through the silicon substrate (etching rate may change depending on the temperature of the surface, inspection can be done with some of the designed big inspection area.)
- Do RIE on the front side of the wafer using CNL Plasmatherm 540/540 Dual Chamber RIE system: etch for 1hr minutes using parameter of 4 sccm O_2 + 16 sccm CF_4 @ 150W, until the polyimide is etched through and the metal is exposed which is look shiny; similarly, etching rate may change depending on the temperature of the surface, inspection can be done with some of the designed big inspection area

(m) Metal release

- Quickly etch away the copper on the top which is for polyimide mask using a standard copper etchant (Transene CE-100*). Then etch away the titanium on top
- This is to remove the top metal layers so that the etching of the metal in channels can be monitored since the polyimide is semi-transparency
- The sacrificial layers of copper were etched away at the end in a standard copper etchant (Transene CE-100*) at 45°C to 60°C to form the embedded micro channels in the HX and free the whole HX structure. The etch time to fully release the structure was approximately 48 hours. Notice that the hotplate temperature set should be higher than the etchant temperature depends on the thermal mass of the beaker and etchant
- Do inspection every day when the device is under releasing
- After fully etch away the copper (yellow metal is gone), etch away the titanium layers for about 10 minutes
- Immerse the device in DI water for at least 10 hrs to make cleaning. It takes a long time for the etchant inside the channels to diffuse out to the water bath.
- Clean the device with IPA bath for at least 5 minutes and dry with nitrogen gun

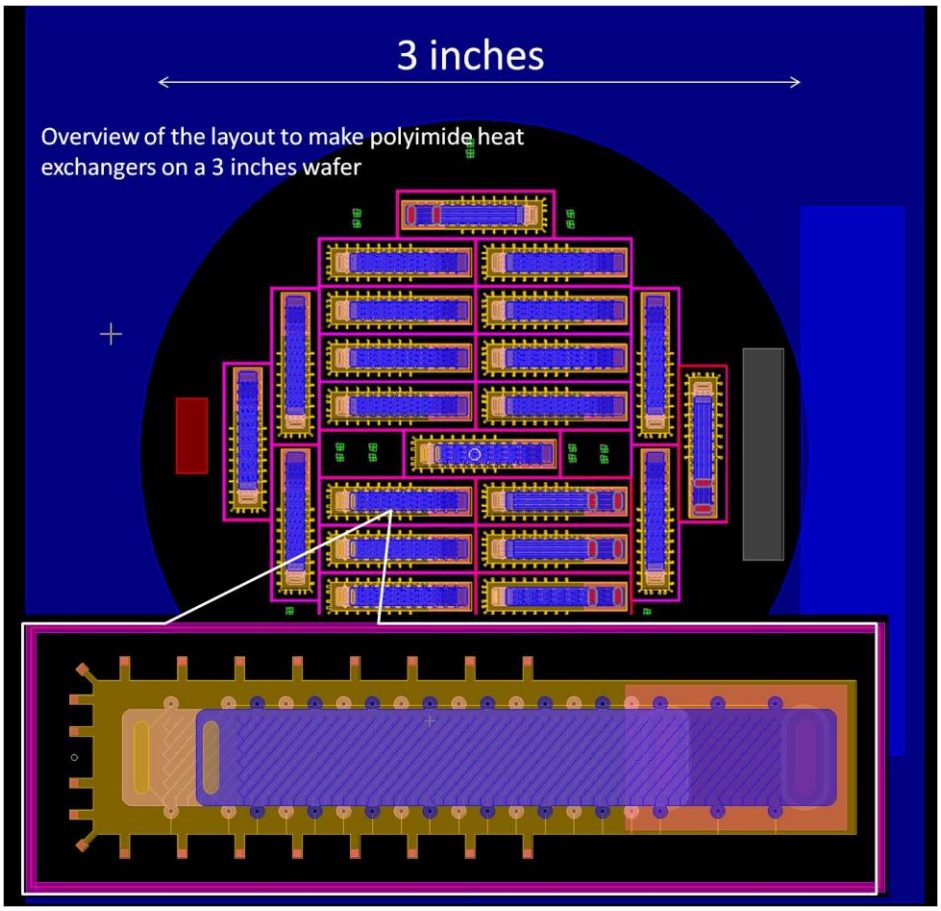

Figure A.2: Overview of the layout to make polyimide HXs on a 3 inches wafer.

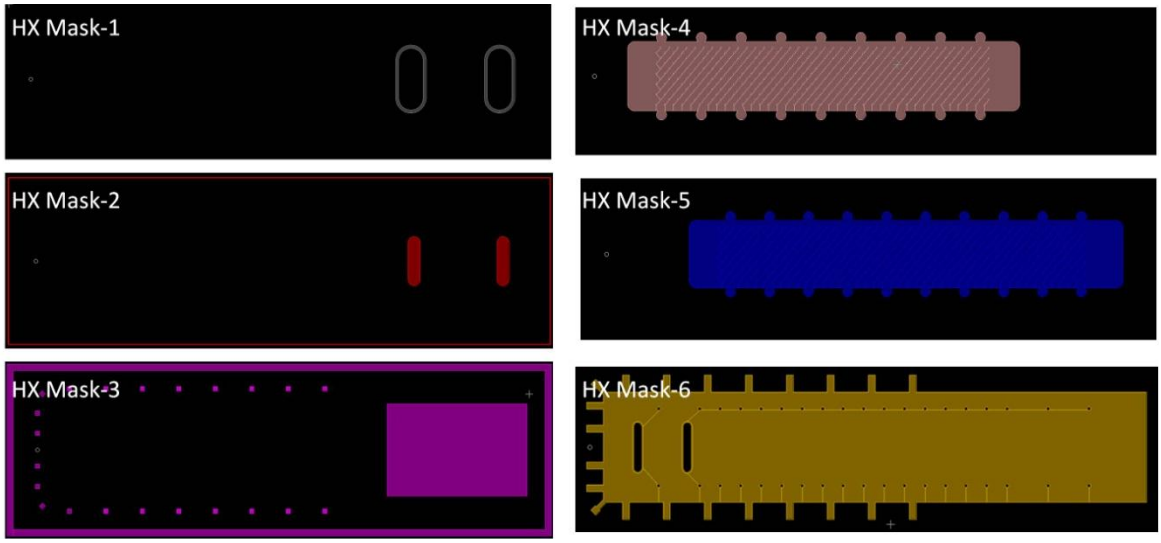

Figure A.3: The layout to make polyimide HXs for each mask of one device unit.

Appendix D: Standard operation of procedure of fabrication of the monolithic polyimide MCC

(1) Thermal oxidation.

- Prepare double side polished (DSP) 3 inch (76 mm) n-type <100> silicon wafer of 550 μm in thickness
- Wet thermal oxide use CNL standard oxidation Instruction on CNL's Lindberg Diffusion/oxidation/annealing furnace 85304
- Wet oxidation of 1.8 μm SiO_2 for about 7 hrs

(2) O-ring shapes trench making.

- Spin coat photoresist AZ- 4620 on front side at 1600rmp for 60 s
- Prebake on hotplate @ 110 ℃ for 4 minutes
- Expose using CNL Karl Suss MJB3 Mask aligner-I to expose for 3'15'' @ 195W (using MP Mask-1)
- Develop in developer (AZ400K:H_2O=1:2.5) for 5-10 minutes (inspection under micro scope is needed to make sure the photoresist are properly developed)
- O_2 plasma for 1 minute to clean (repeat if required)
- Post bake the wafer for 2 minutes @ 110 ℃
- Conduct RIE on the front side of the wafer using CNL Plasmatherm 540/540 Dual Chamber RIE system: etch for 20 minutes for Silicon oxide (4 sccm O_2 + 16 sccm CF_4 @ 150W); rotate the wafer and etch for another 20 minutes
- Do RIE etching on the front side of the wafer using CNL Plasmatherm 540/540 Dual Chamber RIE system: etch for 4 minutes for silicon (5 sccm SF_6 @ 150W)
- Strip off the photoresist use the standard acetone + IPA procedure in CNL

(3) Backside SiO_2 was patterned using RIE.

- Spin coat photoresist AZ- 4620 on back side at 1600rmp for 60 s
- Prebake on hotplate @ 110 ℃ for 4 minutes
- Expose using CNL Karl Suss MJB3 Mask aligner-II (front-to-back alignment) to expose for 2'15'' @ 275 W (using MP Mask-2)
- Develop in developer (AZ400K:H2O=1:2.5) for 5-10 minutes (inspection under micro scope is need to make sure the photoresist are properly developed)
- O_2 plasma for 1 minute (repeat if required)
- Post bake the wafer for 2 minutes @ 110 ℃
- Do RIE etching on the back side of the wafer using CNL Plasmatherm 540/540 Dual Chamber RIE system: etch for 20 minutes for silicon oxide (4 sccm O_2 + 16 sccm CF_4 @ 150W); rotate the wafer and etch for another 20 minutes
- Strip off the photoresist use the standard acetone + IPA procedure in CNL

(4) Plate and pattern the first sacrificial layer

- Do E-beam evaporation to coat chromium 100 nm in thickness followed by an electroplating seed layer of copper 500 nm in thickness using Thermal evaporator CNL
- Copper of 15 μm was electroplated with a current density of approximate 5 mA/cm^2 in CU MEMS lab, thickness is monitored using profilometer
- Spin coat photoresist AZ- 4620 on front side at 1600rmp for 60 s
- Prebake on hotplate @ 110 ℃ for 4 minutes

- Expose using CNL Karl Suss MJB3 Mask aligner-I to expose for 3’15’’ @ 195W (using MP Mask-3)
- Develop in developer (AZ400K:H_2O=1:2.5) for 5-10 minutes (inspection under micro scope is needed to make sure the photoresist are properly developed)
- Do O_2 plasma for 1 minute to remove the photo resist residue (add more time if required)
- Post bake the wafer for 2 minutes @ 110 °C
- Do wet etching of the copper using Transene CE-100, the etching can be conducted both at room temperature or up to 40 °C giving different etching rate.
- Dip the wafer in to DI water for 5 minute and then dry it with N_2 gun
- Do wet etching of the chromium using 30% HCl solution (HCl is supposed not to etch chromium Cr, however, there could be some electrochemical reaction when there are both Cr and Cu that enable the etching of Cr)
- Dip the wafer in to DI water for 5 minute and then dry it with N_2 gun
- Strip off the photoresist use the standard acetone + IPA procedure in CNL

(5) Coat the bottom PI layer

- Dilute the adhesion promoter VM 251 with DI water as in a volume ratio of 1:999 for VM251 to DI water. (Please notice that this diluted solvent is only good to use in one day)
- Dispense the promoter onto the substrate, hold for 20 sec and spin dry for 30 sec.
- Polyimide (DuPont PI-2611) was deposited onto the wafer in two spin coats of 2000 rpm for 30 seconds followed by a soft bake after each at 100 °C for 120 seconds.

- After all the spin coats, the polyimide was cured at 260 °C for 1.5 hours in nitrogen environment use the hotplate in fab lab arriving at an after- cure thickness of about 20 µm. When doing the curing, use the fixture with clampers to keep the wafer flat. Increase and decreasing the temperature very slowly to reduce thermal shock or thermal stress.

(6) Plate and pattern the second sacrificial layer

- Do E-beam evaporation to coat titanium of 30 nm in thickness followed by an electroplating seed layer of copper 500 nm in thickness using Egun-2 evaporator in NIST BMF cleanroom
- Copper of 20 µm was electroplated with a current density of approximate 5 mA/cm^2 in CU MEMS lab, thickness is monitored using profilometer
- Spin coat photoresist AZ- 4620 on front side at 1600rmp for 60 s
- Prebake on hotplate @ 110 °C for 4 minutes
- Expose using CNL Karl Suss MJB3 Mask aligner-I to expose for 3’15’’ @ 195 W (using MP Mask-4)
- Develop in developer (AZ400K:H_2O=1:2.5) for 5-10 minutes (inspection under micro scope is needed to make sure the photoresist are properly developed)
- Do O_2 plasma for 1 minute to remove the photo resist residue (add more time if required)
- Post bake the wafer for 2 minutes @ 110 °C
- Do wet etching of the copper using Transene CE-100, the etching can be conducted both at room temperature or up to 40 °C giving different etching rate.
- Dip the wafer in to DI water for 5 minute and then dry it with N_2 gun

- Do wet etching of the chromium using 30% HCl solution (HCl is supposed not to etch chromium Cr, however, there could be some electrochemical reaction when there are both Cr and Cu that enable the etching of Cr)
- Dip the wafer in to DI water for 5 minute and then dry it with N_2 gun
- Conduct RIE etching on the front side of the wafer to etch Ti using CNL Plasmatherm 540/540 Dual Chamber RIE system: etch for 10 minutes with 4 sccm O_2 + 16 sccm CF_4 @ 150W, more time can be added when needed
- Strip off the photoresist use the standard acetone + IPA procedure in CNL

(7) Coat the center (second) PI layer

- Dilute the adhesion promoter VM 251 with DI water as in a volume ratio of 1:999 for VM251 to DI water. (Please notice that this diluted solvent is only good to use in one day)
- Dispense the promoter onto the substrate, hold for 20 sec and spin dry for 30 sec.
- Polyimide (DuPont PI-2611) was deposited onto the wafer in spin coat of 2000 rpm for 30 seconds followed by a soft bake after each at 100 °C for 120 seconds.
- After all the spin coats, the polyimide was cured at 260 °C for 1.5 hour in nitrogen use the hotplate in fab lab arriving at an after- cure thickness of about 20 μm. When doing the curing, use the fixture with clampers to keep the wafer flat. Increase and decreasing the temperature very slowly to reduce thermal shock or thermal stress.

(8) Plate and pattern the third sacrificial layer

- Do E-beam evaporation to coat titanium of 30 nm in thickness followed by an electroplating seed layer of copper 500 nm in thickness using Egun-2 evaporator in NIST BMF cleanroom
- Copper of 20 μm was electroplated with a current density of approximate 5 mA/cm^2 in CU MEMS lab, thickness is monitored using profilometer in CNL
- Spin coat photoresist AZ- 4620 on front side at 1600rmp for 60 s
- Prebake on hotplate @ 110 °C for 4 minutes
- Expose using CNL Karl Suss MJB3 Mask aligner-I to expose for 3'15'' @ 195 W (using MP Mask-5)
- Develop in developer (AZ400K:H_2O=1:2.5) for 5-10 minutes (inspection under micro scope is needed to make sure the photoresist are properly developed)
- Do O_2 plasma for 1 minute to remove the photo resist residue (add more time if required)
- Post bake the wafer for 2 minutes @ 110 °C
- Do wet etching of the copper using Transene CE-100, the etching can be conducted both at room temperature or up to 40 °C giving different etching rate.
- Conduct RIE etching on the front side of the wafer to etch Ti using CNL Plasmatherm 540/540 Dual Chamber RIE system: etch for 10 minutes with 4 sccm O_2 + 16 sccm CF_4 @ 150W, more time can be added when needed
- Bath the wafer in to DI water for 5 minute and then dry it with N_2 gun
- Strip off the photoresist use the standard acetone + IPA procedure in CNL

(9) Coat the sacrificial layer for J-T valve

- Spin coat photoresist AZ- 4620 on front side at 1600rmp for 60 s

- Prebake in oven @ 110 ℃ for 4 minutes
- Expose using CNL Karl Suss MJB3 Mask aligner-I to expose for 3’15’’ @ 195W (using MP Mask-6)
- Develop in developer (AZ400K:H_2O=1:2.5) for 5-10 minutes (inspection under micro scope is needed to make sure the photoresist are properly developed)
- Do O_2 plasma for 1 minute to remove the photo resist residue (add more time if required)
- E-beam evaporation to coat titanium 20 nm in thickness followed by an electroplating seed layer of copper 3 nm in thickness using thermal evaporator (E-gun2) in NIST BMF cleanroom.
- Put the device in the acetone bath to lift-off and pattern the metal. Scotch tape was used to help to delaminate the potoresist supposed to be removed*

*(For this lift-off process, the photo resist used here is not a good candidate since for positive photoresist, Since these temperatures often occur during typical coating processes, the resist features will rounden and become coated overall making lift-off hard or impossible. Even if the resist features do not soften, positive resists allow only positive or - in best case - 90° sidewalls which also promotes the coverage of the sidewalls during coating [48]. The AZ 4620 is chose here for an development efficiency reason since it’s lithography on such a polyimide/copper surface has been developed during the previous process. Some other negative photoresists with a similar thickness are suggested to replac the AZ 4620 for the future fabrication.)

(10) Coat the top PI layer

- Polyimide (DuPont PI-2611*) was deposited onto the wafer in two spin coats of 2000 rpm for 30 seconds followed by a soft bake after each at 100 ℃ for 120 seconds.
- After all the spin coats, the polyimide was cured at 260 ℃ for 1.5 hours in nitrogen use the hotplate in fab lab arriving at an after- cure thickness of about 20 µm. When doing the curing, use the fixture with clampers to keep the wafer flat. Increase and decreasing the temperature very slowly to reduce thermal shock or thermal stress.

(11) Coat and pattern final mask layer

- E-beam evaporation to coat titanium 30 nm in thickness followed by an electroplating seed layer of copper 1.8 µm in thickness using thermal evaporator (E-gun2) NIST BMF cleanroom
- Spin coat photoresist AZ- 4620 on front side at 1600rmp for 60 s
- Prebake in oven @ 110 ℃ for 4 minutes
- Expose using CNL Karl Suss MJB3 Mask aligner-I to expose for 3’15’’ @ 195W (using MP Mask-7)
- Develop in developer (AZ400K:H_2O=1:2.5) for 5-10 minutes (inspection under micro scope is needed to make sure the photoresist are properly developed)
- Do O_2 plasma for 1 minute to remove the photo resist residue (add more time if required)
- Post bake the wafer for 2 minutes @ 110 ℃
- Do wet etching of the copper using Transene CE-100 at room temperature
- Dip the wafer in to DI water for 5 minute and then dry it with N_2 gun

- Conduct RIE etching on the front side of the wafer to etch Ti using CNL Plasmatherm 540/540 Dual Chamber RIE system: etch for 10 minutes with 4 sccm O_2 + 16 sccm CF_4 @ 150W, more time can be added when needed
- Strip off the photoresist use the standard acetone + IPA procedure in CNL

(12) RIE etch to expose the sacrificial layers and define the shape of the heat exchanger

- Do RIE on the front side of the wafer using CNL Plasmatherm 540/540 Dual Chamber RIE system: etch for 30 minutes using parameter of: 4 sccm O_2 + 16 sccm CF_4 @ 150W
- Rote the wafer for 45° and repeat the previous etching step
- Repeat the previous rotation and etching for about 8 times until the first layer of the sacrificial metal to be exposed which is looks shiny (this rotation and etching is to keep a good uniformity of the whole etching in order to keep the under cutting of the polyimide to be uniform, more or less of this etching might required depending the variation of the etching rate)

(13) Etch the backside via holes

- Apply the Crystalbond™ 555 on a silicon wafer when heat it up to 95 °C with a hotplate; disperse the Crystalbond™ even onto the wafer, this wafer is a backup wafer for doing the later DRIE.
- Place the wafer processed to the backup wafer (backside up) when keep the heating, press gently to make a better contact and shut done the hotplate, let the wafer cool down to room temperature.

- Do DRIE in NIST cleanroom using standard silicon process setup for a etching rate of silicon of about 1.1 um/cycle, etch for about 3hrs until it etch through the silicon substrate (etching rate may change depending on the temperature of the surface, inspection can be done with some of the designed big inspection area).
- Do RIE on the front side of the wafer using CNL Plasmatherm 540/540 Dual Chamber RIE system: etch for 1hr minutes using parameter of 4 sccm O_2 + 16 sccm CF_4 @ 150W, until the polyimide is etched through and the metal is exposed which is look shiny; similarly, etching rate may change depending on the temperature of the surface, inspection can be done with some of the designed big inspection area.

(14) Metal release

- Quickly etch away the copper on the top which is for polyimide mask using a standard copper etchant (Transene CE-100*). Then etch away the titanium on top. This is to remove the top metal layers so that the etching of the metal in channels can be monitored since the polyimide is semi-transparency.
- The sacrificial layers of copper were etched away at the end in a standard copper etchant (Transene CE-100*) at 45°C to 60°C to form the embedded micro channels in the HX and free the whole HX structure. The etch time to fully release the structure was approximately 48 hours. Notice that the hotplate temperature set should be higher than the etchant temperature depends on the thermal mass of the beaker and etchant. Do inspection every day when the device is under releasing.
- After fully etch away the copper (yellow metal is gone), etch away the titanium layers for about 10 minutes.

- Immerse the device in DI water for at least 10 hrs to make cleaning. It takes a long time for the etchant inside the channels to diffuse out to the water bath.
- Clean the device with IPA bath for at least 5 minutes and dry with nitrogen gun.

(15) Cap the front side etching hole

- Cut a piece of Kapton film with 50 µm thickness
- Place onto the hole to cap it and seal it with epoxy

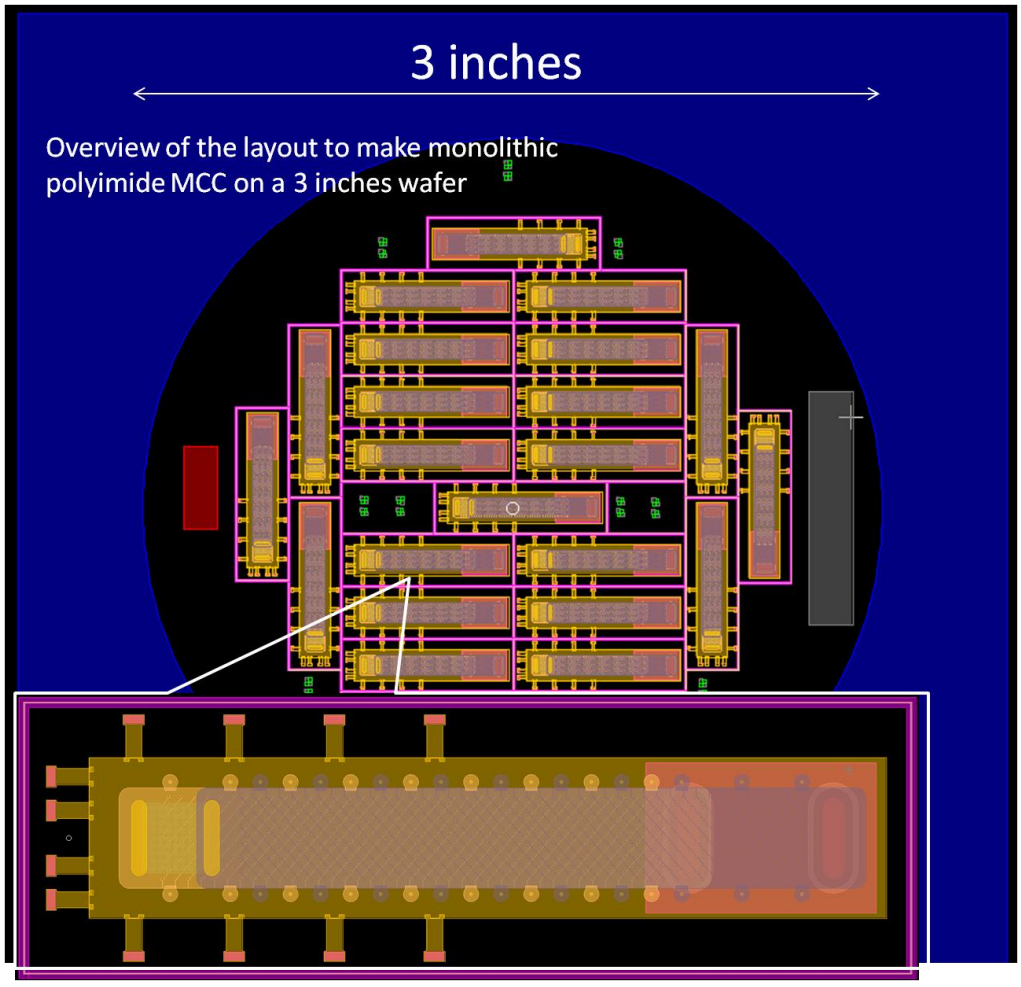

Figure A.4: Overview of the layout to make monolithic polyimide MCCs on a 3 inches wafer.

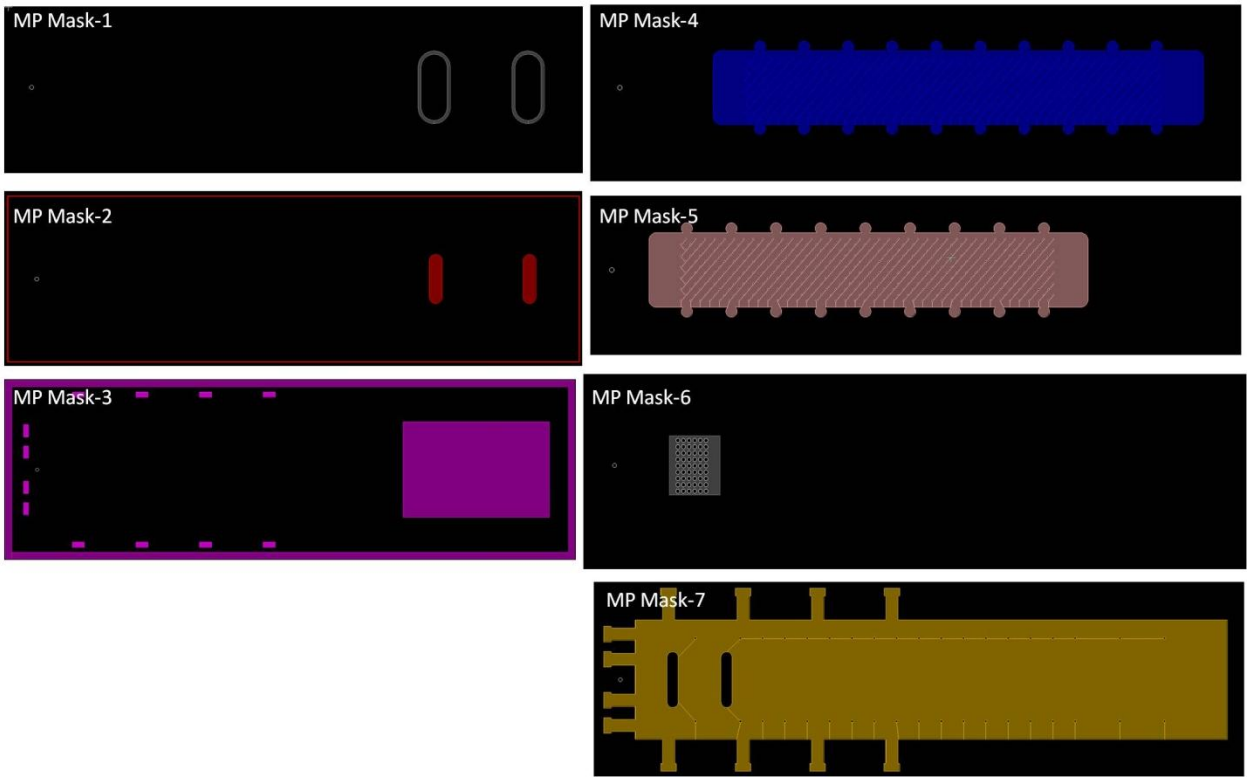

Figure A.5: The layout to make monolithic polyimide MCCs for each mask of one device unit.

Appendix E: Raw data of the valve restriction tests

The following are the raw data of the tests of valves flow-rates and pressure drops using the 275 K- 160 K refrigerant.

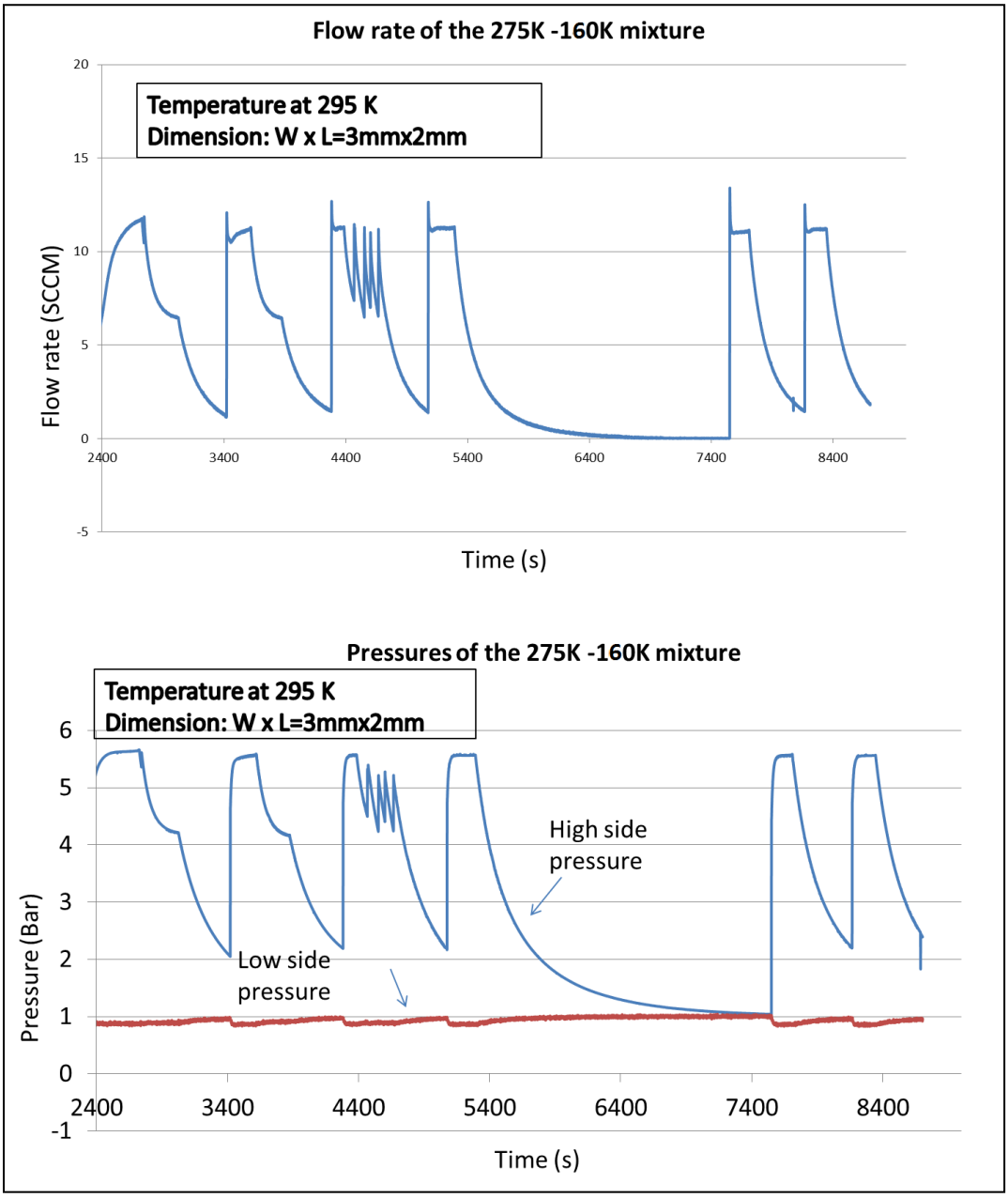

Figure A.6: Flow-rate and according pressures for a J-T valve with W × L = 3 mm × 2mm tested with 275- 160 K mixture when the temperature of the valve assembly is at 295 K.

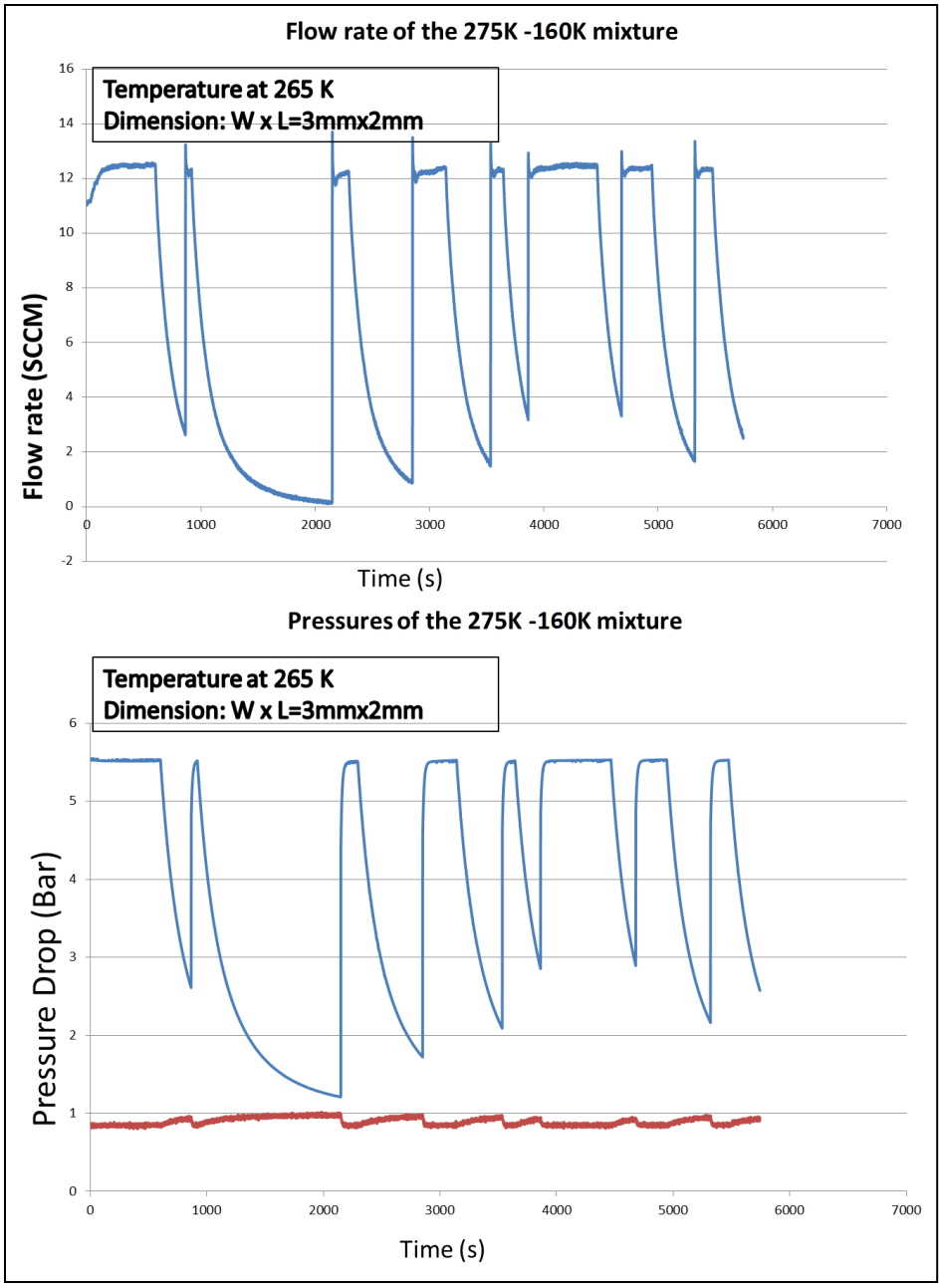

Figure A.7: Flow-rate and according pressures for a J-T valve with W × L = 3 mm × 2mm tested with 275- 160 K mixture when the temperature of the valve assembly is at 265 K.

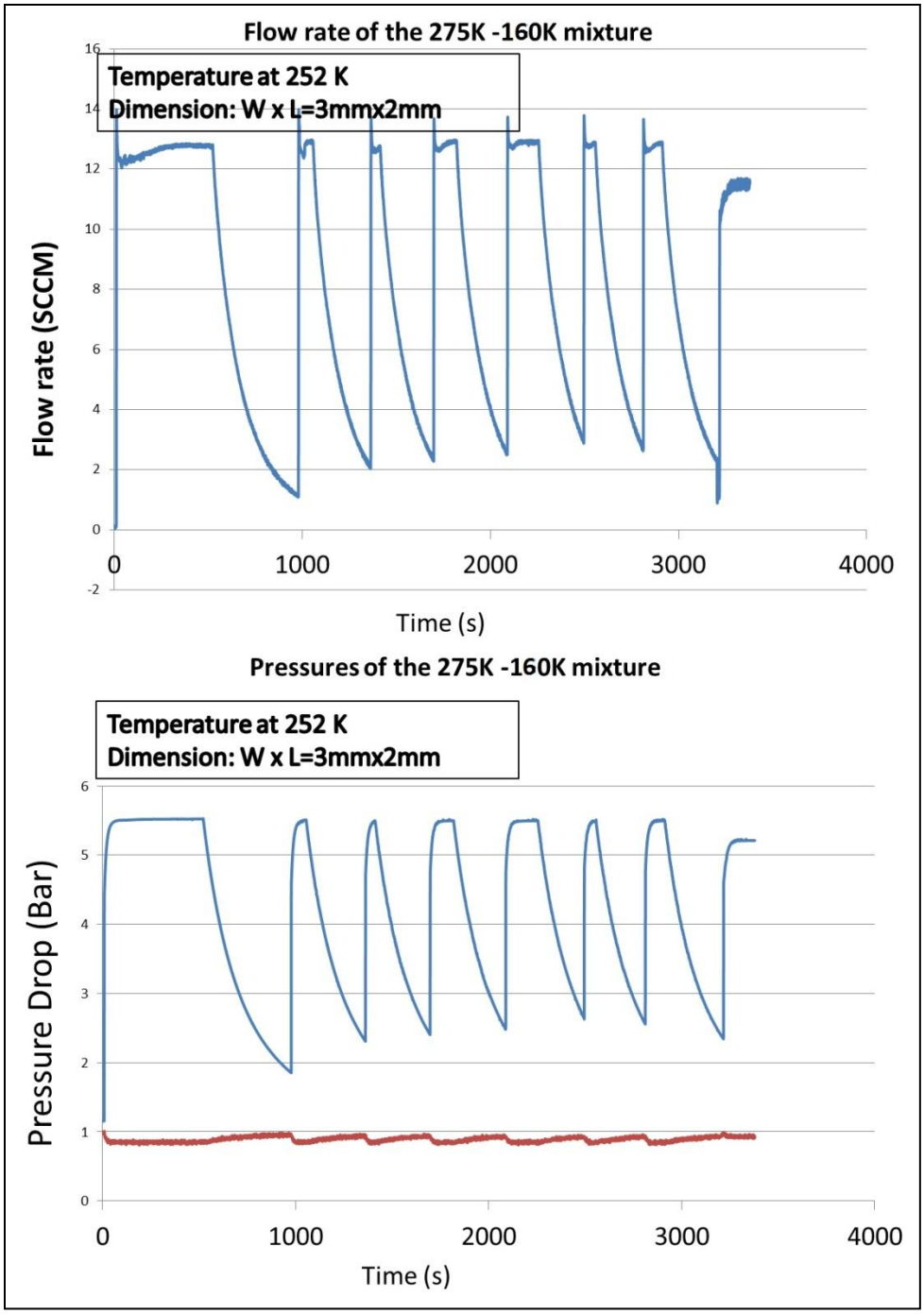

Figure A.8: Flow-rate and according pressures for a J-T valve with W × L = 3 mm × 2 mm tested with 275- 160 K mixture when the temperature of the valve assembly is at 252 K.

REFERENCE

[1] M.-H. Lin et al. “Design, Fabrication, and Assembly of a Hollow-Core Fiber-Based Micro Cryogenic Cooler” Transducers’09, Denver, June 21-25, 2009, pp. 1114-1117, 2009.

[2] Yung-Cheng Lee, Victor M. Bright, Ray Radebaugh, Eyal Gerecht, and James C. Booth “Micro Cryogenic Coolers (MCC) for Terahertz Imagers Utilizing Superconducting Hot Electron Bolometers” DARPA project proposal

[3] http://www.darpa.mil/MTO/programs/mcc/index.html DARPA MTO MCC program

[4] W.A. Little “Microminiature refrigeration” Transactions of Cryogenic engineering conference, Vol.53, 2008

[5] Y.D. Wang et al. “Wafer-Level Processing for Polymer-Based Planar Micro Cryogenic Coolers” Proc. of IEEE MEMS'12, Paris, France, Jan. 29 - Feb. 2, 2012, pp.341-344, 2012

[6] Lewis, R, Wang, Y., Cooper, J., Lin, M.-H., Bright, V.M., Lee, Y.C., Bradley, P.E., Radebauth, R., and Huber, M.L., “Micro Cryogenic Coolers for IR Imaging,” SPIE 2011. 8012-75, 2011

[7] J. E. Mercereau and W. A. Little “Microminiature Refrigeration System and Integrated Superconducting Magnetometer” Research Advisory Institute proposal submitted to the Office of Naval Research, May 5, 1972.

[8] P P P M Lerou et al “All-Micromachined Joule-Thomson Cold Stage” 14th International Cryocooler Conference, 16-20 July 2007, Annapolis, MD, USA.

[9] P P P M Lerou, H J M ter Brake, J F Burger, H J Holland and H Rogalla, “Characterization of micromachined cryogenic coolers” J. Micromech. Microeng, 17 (2007) 1956–1960.

[10] Martin Lin “Fabrication, Assembly, and Characterization of a Hollow-Core Fiber-Based Micro Cryogenic Cooler” Ph.D. thesis defense in University of Colorado- Boulder, Aug, 2009.

[11] Radebaugh, R., "Recent Developments in Cryocoolers " 19th Int. Congress of Refrigeration, 973 , 1995.

[12] D. J. Missimer "Auto-Refrigerating Cascade (ARC) systems-an Overview" Tenth Intersociety Cryogenic Symposium, AIChE Spring National Meeting, 1994.

[13] M. J. Boiarski, V.M. Brodianski, and R.C. Longthworth "Retrospective of mixed refrigerant technology and modern status of cryocoolers based on one-stage, oil-lubricated compressors" Adv. in Cryogenic Engineering 43, 1701-1708, 1998.

[14] M. Fuderer. A. Andrija et al. German Patent 1426956, 1969.

[15] R. Radebaugh "Microscale heat transfer at low temperatures" Microscale Heat Transfer – Fundamentals and Applications, Springer, pp. 93–124, 2005.

[16] NIST Standard Reference Database 4. NIST Thermophysical Properties of Hydrocarbon Mixtures (SuperTrapp): Version 3.2, National Institute of Standards and Technology, Gaithersburg, MD; 2007.

[17] Ryan Lewis, M.-H. Lin, Jill Cooper, Yunda Wang, Marcia Huber, Peter Bradley, Ray Radebaugh and Y.C. Lee "Demonstration of an Integrated Micro Cryogenic Cooler and Miniature Compressor for Cooling to 200K," Proc. IMECE2011, Denver, CO, Nov. 11-17, 2011.

[18] S. Garvey, S. Logan, R. Rowe, and W.A. Little "Performance characteristics of a low-flow rate 25 mW, LN2 Joule-Thomson refrigerator fabricated by photolithographic means" Appl. Phys. Lett, 42:1048-1050, June 1983.

[19] W.A. Little. "Microminiature refrigeration" Rev Sci Instrum, 55:661-680, 1984

[20] P P P M Lerou, G C F Venhorst, C F Berends, T T Veenstra, M Blom, J F Burger, H J M ter Brake and H Rogalla "Fabrication of a micro cryogenic cold stage using MEMS-technology" J. Micromech. Microeng. 16 (2006) 1919–1925

[21] MMR Technologies, Inc. Website resource: http://www.mmr.com

[22] Clemens, J.M. Lasance, Electronic cooling, Technical Data, http://www.electronics-cooling.com, Nov 2002.

[23] Holman, J.P., "Heat Transfer", 8th ed., McGraw-Hill

[24] NIST Material measurement laboratory. Website resource:

http://cryogenics.nist.gov/MPropsMAY/Polyimide%20Kapton/PolyimideKapton_rev.htm

[25] Shigley, Joseph et al. "Mechanical Engineering Design" 7th ed., McGraw-Hill

[26] M. Van de Voord "Results of physical tests on polymers at cryogenic temperatures" Cryogenics 16 (1976) 296.

[27] E. Tschegg "Mechanical properties and fracture behaviour of polyimide (SINTIMID) at cryogenic temperatures" Cryogenics 31, pp. 878-883, 1991.

[28] H. Yokoyama "Thermal conductivity of polymide at cryogenic Temperature," Cryogenics 35, pp.798-799, 1995.

[29] M.A. Schmidt, R.T. Howe, S.D. Senturia, and J.H. Haritonidis, "Design and Calibration of a Microfabricated Floating Element Shear-Stress Sensor", IEEE Transacw on E l m Devices, vol. 35, no. 6, pp. 750-757, 1988.

[30] R,J. Jensen, J.P. Cummings, and H. Vora, "Copper/Polyimide Materials System for High Performance Packaging", Transactions on components Technology, v o l m o . 4, pp.384-393, 1984.

[31] Y. W. Kim and M. G. Allen "Surface micromachined platforms using electroplated sacrificial layers," Solid-State Sens. Act., pp. 651-654, 1991.

[32] Y. W. Kim and M. G. Allen, "Single- and multi-layer surfacemicromachined platforms using electroplated sacrificial layers," Sensors and Actuorors A, vol. 35, pp. 61-68, 1992.

[33] P. P. P. M. Lerou, et al. “Insight into clogging of micromachined cryogenic coolers,” Appl. Phys. Lett. 90, pp. 064102, 2011.

[34] D. J. Missimer “Auto-Refrigerating Cascade (ARC) systems—an Overview,” Tenth Intersociety Cryogenic Symposium, AIChE Spring National Meeting, 1994.

[35] M. J. Boiarski et al. “Retrospective of mixed refrigerant technology and modern status of cryocoolers based on one-stage, oil-lubricated compressors,” Adv. in Cryogenic Engineering 43, pp. 1701-1708, 1998.

[36] M. Fuderer et al., German Patent 1426956, 1969.

[37] R. Lewis, “Two-phase Flow Patterns and Cooling Power of Mixed Refrigerant in Micro Cryogenic Coolers” ASME ICNMM2012, July 8-12, 2012.

[38] Ryan Lewis, Yunda Wang, Mu-Hong Lin, Marcia L. Huber, Ray Radebaugh, Y.C. Lee, “Enthalpy Change Measurements of a Mixed Refrigerant in a Micro Cryogenic Cooler in Steady and Pulsating Flow Regimes” Cryogenics, in press.

[39] R. Lewis “Testing and Analysis of Micro Cryogenic Coolers with Mixed Refrigerant” Ph.D. thesis defense in University of Colorado- Boulder, Dec. 2012

[40] http://www.engr.sjsu.edu/ahashemi/Joule%20Thompson%20Expansion.pdf

[41] Souza, A.L., Chato, J.C., Jabardo, J.M.S., Wattelet, J.P., Panek, J., Christoffersen, B.,Rhines, N.. “Pressure drop during two-phase flow of refrigerants in horizontal smooth tubes” Air Conditioning and Refrigeration Center TR-25.1992.

[42] I.Y. Chen, K.S. Yang, C.C. Wang An empirical correlation for two-phase frictional performance in small-diameter tubes Int J Heat Mass Transfer, 45 (17) (2002), pp. 3667 – 3771

[43] R.W. Lockhart, R.G. Martinelli, Proposed correlations for isothermal two-phase two-component flow in pipes, Chem. Eng. Prog. 45 (1) (1949) 39–48.

[44] L. Friedel, Improved friction pressure drop correlations for horizontal and vertical two-phase pipe flow, European Twophase Group Meeting, Ispra, Italy, Paper E2, June, 1979.

[45] K.A. Triplett, S.M. Ghiaasiaan, S.I. Abdel-Khlik, A.LeMouel, B.N. McCord, Gas–liquid two-phase flow in microchannels Part II: void fraction and pressure drop, Int. J. Multiphase Flow 25 (3) (1999) 395–410.

[46] C.C. Wang, K.S. Yang, Y.J. Chang, D.C. Lu, Characteristics of air–water two-phase flow in a 3-mm smooth tube, Can. J. Chem. Eng. 78 (2000) 1011–1016.

[47] K.Y. Yang, I.Y. Chen, R. Hu, C.C. Wang, Some observations of the two-phase flow characteristics within a 3-mm diameter tube, ASHRAE Trans., accepted.

[48] MIT online text book chapter:

http://web.mit.edu/16.unified/www/FALL/thermodynamics/notes/notes.html

[49] John Taylor, "An introduction to error analysis: the study of uncertainties in physical measurements "Oxford University Press, 1981. pp 50

[50] Online thermopedia book http://www.thermopedia.com

[51] C. A. Wilson, R. K. Grubbs, and S. M. George, "Nucleation and Growth during Al2O3 Atomic Layer Deposition on Polymers", Chem. Mate. 2005, 17, 5625-5634

[52] A. S. da Silva Sobrinho, G. Czeremuszkin, M. Latreche, and M. R. Wertheimer, "Defect-permeation correlation for ultrathin transparent barrier coatings on polymers," J. Vac. Sci. Technol. A, vol. 18, pp.149–157, 2000.

[53] A. P. Roberts, B. M. Henry, A. P. Sutton, et al., "Gas permeation in silicon-oxide/polymer (SiOx/PET) barrier films: role of the oxide lattice, nano-defects and macro-defects", J. Membr. Sci. 208, 75, 2002.

[54] A. G. Erlat, B.-C. Wang, and R. J. Spontak, "Morphology and gas barrier properties of thin SiOx coatings on polycarbonate: Correlations with plasma-enhanced chemical vapor deposition conditions" J. Mater. Res. 15, 704, 2000.

[55] Ryan Lewis, Collin Coolidge, Paul Schroder, Y.C. Lee, Victor Bright, "Fabrication, assembly, and testing of a MEMS-enabled micro gas compressor for a 4:1 pressure ratio," Submitted to Sensors and Actuators A: Physicsal, September 2012.